ΝΤΑΓΚΡΑΣ ΔΗΜΗΤΡΙΟΣ

Σχεδιασμός και οικονομική αξιολόγηση υπερκρίσιμου κύκλου CO_2

ΣΧΟΛΗ ΜΗΧΑΝΟΛΟΓΩΝ ΜΗΧΑΝΙΚΩΝ

Τομέας: Θερμότητας

Επιβλέπων: Σωτήριος Καρέλλας, Καθηγητής ΕΜΠ

Αθήνα 2020

NTAGKRAS DIMITRIOS

SCHOOL OF MECHANICAL ENGINEERING

Design and economic evaluation of a supercritical CO_2 cycle

Section: Thermal Engineering

Supervisor: Sotirios Karellas, Professor

Athens 2020

Ευχαριστίες

Νομίζω είναι εύλογο ως πρώτο πρόσωπο να ειπωθεί το όνομα του καθηγητή μου, κ. Σωτήριου Καρέλλα, ο οποίος με εμπιστεύτηκε για την εκπόνηση αυτού του θέματος υπό την επίβλεψη του καθώς και για την αμέριστη κατανόηση του.

Ιδιαίτερη μνεία θα ήθελα να κάνω στον υποψήφιο διδάκτορα Ρουμπεδάκη Τρύφωνα, ο οποίος με απεριόριστη θέληση και προθυμία, ήταν δίπλα μου σε κάθε κώλυμα που μπορεί να δημιουργήθηκε κατά τη διερεύνηση των κατάλληλων λύσεων. Ειλικρινά χωρίς την βοήθεια του και την στήριξη του, η περάτωση αυτού του θέματος θα έμοιαζε Γολγοθάς.

Οι δύο συνάδελφοι, Νίκος και Μιχάλης, οι οποίοι με την πάροδο του χρόνου έγιναν δύο πολύ καλοί φίλοι, συνεισέφεραν τα μέγιστα στη κατανόηση του σχεδιαστικού κομματιού της εργασίας, αλλά επίσης η ντοπαμίνη ψυχολογίας που μου έδιναν όταν ήμουν σε κάποιο αδιέξοδο ήταν το μεγαλύτερο όπλο στη φαρέτρα μου.

Οι γονείς μου, Χρήστος και Θεοδώρα, είναι αναπόσπαστο κομμάτι σε ό,τι και να κάνω και όπως είναι λογικό ήταν και σε αυτό το κεφάλαιο της ζωής μου δίπλα, παρόλο που γκρίνιαζαν ή μπορεί να τους μιλούσα για πράγματα που ούτε τους ενδιέφεραν ούτε καταλάβαιναν. Η επιμονή και υπομονή, αλλά και η διάπλαση του χαρακτήρα μου εξαρτάται από αυτούς, έχοντας ως γνώμονα τα όνειρα μου ώστε να γίνω η καλύτερη εκδοχή του εαυτού μου.

Σημαντικός αρωγός στη κονιορτοποίηση κάθε είδους εμποδίου ήταν η κοπέλα μου, Ελευθερία, η οποία έπαιζε το ρόλο του σωτήρα, κάθε φορά που έχανα τον έλεγχο, και βάζοντας με πάλι στις ράγες του τρένου που οδηγούσε στο τέλος της εργασίας.

Θα ήθελα επίσης να αναφέρω τους αδερφικούς φίλους μου, Στάθη, Αντώνη, Ανάσταση, Λεωνίδα, Τάσο, Άγγελο, Σεραφείμ και Γιάννη με τους οποίους έχουμε περάσει πάρα πολλά και η σκέψη τους μου έδινε δύναμη.

Τελευταίους αλλά εξίσου σημαντικούς ανθρώπους, με τους οποίους είμαι αυτή τη στιγμή που γράφω τις ευχαριστίες, είναι η διμοιρία μου, θάλαμος Β4, 2η μοίρα, που με καλύπτουν σε κάθε ενέργεια μου προκειμένου να ξεκλέψω λίγο χρόνο και να γράψω τη διπλωματική μου. «ΑΝΤΟΧΗ:Α-ΤΕ-ΛΕΙ-Ω-ΤΗ».

<u>Υπεύθυνη δήλωση</u> για λογοκλοπή και για κλοπή πνευματικής ιδιοκτησίας:

Έχω διαβάσει και κατανοήσει τους κανόνες για τη λογοκλοπή και τον τρόπο σωστής αναφοράς των πηγών που περιέχονται στον οδηγό συγγραφής Διπλωματικών Εργασιών. Δηλώνω ότι, από όσα γνωρίζω, το περιεχόμενο της παρούσας Διπλωματικής Εργασίας είναι προϊόν δικής μου εργασίας και υπάρχουν αναφορές σε όλες τις πηγές που χρησιμοποίησα.

Ονοματεπώνυμο

Δημήτριος Ντάγκρας

Contents

Σύνοψη

Ο σκοπός της διπλωματικής εργασίας είναι η εξέταση ενός κύκλου Rankine που χρησιμοποιεί ως εργαζόμενο μέσο διοξείδιο του άνθρακα το οποίο βρίσκεται σε υπερκρίσιμη κατάσταση. Στην εισαγωγή αναφέρονται οι ορισμοί της συμπαραγωγής και της τριπαραγωγής και πως είναι πιθανό να πετύχουμε τριπλή παραγωγή ενέργειας ταυτόχρονα χρησιμοποιώντας υπερκρίσιμο διοξείδιο του άνθρακα. Το κύριο μέρος της ανάλυσης αποτελείται από δύο πεδία, την θερμοδυναμική ανάλυση του κύκλου σύμφωνα με την επίτευξη του μέγιστου ενεργειακού και εξεργειακού έργου, και ο σχεδιασμός των εξαρτημάτων σε 3D απεικόνιση μέσω του προγράμματος SOLIDWORKS.Η λεπτομερής επιλογή, το μέγεθος και το τελικό σχέδιο των στοιχείων μας δίνει την δυνατότητα κατασκευής ενός πίνακα υλικών ώστε να υπολογιστεί με μεγαλύτερη ακρίβεια το συνολικό κόστος μιας τέτοιας κατασκευής. Τα αποτελέσματα από την θερμοδυναμική ανάλυση εφαρμόζονται στην κατάλληλη επιλογή της διαστασιολόγησης και του σχεδίου των εξαρτημάτων καθώς και στο υπολογισμό για την λειτουργία του συστήματος. Για αυτό το λόγο η οικονομική ανάλυση που δημιουργήθηκε έχει σκοπό την ανάδειξη της ανταγωνιστικότητας αυτής της διάταξης στην ελληνική αγορά. Ως αποτέλεσμα, για μια επένδυση 20 χρόνων το LCOE υπολογίστηκε 0.063 €/kWhel,την ίδια στιγμή που η τιμή της πώλησης 1 kWh κυμαίνεται ανάμεσα στα 0.021-0.088 €/kWhe για τον μήνα Σεπτέμβριο του 2020.Αξιοσήμειωτο είναι ότι ο χρόνος αποπληρωμής(PbP) ήταν 15.69 χρόνια με την προϋπόθεση λειτουργίας της εγκατάστασης 6570 ώρες/χρόνο.

Abstract

The reason of this research is to examine a Rankine cycle with carbon dioxide as working fluid, at a supercritical state for electricity production. The study starts with an introduction in the basic configurations for cogeneration and trigeneration and how it is possible to produce three different energies (electric, thermal, cooling) simultaneously, based on supercritical carbon dioxide (sCO_2). The main body of the research is divided to two fields, the thermodynamical analysis of the cycle towards the maximization of the net energy and exergy outputs, and the design of the system components for a medium scale setup along with the assembly of the layout in 3D drawing using SOLIDWORKS. The detailed selection, sizing and final design of the involved components allows the development of a detailed bill of materials required for one such setup and eventually estimate with high accuracy the capital costs for the development of one such system. The results of the thermodynamic analysis are both implemented in the selection/sizing of the components as well as in the estimation of the operational performance of the sCO_2 system. In this way, a detailed economic analysis is conducted to evaluate the system's competitiveness for the Greek market. In fact, for a 20-year period of investment the LCOE of the system was estimated at 0.063 €/kWhel, while the system marginal price for the Greek market ranged between 0.021-0.088 €/kWhe for September 2020. Moreover, the corresponding payback period was estimated at 15.69 years for 6570 operating hours per year.

Nomenclature

A	*Surface*	*[m²]*
B	*Height*	*[m]*
C	*Cost*	*[$]*
D	*Density*	*[kg/m²]*
Ex	*Exergy*	*[kW]*
h	*Enthalpy*	*[J/kg]*
IRR	*Internal rate of return*	-
L	*Length*	*[m]*
LCOE	*Levelized cost of electricity*	
MSC	*Marginal System Cost*	*[€/kWh]*
N	*Rotation speed*	*[rpm]*
NPV	*Net present value*	*[€]*
p	*Pressure*	*[bar]*
PbP	*Pay-back period*	*[years]*
Pr	*Pressure ratio*	-
R	*Resistance*	-
r	*Radius*	*[m]*
s	*Entropy*	*[J/kg K]*
T	*Temperature*	*[K]*
t	*Thickness*	*[m]*
U,u	*Velocity*	*[m/s]*
W	*Power output*	*[kW]*
X	*Velocity ratio*	-
Z	*Number of rotor*	-

Greek Symbols

α,β	*Angles*	*[°]*
Δp	*pressure drop*	*[bar]*
η	*Efficiency*	-
φ	*Velocity coefficient of the rotor*	-
ψ	*Velocity coefficient of the stator*	-
Ω	*Degree of reaction*	*[°]*

Subscripts

BM	*component*
cond	*Condenser*
CT	*Constants for pressure factor*
ex	*Exergy*
F	*Factor*
h	*Hub*
HT	*High temperature*
HX	*Heat exchanger*
is	*Isentropic*
LT	*Low temperature*
M	*Maintenance*
net	*Net output*
P	*Cost of material*
prod	*Production*
R	*Rotor*
S	*Expense*
s	*Shroud*
SIC	*Specific investment cost*
st	*Turbine*
Tcrit	*Critical temperature*
th	*Thermal*
TIT	*Turbine inlet temperature*

1. Introduction

1.1 Combined Heat and Power (CHP)

Combined heat and power (CHP) is the use of a heat engine to create electricity and useful heat at the same time. On the other hand, the term trigeneration is used when cooling production is added to the other two processes.

The goal of combined heat and power is to use the waste heat to provide an additional useful output, namely heat or electricity, which is more efficient than the traditional standalone facilities. Furthermore, CHP revitalizes the environment as it recycles the waste heat and reduces the pollution. In fact, CHP is a procedure that is not limited to stationary power plants; many automotive corporations try to enhance the efficiency of the vehicles by recapturing the exhaust heat to cover auxiliary electrical or cooling loads.

As referred above, to create a trigeneration plant, it could only be realized by adding in a CHP unit an absorption chiller unit to convert the heat to cold. Combining a CHP or cogeneration plant with an absorption refrigeration system allows the utilization of seasonal excess heat for cooling.[1] The hot water from the cooling circuit of the plant serves as driving energy for the absorption chiller. The hot exhaust gas from the gas engine can also be used as an energy source for steam generation, which can then be utilized for a highly efficient, double-effect steam chiller. Up to 80% of the thermal output of the CHP plant is thereby converted to chilled water. In this way, the year-round capacity utilization and the overall efficiency of the cogeneration plant can be increased significantly.

1.1.1 CHP analysis

A fossil fuel, such as oil, coal, or natural gas, can be combusted in an engine realizing a steam turbine plant, a gas turbine, an internal combustion engine or a Stirling engine. This engine actuates an alternator (inverter-generator module) which generates eventually electrical power [2]. The rotation of this alternator produces heat and a coolant is used therefore to prevent its overheating. A heat exchanger recovers this heat to achieve the preferable heating or cooling effect. The main advantages and disadvantages of a CHP are listed below

Advantages

- CHP can achieve 90% efficiency or even more while, at a conventional plant, the corresponding combined efficiency rates 60%.
- Helps to reduce the global warming by reducing emissions of CO_2 and using part of these emissions to drive a chiller in a trigeneration system
- Reduces energy costs

- Renewable heat incentives: the versatility of these systems allow for coupling with renewable sources and thus exploit also the funding schemes to improve overall economics
- Replacing huge power plants with more CHP plants reduces the dependency on the centralized energy network and, in theory, major system failures and outages

Disadvantages

- The technology is currently more expensive and complex, so developing CHP plants typically requires higher initial investment
- Maintenance costs can also be higher for CHP
- Smaller-scale CHP plants produce electricity more expensively than larger-scale ones.

Trigeneration has the same benefits with the CHP systems but can also be used to produce steam or hot water for in situ domestic use. Trigeneration finds commonly application in hospitals and nursing/care facilities, food production factories as well as in fruit and vegetable growing facilities[3]. The only problem, which has to be mentioned is that trigeneration systems limits available distance to transfer the energy due to the danger of excessive heat losses through the pipe network. There are a number of different configurations of CHP units, on which refrigeration can be produced. These include:

- **Absorption chillers:**1) Operation using hot water 2) Operation using steam 3) Direct heat via combustion
- **Compression-type refrigeration machines:**1) Direct drive power 2) electrical drive power.

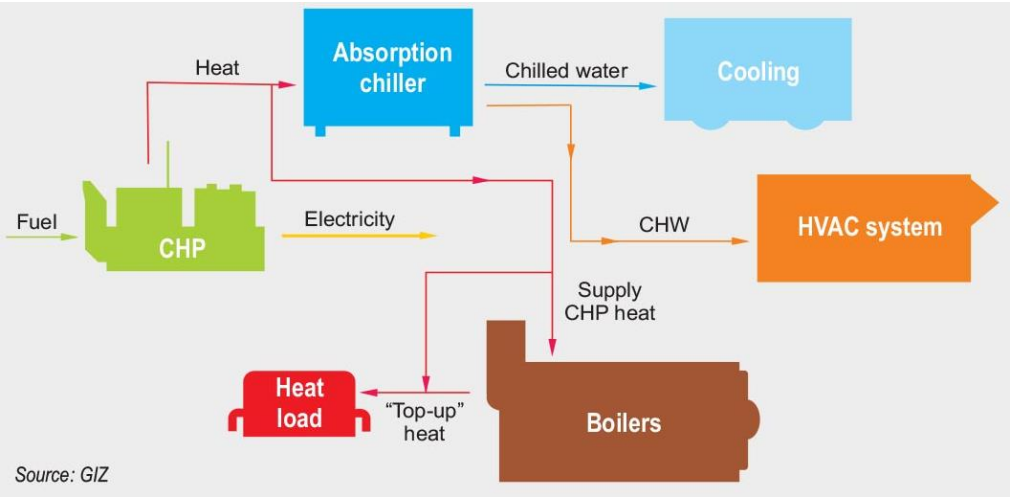

Fig. 1.1. Schematic of a trigeneration system

Some researchers argue that CHP is less efficient it is considered. The late Cambridge physicist David MacKay, for example, pointed out a theoretical flaw with the technology [4]. Heat is not wasted in conventional power plants in quite such an arbitrary way as we often assume: the "lost" heat is actually a fundamental part of making electricity as efficiently as possible in a conventional power plant—and optimizing the process to recover that heat can reduce the efficiency with which the electric power is produced. That's a problem, because electricity is a much more useful form of energy than heat (we can do far more things with it).
CHP is most efficient when heat can be used on-site or very close to it. Overall efficiency is reduced when the heat must be transported over longer distances [5]. This requires heavily insulated pipes, which are expensive and inefficient; whereas electricity can be transmitted along a comparatively simple wire, and over much longer distances for the equivalent energy loss. A car engine becomes a CHP plant in winter when the rejected heat is used for space heating of the vehicle's interior. The example illustrates the point that deployment of CHP depends on heat uses in the vicinity of the heat engine.

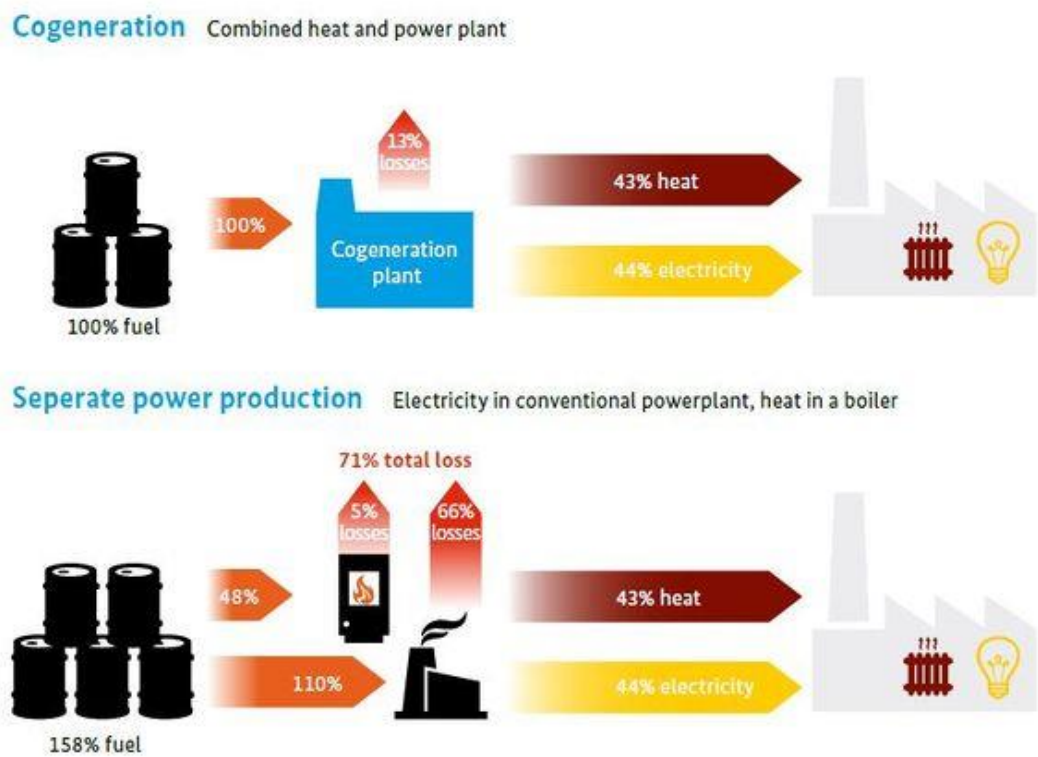

Fig. 1.2. Difference between separate power production and cogeneration

1.1.2 Micro CHP

Micro-generation relies to the same principles as larger CHP systems but these units are smaller in scale/size and usually they are decentralized, so as to be close to the consumption, thus, the efficiency will be higher [6].
The systems are usually powered by a small fuel cells or via a heat engine. The main purpose of a micro CHP is the heat production, therefore the electricity which is not used can be sold back to the grid. The benefits of micro CHP are similar with the CHP systems, but the most significant role of these units is the reduction of CO_2. As it is expected the smaller scale and the adaptation of the components technology results in a more complicated design.

1.2 CO_2 cycles

1.2.1 S-CO_2 properties

When a CO_2 stream is in a pressure and temperature above the critical point, then the fluid is in a state called supercritical. The main characteristic is the coexistence of a gas and a liquid. The unique properties of CO_2, which turn it in an attractive alternative to common refrigerants include:

- At temperatures in the vicinity of the critical point, the enthalpy of vaporization is reduced. This leads to a reduction in heating capacity and poor performance of the system. To be more specific, a conventional heat pump should avoid operating at a heat rejection temperature near T_{crit}. In a transcritical heat pump, heat rejection pressures are greater than the supercritical pressure and heat delivery temperatures are no longer limited by T_{crit}. Because of the high working pressure to achieve the demanding efficiency occur some design challenges, which with other refrigerant we don't have.
- CO_2 has a relatively high vapor density and correspondingly a high volumetric heating capacity. This allows a smaller volume of CO_2 to be cycled to achieve the same heating demand which allows for smaller components and a more compact system
- CO_2 becomes a supercritical fluid at 31.1 ^oC and pressure of 73.7 bar. In a conventional (subcritical) heat pump cycle, low critical temperature (T_{crit}) is a disadvantage because it limits the operating temperature range [7].

1.2.2 CO_2 as a refrigerant

In an analysis from EMERSON climate technologies [8], it is confirmed that the CO_2 (R744) is eligible to different conditions and criteria. As compared with the other conventional refrigerants, the cooling capacity is much bigger than the most common HFCs, HFOs and HCFCs.

Because of its availability, CO_2 cost is low but the components costs are high; the pressure is significant high so the materials of the components have to be resistant [9]. In addition, the carbon dioxide is a low toxicity substance and has the ability not to be flammable. An important characteristic that is created with the pressure flexibility (the use of different pressure states in a single layout) is the opportunity to be implemented in both simple as well as complex systems.[10]

1.2.3 Subcritical cycle

The cycle that is realized between the triple and the critical point is called subcritical. The triple point occurs at 5.18 bar and -57 °C, below this point there is no liquid phase. The most common characteristic in subcritical cycles is that the CO_2 plays the role of a refrigerant for the low temperature stage, thanks to its low temperature of the triple point and the corresponding saturation pressures at temperatures near and below 0 ^{o}C [11].

1.2.4 Transcritical cycle

When parts of a cooling cycle take place above the critical pressure (but not the entire cycle), the cycle is called transcritical. One main characteristic is that the gas cooler exit temperature has to be above 31°C, when CO_2 is considered. One difference between the subcritical and transcritical cycle is the cooling capacity (in the transcritical phase the cooling is much less). This is the reason why the heat rejection in a transcritical cycle is referred as gas cooling. Therefore, the implementation of a system to control the high side pressure is necessary. The most significant advantage of this type of cycle is the opportunity of having different pressures in a layout resulting in a good equilibrium between efficiency and cost investments-maintenance of the components.

Fig. 1.3. Difference between subcritical and transcritical cooling cycle using CO_2

1.2.5 s-$C0_2$ brayton cycle

Among various candidates, the s-CO2 power cycle is considered as one of the most promising alternatives to potentially provide high efficiency, higher stability with conventional structure materials, and eventually improved safety and reliability of the power conversion system. The s-CO_2 cycle combines the benefits of a Rankine cycle and the gas turbine system.

<u>Advantages</u>

- One of the most important benefits of this cycle is its compact turbomachinery. Because of the minimum pressure, the fluid remains dense throughout the entire system. Therefore, the volumetric flow rate decreases as the fluid density is higher, resulting in 10 times smaller turbomachinery compared with the turbomachinery of a steam Rankine cycle.

- The thermal efficiency can be increased up to 5% point compared with the steam Rankine cycle
- As the minimum pressure is higher than the CO_2 critical pressure (7.38 MPa), the purification system requirements are lower than those of the steam Rankine cycle to prevent air ingress. Thus, the power conversion system can be much simpler. In the steam cycle case, the low pressure in the condenser causes gas ingression and complex purification systems are required
- Among various fluids, CO_2 is relatively cheaper and less harmful when an appropriate ventilation system is installed.

1.3 Single flow layouts

According to recent studies, various layouts can be utilized for the s-CO_2 power cycle depending on the application. This is because the s-CO_2 cycle is similar to a steam Rankine cycle in terms of layout while the s-CO_2 cycle is similar to a gas turbine system from the main component design point of view.
One of the s-CO_2 Brayton cycle characteristics is that the specific heat of the cold side flow is two to three times higher than that of the hot side flow in recuperators. It is especially important for the s-CO_2 cycle layout design and also explains why the recompressing layout (Fig. 1.4) can have high efficiency.

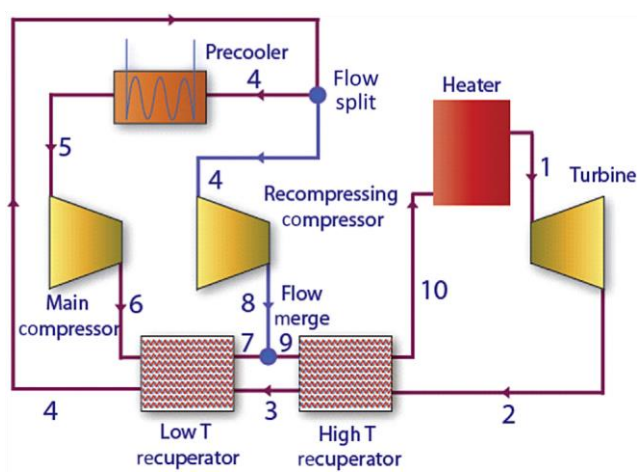

Fig. 1.4. S-CO_2 recompressing cycle layout

Before starting the analysis of recompressing layout, it is significant to discuss other s-CO_2 cycle layouts, thus, we can yield in more specific results The CO_2 flow can be separated depending on the application. Therefore, the cycle can be categorized depending on whether the flow is split

or not. Single (non-split) flow layouts can be distinguished into intercooling, reheating, precompression, inter-recuperation and split-expansion cycles [12].

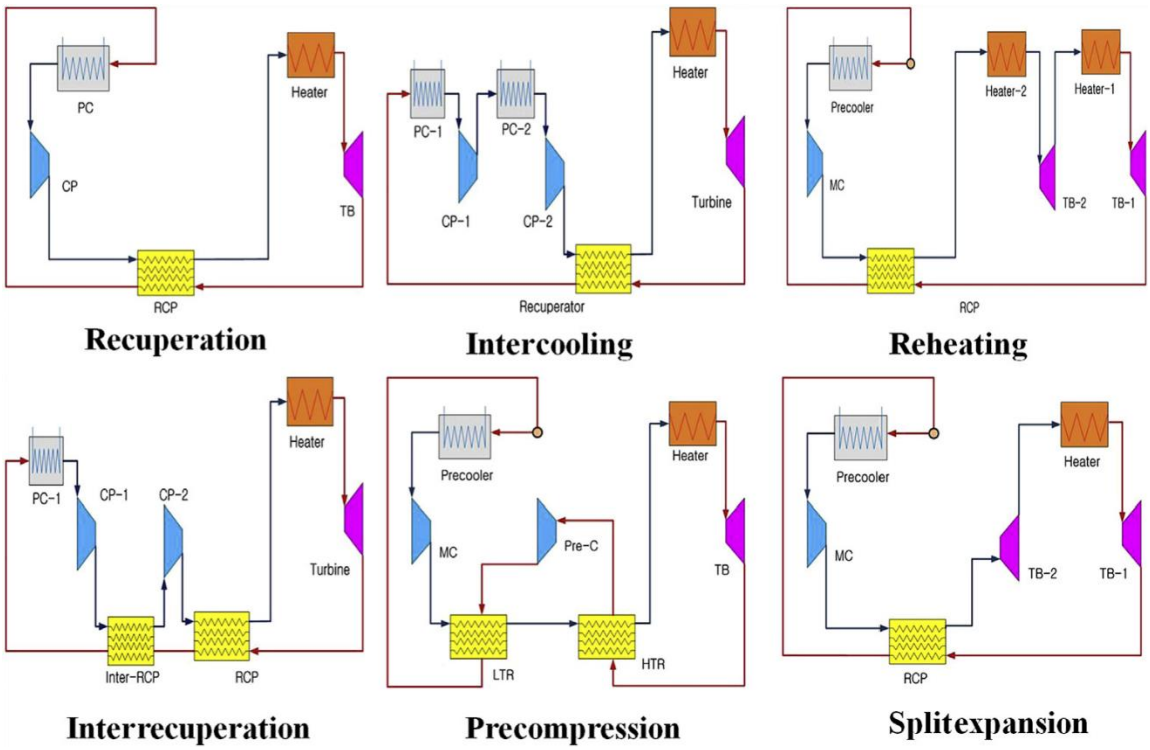

Fig. 1.5. s-CO_2 cycle single-flow configurations

The main role of *intercooling* and *reheating* configurations is to minimize or maximize the compression or expansion work, respectively. As the exhaust CO_2 temperature in the turbine is still high due to the low cycle pressure ratio, the heat can be recuperated in several ways. In *inter-recuperation*, *precompression* and *split-expansion* layouts, the application is directly dependent on the recuperation.

1.3.1 Intercooling

The main characteristic of the intercooling layout is that the compressor "breaks" in two stages and between these stages there is a second pre-cooler (the first is located before the compressors). The influence of the intercooling is more visible in the reduction of the compression work; however, in the s-CO_2 cycle the compression work is small anyway, thus the result is a small increase in the thermal efficiency. Another significant characteristic is that with the second pre-cooler, the temperature in the compressor outlet and in the recuperator drops, which the main problem is the proximity to the critical point.

1.3.2 Reheating

In order to create a s-CO_2 cycle with many features like the ideal gas Brayton cycle, a heater and an additional turbine (low pressure turbine mostly) can be introduced. The main difference is that after the first heater, the working fluid flows to the turbine, but after the turbine discharge enters the second heater and then flows through the second turbine before the recuperator.

1.3.3 Inter-recuperation

Inter-recuperation is similar to the intercooling cycle, with a second recuperator in lieu of a second precooler. The inter-recuperator has the function to drop the temperature so as to prevent the stream reaches the critical point in the recuperator and to reduce the heat waste. As a result, the thermal efficiency is higher and the heater performance is much better. It is important to be mentioned, that the recuperator is responsible for the biggest amount of the heat transfer.

1.3.4 Precompression

In this layout, the recuperator is divided to a high temperature recuperator and to a low temperature recuperator, putting between these two heat exchangers, a pre-compressor. The outlet of the main compressor flows through both recuperators and the working fluid returns to the pre-compressor and reflows through LTR and HTR. The main purpose is to allow for further regeneration, when the temperature difference is small so as to avoid the outlet turbine pressure influences the inlet main compressor pressure

1.3.5 Split-expansion

Split expansion is similar to the recuperation cycle with a turbine prior and after the heater. The additional turbine is used to split the expansion and to reduce the stress of the hottest component of the cycle(heater).
According to [12] the intercooling and reheating layouts are adopted to minimize or maximize the compression or expansion work, respectively. One of the major characteristics of the s-CO_2 cycle is its low pressure ratio because the limit of minimum pressure in the system is influenced by the critical pressure (7.38 MPa), which is relatively high compared with the steam Rankine cycle (~0.07 MPa) or air Brayton cycle(~0.1 MPa).

1.4 Split flow layouts

Apart from the two parameters with the highest sensitivity, namely turbine inlet temperature (TIT) and the pressure ratio, the flow split ratio, as it is presented in Fig. 1.6, has a significant role. The best example about the split flow is the three turbine split flow layouts, which have

the same components but the flow merges in different points. Each layout has a unique correlation between cycle efficiency and the split flow ratio to maximize the net output.

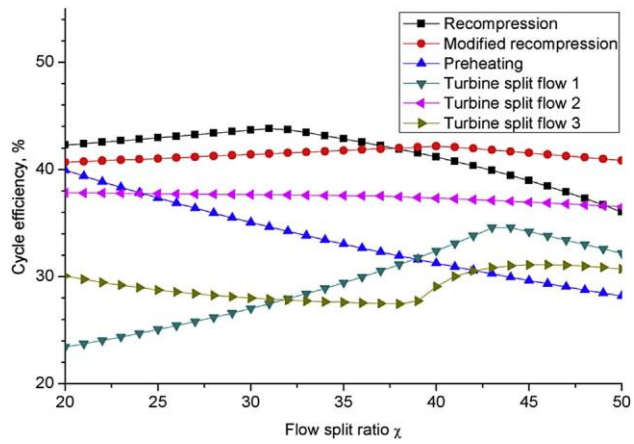

Fig. 1.6. The efficiencies of s-CO_2 split flow layouts for various flow split ratio. S-CO_2

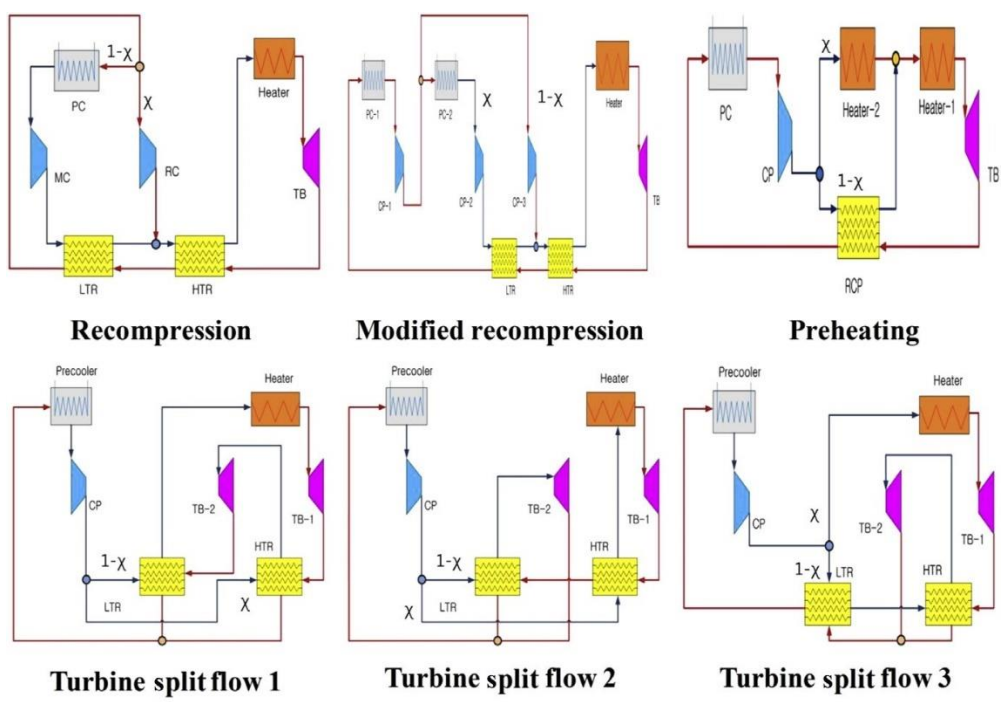

Fig. 1.7. s-CO_2 cycle split flow layouts

The difference between the *recompression* layout and the others is the recuperation process. In the recompression layout, the flow is split and the high specific heat in the cold side stream is matched with the hot side's large flow with lower specific heat in the low temperature recuperator (LTR) to maximize the cycle efficiency. In the *modified recompression* layout, the

turbine expands the flow below the critical pressure to produce more work. Compressor 1 compresses CO_2 near the critical point and the other processes are similar to the original recompression layout.
The other layouts, such as the *preheating* and *turbine split flow 1, 2,* and *3* layouts, maximize the temperature difference in the intermediate heat exchanger. Thus, these layouts can be implemented in co-generation or tri-generation plant systems because of the proportional temperature change in the heat source and the heat flowing into the conventional power system. Therefore, more power can be achieved with a lower efficiency if the absorbed heat is large.

1.4.1 Modified recompression

The main difference is the existence (i) of a third compressor between the second precooler and the HTR and (ii) the precooler before the first compressor. The operation of this layout is the same with the recompression cycle; the working fluid flows through the precooler before going to the first and second compressor. Then, the flow splits before the second precooler to go through the third compressor without dropping the temperature. The flow merges after the LTR and the third compressor (before HTR)

1.4.2 Preheating

The flow splits so as to go through the recuperator and the first preheater. Then merges after the increase of the temperature of the one flow (after the heater) so as to go together to the main heater and finally go to the state where occurs the lowest pressure of the cycle. The basic principle is to annihilate the temperature glide between the working fluid and the hot source so as to exploit greater heat transfer.

1.4.3 Turbine split flow 1,2,3

This layout has two turbines and their operation is like the split-expansion of the single flow layouts. The flow splits in the same state in these three layouts but the difference is where the flow goes after the split. In the first two layouts goes to the LTR and HTR and the third to the LTR and the heater. In each layout the working fluid goes to other component and the flow merges before the precooler in the first two configurations and before the LTR in the third. The distinctive feature of these architectures is the maximization of the waste heat utilization of the hot source and hence of the electrical net power output.
The differences between the basic split flow recompression layout and the other layouts are small but not negligible. In the modified compression, the turbine expands below the critical pressure to produce more work. All the above layouts have as main principle the maximization of the temperature difference in the intermediate heat exchanger.[12]

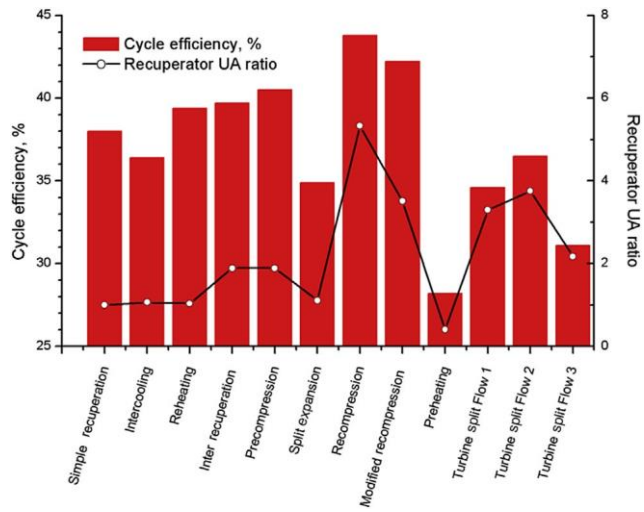

Fig. 1.8. Performance comparison of s-CO_2 layout

It is important to point that as the layout becomes more complex, the cycle efficiency is higher but also the cost of this operation increases.

1.5 s-CO_2 application

The s-CO_2 cycle is coupled with many nuclear heat sources, because it can replace the steam Rankine cycle with a number benefits by the substitution. Depending on the utilization of the s-CO_2 cycle, it can be an alternative as a topping cycle for fossil fuel powered plants and a bottoming cycle of gas combined cycle plants. There are also promising heat sources soon to be coupled with the s-CO_2 cycle, which include several renewable energy sources such as high temperature fuel cells, concentrated solar power, and geothermal power [13].

1.5.1 Nuclear application

Extensive research has taken place about the replacement of the malevolent water reactors from the mild sodium-CO_2 fast reactors. Despite the fact that the nitrogen Brayton cycle can eliminate the chemical reaction between sodium and the nitrogen Brayton cycle can achieve performance competitive to the superheated steam Rankine cycle, it can only be utilized in the sodium-cooled fast reactor application and unfortunately outside the nuclear application no immediate application field can be found. In contrast, the s-CO_2 power cycle can potentially be utilized for small and medium sized Reactors (SMR) such as SMART [14], large size conventional water-cooled reactors, and fusion reactor applications, as well as other energy sources such as coal, natural gas, and renewable energies.

1.5.2 Coal power application

The s-CO_2 cycle is also considered to be a promising candidate for the coal-fired power plant as a topping cycle to improve thermal efficiency. After some researches, the results show that this innovative s-CO_2 topping cycle can produce the same amount of net electricity as a non-CO_2 capturing steam power plant while, as expected, is reducing the CO_2 emissions significantly [15].

1.5.3 Exhaust/waste heat recovery application

The exhaust gas temperature from a gas turbine or general topping cycle is usually > 450 ^oC and the conventional steam Rankine cycle utilizes this exhaust gas to improve its thermal efficiency. The s-CO_2 Brayton cycle can potentially replace the steam Rankine cycle to further improve the thermal efficiency and can be utilized to recover waste heat from a small gas turbine as well, which is not practically feasible with the steam Rankine cycle. Using s-CO_2 power cycles for waste heat recovery, it is very important to maximize the net output power by incorporating the utilization efficiency of the waste heat along with the thermal efficiency of the cycle.

1.6 s-CO_2 Rankine cycle

Three types of Rankine cycles (**simple, cascade, and split**) will be discussed in this section, comparing the characteristics in the upper pressures of the cycle. In order to optimize their performance, it is very significant to maximize the net output power by combining the utilization efficiency of the waste heat and the thermal efficiency. To improve the thermal efficiency of the cycle, the turbine inlet temperature must be increased.
Because of the convenience of the CO_2 to reach the critical temperature (31.1 ^oC) and the critical pressure(7.38MPa), low and medium temperature heat sources can be exploited, which will reduce the temperature difference and promote the overall efficiency.

1.6.1 Simple s-CO_2 Rankine cycle

To improve the thermal efficiency of the cycle, the turbine inlet temperature must be increased as much as possible using a recuperator. However, a higher turbine inlet temperature results in a lower utilization (heat recovery) efficiency of the exhaust gas waste heat.[16] The reason for this is that the working fluid is preheated by the recuperator to a higher temperature. Because of this trade-off between the thermal efficiency and the utilization efficiency, it is impossible for a simple s-CO_2 Rankine cycle to fully utilize the waste heat from a gas turbine.

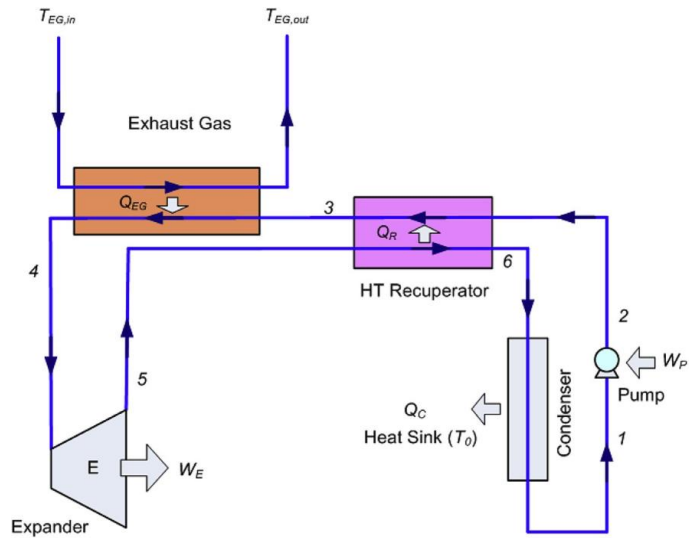

Fig. 1.9. Layout of simple S-CO_2 cycle for WHR from a gas turbine

1.6.2 Cascade supercritical CO2 Rankine cycle

An additional s-CO_2 Rankine cycle can be used to recover the remaining waste heat from the previous simple cycle. As mentioned before, it is impossible to fully utilize the waste heat of the exhaust gas of a gas turbine with a simple s-CO_2 rankine cycle. Therefore, a low temperature loop is introduced to the high temperature loop. The thermal efficiency of the cycle is lower than that of the simple cycle at a given turbine inlet temperature because it is the average of the efficiencies of the LT and HT loops. However, the heat recovery efficiency of the cycle is much higher than that of the simple cycle and decreases very slightly as the turbine inlet temperature increases.

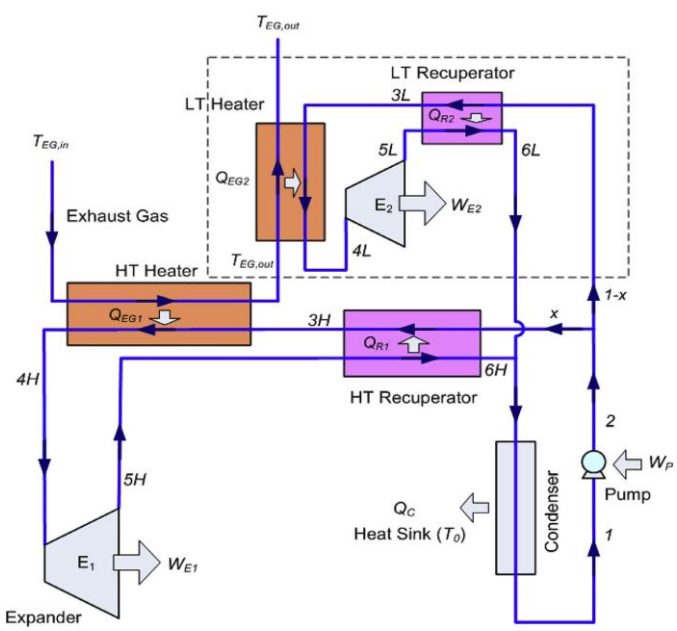

Fig. 1.10. Layout of cascade S-CO_2 cycle for WHR from a gas turbine

Because the cascade cycle is composed of two cycles, it is important to highlight the main difference between the topping and the bottoming cycle. In the topping cycle, the fuel is used in a gas turbine and the main heat source generates high-enthalpy and electricity. The hot exhaust afterwards is used for partial heating, cooling or other utility. As it pointed in the study [16], there are some subcategories about the topping cycle plant such as Steam electric plant with steam extraction from a condensing turbine. On the other hand, the bottoming cycle is not only more expensive than the topping cycle but also not so efficient. The low-enthalpy waste heat is used to drive the power generation cycle via a heat exchanger, recuperator or a boiler. This cycle finds application in function with high temperature energy production and high temperature heat rejection [17].

1.6.3 Split supercritical CO_2 Rankine cycle

Another way to recover the remaining waste heat from the previous simple cycle is to use a split s-CO_2 Rankine cycle. In the previously described simple s-CO_2 Rankine cycle, the temperature of the CO_2 after the recuperator on the high-pressure side is considerably lower than the temperature of the CO_2 before the recuperator on the low-pressure side, even with a high efficiency recuperator. This is because the isobaric specific heat of the CO_2 on the high-pressure side is much higher than that on the low-pressure side. Therefore, in the split s- CO_2 Rankine cycle shown in Fig. 1.11, it is possible to utilize the remaining waste heat from the simple s- CO_2 Rankine cycle to make up the difference in the isobaric specific heat of the CO_2 between the high- and low-pressure sides for a maximum temperature of CO_2 after the recuperator (state 3). The flow that is split after the pump is preheated by the recuperator and the LT heater to the same temperature.

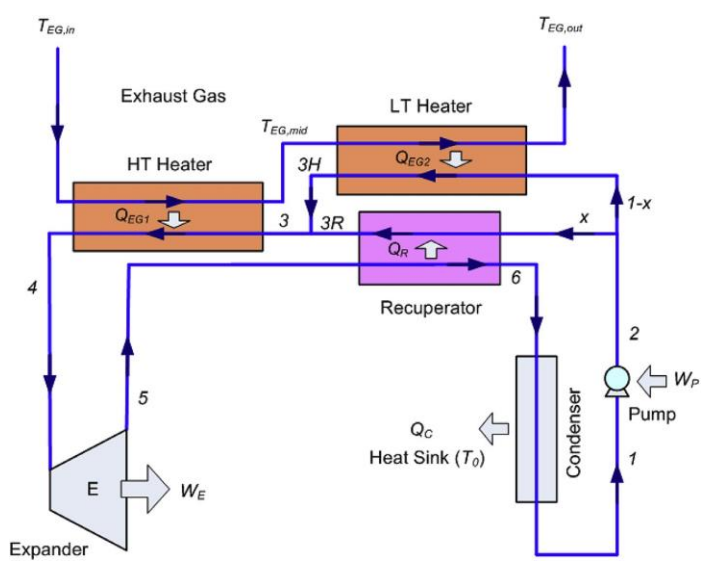

Fig. 1.11. Layout of split S-CO_2 cycle for WHR from a gas turbine

1.6.4 Poly-generation systems using s-CO_2

Poly-generation has had many meanings, however, has being defined as a thermochemical process which simultaneously produces at least two different products and at least one product is chemical or fuel and one at least electricity [18]. Nowadays, poly-generation has developed to be a multi-input and multi-output energy system that is assumed as the most promising technology to "bridge" the gap between the different industrial sectors.

At the beginning, these systems utilized as feedstock coal, but in order to save energy and solve the environmental problem, started to exploit renewable energy sources such as biomass or CO_2 based systems. Below are listed the key principles of a poly-generation system:

- Utilization of different types of fuels: According to the characteristics and the advantages of the fuels, a multi-fuel feedstock input could be used to succeed high energy chemical efficiency.
- Step by step conversion of effective components: Instead of complex composition adjustment processes, step by step conversion is implemented so as to achieve the requirements of different chemical production processes.
- Cascade utilization of both chemical and thermal energies: Heat produced in the chemical production can be utilized in power generation according to its energy level and at the same time a power subsystem can provide heat to the chemical production with a matching energy level
- Energy utilization and pollutant control: A major problem of the systems which create electricity or chemical fuels is the environmental pollution. Poly-generation systems can bring a solution to energy production and reduction of the environmental problems. The pollutants can be concentrated without extra energy consumption accompanied with products.

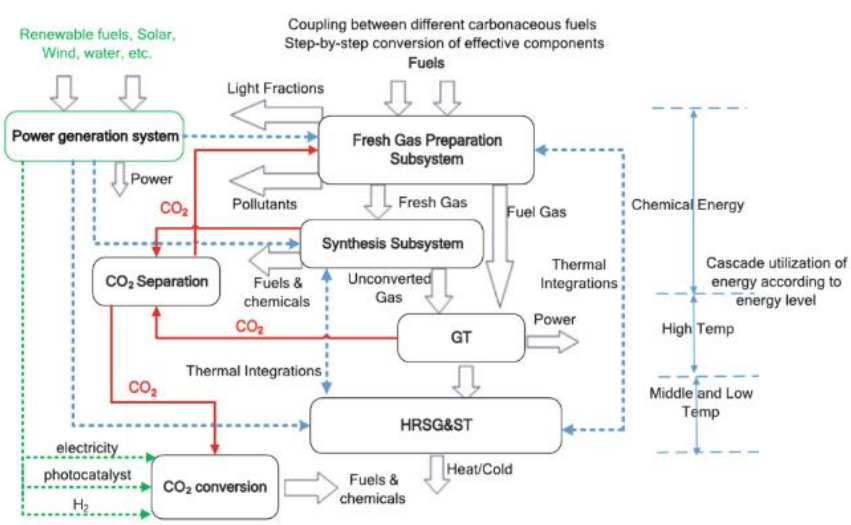

Fig. 1.12 Basic principles of a poly-generation system

In Fig. 1.12 is presented the primary function of the fresh gas preparation subsystem and the syngas which will not be converted can be used as fuel to power generation. more importantly, CO_2 can be recovered with less energy penalty from synthesis subsystem and flue gas. CO_2 can recycle from fresh gas preparation subsystem, from power generation and also can be converted by electricity, photocatalytic conversion and hydrogeneration reduction.

1.6.5 Utilization of CO_2 recycle in poly-generation systems

- CO_2 recycle as a gasifying agent at a coal-based poly-generation system
- In order to increase the carbon efficiency, CO_2 produced during the process as a gasifying agent into the gasifier can be reused, without increasing the level of C but keeping cycling from high to low [19].
- Because of the high temperature of the gasifier, we have the opportunity to increase the amount of CO so as to exploit the downstream chemical output. CO_2 recycling into the gasifier has great potential, but the key challenge is the control of the recycling ratio; too much recycling mass flow yields low gasification temperature reducing the efficiency and the chemical output.
- CO_2 as feedstock in poly-generation systems
- CO_2 is non-toxic and economic as a feedstock. One of the most important research is to replace the phosgene with CO_2 for synthesis of various chemicals. This conversion has provided huge potential on the CO_2 recycle and the coal reduction. The CO_2 which produced in chemical production and power plant can both serve as raw material to produce new fuels or chemicals.
- CO_2 recycle in multi-feedstock energy poly-generation system
- CO_2 produced from energy system can be converted in fuels by hydrogeneration, electrochemical and photochemical processes. These sources could be energy zero carbon footprint (solar, geothermal, wind etc.).if we could control the use of CO_2 recycle and the conversion technologies, the MFEPS will provide the opportunity to have higher efficiency lower investment and lower environmental impact [20].

1.6.6 Barriers for poly-generation systems with CO_2 recycle

- Costs of CO_2 capture, purification and transportation to user site
- Energy requirements of CO_2 chemical conversion
- Lack of industrial commitments for CO_2-based chemicals; because the technologies of CO_2 are in laboratory research and uncertainties exist. Especially energy poly-generation systems that integrate different sources and processes lack of design and operational experience

- Without supporting policies, the financial investment and the technological research is difficult to be understood

1.7 Scientific question

Considering the above, it is crucial to analyze the and assess the viability of medium scale CO_2 systems for power generation, mainly driven by the exhaust gases of gas turbines -to match the temperature levels of a supercritical CO_2 cycle. More specifically, the main scientific questions to be answered on this thesis are listed below:

- Which are the most common supercritical CO_2 configurations and how can be one such cycle further optimized?
- How can a supercritical CO_2 system be designed and which are the specific components required for this procedure?
- Which are the total costs for the development of the system and how competitive can it be based on the local electricity prices?

2. Components of the s-CO_2 Rankine cycle

2.1 Heat Exchanger

As heat exchanger (HX) is defined the component which facilitates ae heat transfer process. It is composed of two streams with different temperatures. In most applications, the two streams are kept separate (no mixing) to achieve the heat transfer.

2.1.1 Main characteristics of HX

I. Fluid allocation

One key categorization between the heat exchangers is in how the hot and the cold flow are flowing inside the tubes and annulus. When these flows have the same direction, the HX is called parallel; on the contrary is called counterflow (the hot flow and the cold flow have opposite direction). The temperature difference before the parallel heat exchanger is big allowing to be used in layouts with temperature flexible demands, as shown in Fig. 2.1.

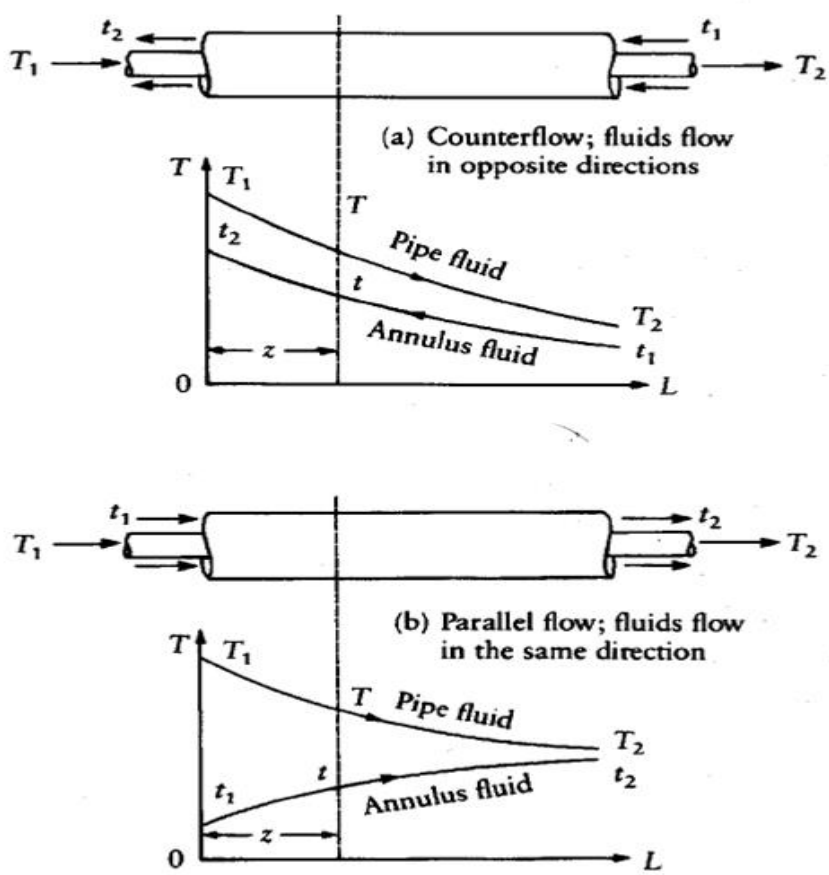

Fig. 2.1. Diagram of Temperature-length of counterflow and parallel flow HX

II. Compactness

The term of area density is the appropriate fraction between HX surface and volume to calculate how compact a heat exchanger is. When this fraction is above 700 then the HX can be called compact (car radiator is close to 1000).

III. Crossflow HX

The crossflow is composed of two perpendicular streams which can be either mixed (can move to the transfer direction because of the temperature gradient) or unmixed(can't move to the transfer direction), as shown in Fig. 2.2.

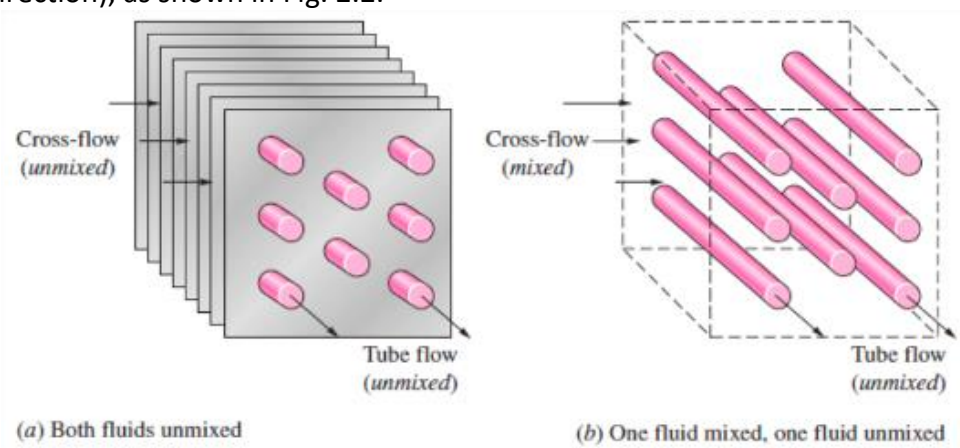

Fig. 2.2. (a) Unmixed and (b) mixed crossflow HX

2.1.2 Types of HX

Prior to the analysis of the shell and tube heat exchanger and the reasons why it is specifically selected, the other types of heat exchangers will be discussed. Heat exchangers can be classified based on three different categorizations, according to:

I. Nature of heat exchanger process

- Regenerative heat exchanger
- Direct contact heat exchanger
- Recuperator
- Condenser
- Boiler
- Evaporator

- Radiator

II. Flow arrangement

- Parallel flow
- Counter flow
- Cross flow

III. Geometry

- Shell and tube heat exchanger
- Plate heat exchanger
- Plate and fin heat exchanger
- Finned tube heat exchanger
- Plate and shell heat exchanger
- Tube-in-tube heat exchanger

2.1.3 Shell and tube heat exchanger

The most common HX with the most applications in industries (especially in industrial processes in scale of kWs or MWs) is the shell and tube HX. Due to its weight and large dimensions, it is not suitable for transport. Their most significant characteristic is that the combination of quality, efficiency and value is the best compared to all the above heat exchangers. It is a counterflow-like HX and the name shows that the main components is a shell and many tubes. Depending on the direction of the flow in the shell, the HX is called one-shell-pass, two-shell-passes HX etc. Furthermore, the addition of a baffle converts the counterflow HX to a crossflow resulting to an enhanced efficiency. If the flow is diverted by inserting a semicircular pattern in the end of the tube, the heat exchanger is called two-tube-pass or U-type shell and tube heat exchanger, as shown in Fig. 2.3.

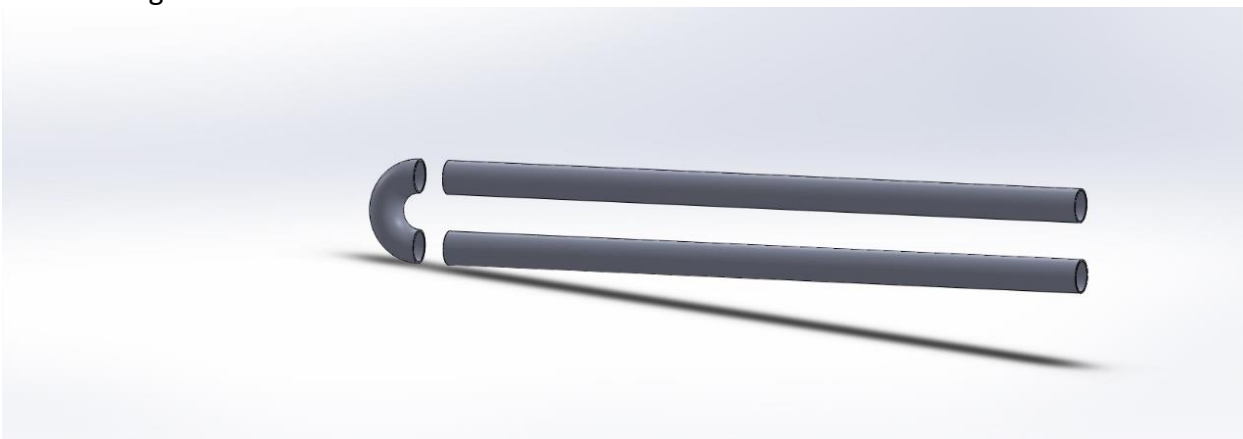

Fig. 2.3. Semicircular pattern in a U-type shell and tube heat exchanger

The tube sheet is a very important sub-component of this type of HX because their implementation holds the tubes in position and establish the pressure boundary for the shell fluid. Apart from the assistance that gives the baffle to the fluid to change direction, it also helps keeping the tubes in alignment. This turbulent flow increases the heat transfer capacity of HX.
In a comparison with the plate heat exchanger, the second most common HX in the industries, it is easier to find the advantages and disadvantages of the shell and tube heat exchanger.

Table 2.1. Advantages and disadvantages of shell and tube heat exchanger

Advantages	*Disadvantages*
Easy to maintain	Less efficient than the plate heat exchanger
Best fraction between price and efficiency	Requires more space
Higher pressures and temperatures	Can't vary cooling capacity
Lower pressure drops	
Easy to find leaks	

2.1.4 Gas cooler

A gas cooler is an essential component of any refrigeration cycle. It is a heat rejection unit and inside it the change of phase from gas to liquid takes place.
The most important requirement so as to harness the condensing ability, is to have an outdoor temperature lower than the condensation temperature. As a secondary fluid can be another substance or another refrigerant not necessarily the air. The required design characteristics are the same with the shell and tube heat exchanger.

2.1.5 Turbine

Turbine is a rotary mechanical device which extracts energy from a fluid flow so as to create useful work. A turbine is composed of a wheel and the blades (stator and rotor) which are attached to the wheel. The two main types of turbines are the *impulse* and the *reaction* turbines. In the impulse turbine, the pressure drop is significant. As the steam passes through the nozzles and the velocity is increased. when the flow goes though the rotor, the velocity is decreased but the pressure remains the same. This is the main principle which distinguishes impulse from a reaction turbine. The velocity profile through the fixed and the moving blades is the same with the impulse turbine (Fig. 2.4). On the other hand, the pressure drops as the stream flows from the entrance (stator) to the turbine until the exit (rotor) [21].

The differences between these two types are many, as listed in Table 2.2, but the main characteristic that plays the most important role for the selection is the control of the pressure and velocity, which is much easier in the impulse turbine. The geometry of the moving blades is the main problem not only for the high cost and maintenance but also to the turbulent flow of the steam [22].

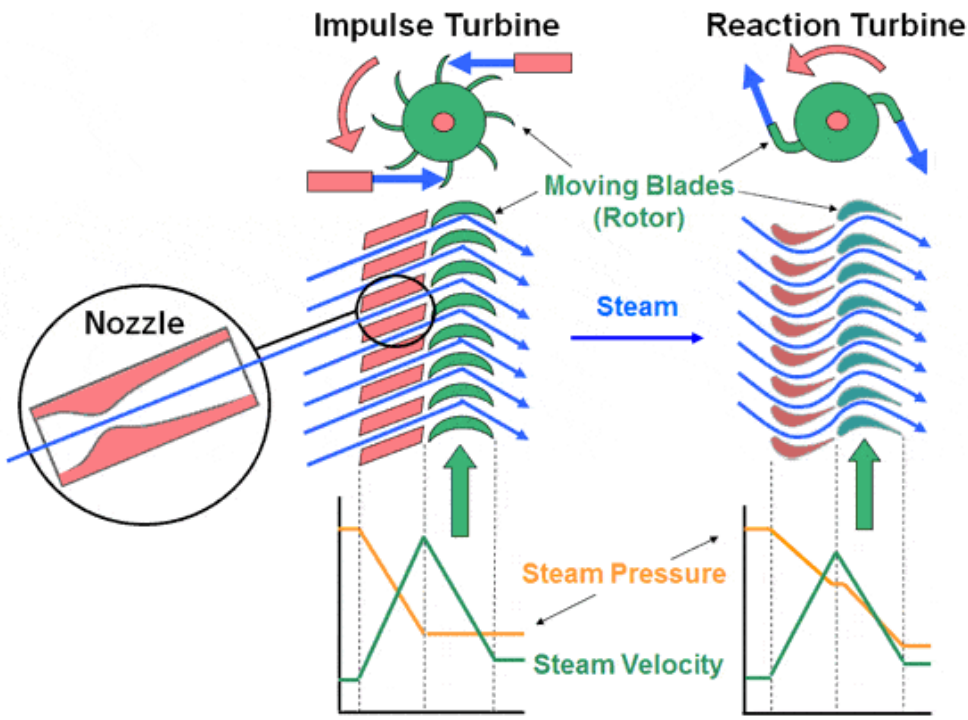

Fig. 2.4. Impulse and reaction turbine operation

Table 2.2. Difference between reaction and impulse turbine

Parameter	*Reaction turbine*	*Impulse turbine*
Maintenance	Not as easy as impulse	Easy
Efficiency	High	Low
Space requirement	High footprint	Very less size
Cost	Higher than impulse	Low

In order to design a specific turbine for the Rankine cycle, Zhou and Jang [23] tried to optimize the s-CO_2 cycle and conduct a radial inflow turbine using CFD simulation and tip clearance

analysis. Based on this research, the design parameters of the turbine are the same as Zhou's research, because the turbine is used for a similar s-CO_2 cycle.

Table 2.3. Basic parameters and their values for the turbine

Parameter	α_4	β_5	φ	ψ	x_α	Ω	μ
Range	14-17°	35-55°	0.90-0.97	0.8-0.9	0.6-0.7	0.4-0.55	0.35-0.5

where x_a is the velocity ratio,
Ω refers to the degree of reaction,
μ is the diameter ratio,
α_4 is the absolute flow angle of rotor inlet,
β_5 is the outlet relative flow angle of rotor,
ψ and φ are the velocity coefficient of the nozzle and the rotor, respectively.

2.1.6 Rotor

The number of rotor blades is estimated using Glassman empirical correlation [24]:

$$Z_R = \frac{\pi}{30}(110 - a_4)\, tan\, a_4 \tag{2.1}$$

Radius and blade thickness at rotor inlet and outlet are given by:

$$\mathrm{r}_4 = \frac{60}{2\pi N} u_4 \tag{2.2}$$

$$r_5 = \mu\, r_4 \tag{2.3}$$

$$t_4 = 0.03\, r_4 \tag{2.4}$$

$$t_5 = 0.02\, r_4 \tag{2.5}$$

The blade heights at the inlet and outlet of the rotor can be expressed as:

$$b_4 = \frac{A_4}{2_{\pi r_4} - z_r t_4} \tag{2.6}$$

$$b_5 = \frac{A_5}{2_{\pi r_5} - z_r t_5} \tag{2.7}$$

The blade surface area is given by the equation [24]:

$$A = [(r_{1a} - r_{2t} + h_s)(r_{1a} - r_{2h}) - (r_{1a} - r_{2t})^2]\frac{\pi}{2} \tag{2.8}$$

The tip and hub wall areas are determined as the surfaces of revolution of the tip and hub curves around the turbine axis.
The rotor outlet radius at hub and shroud can be given as

$$r_{5h} = r_5 - 0{,}5b_5 \tag{2.9}$$

$$r_{5s} = r_5 + 0{,}5b_5 \tag{2.10}$$

The axial length can be then defined as:

$$l_a = 1{,}5(r_{5s} - r_{5h}) \tag{2.11}$$

2.1.7 Stator

It is obvious that the geometry of the nozzle is directly linked with the geometry of the rotor. The nozzle outlet height is assumed to be equal with the blade inlet height.

$$b_3 = b_4 \tag{2.12}$$

The chord length and the relative span of nozzle can be obtained by:

$$\bar{t_n} = \frac{t_n}{l} \tag{2.13}$$

$$l = \frac{\pi\, d_4}{z_n \bar{t_n}} \tag{2.14}$$

The nozzle inlet radius and the nozzle outlet radius can be given by

$$r_2 = \sqrt{r_4^2 + (al)^2 + 2alr_4 \sin a_4} \tag{2.15}$$

$$r_3 = r_4 + 2b_4 \sin a_4 \tag{2.16}$$

3. Thermodynamic analysis of the layout

In this chapter, will be discussed the thermodynamic modeling of the selected simple s-CO_2 layout for WHR with a single recuperator, as shown in Fig. 3.1.

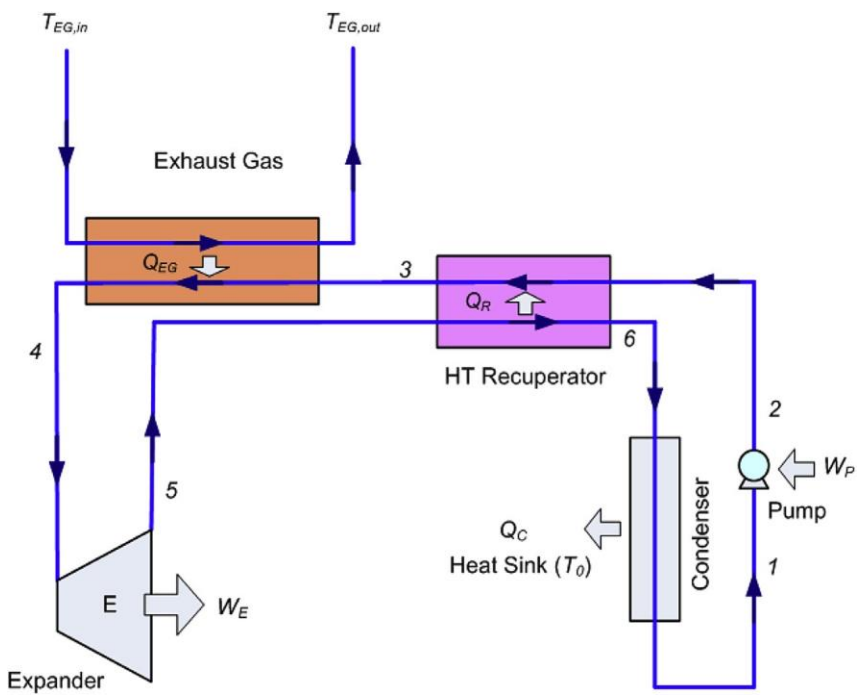

Fig. 3.1. Schematic of the simple s-CO_2 layout for WHR to be investigated

3.1 Assumptions

At first, below are presented the assumptions made in order to conduct the energetic analysis.

- The kinetic and potential energies of the flow, as well as the heat and friction losses were assumed to be negligible.
- Ambient temperature was set at 15°C.
- The pressure drop in the heat exchangers (heater, recuperator and gas cooler) is considered 1 bar (Δp_{heat})
- The temperature in state **(4)** is investigated within the range of 450-750 °C [25]
- With respect to the isentropic efficiencies, the following values were considered:
- Pump: 0.80
- Turbine: 0.90

- Turbine pressure ratio is being investigated at the range of 4 to 12 [26, 27]
- The exit of the gas cooler is at supercritical state.
- Lower pressure of the supercritical cycle is set at least higher than the critical pressure.(state 1)
- The third alternating parameter is a temperature that called T_{test} which is the diferrence between T_{crit} and T_1 (how much above the T_{crit} is the lowest temperature of the cycle)
- Pinch point on recuperator is equal to 10 ^oC
- Mechanical efficiencies:
  i. Turbine:0.95
  ii. Spindle:0.98
- Recuperator effectiveness: 0.95

At this point it has to be mentioned that the fluid properties calculations were conducted using Coolprop library.

3.2 Thermodynamic model of cycle

The equations used for the pressure calculations of the cycle are listed below:

$$p_6 = p_1 + \Delta p_{hex} \tag{3.1}$$

$$p_5 = p_6 + \Delta p_{hex} \tag{3.2}$$

$$p_4 = p_5 \cdot Pr_{ratio,th} \tag{3.3}$$

$$p_3 = p_4 + \Delta p_{hex} \tag{3.4}$$

$$p_2 = p_3 + \Delta p_{hex} \tag{3.5}$$

At the initial scenario for the p_1 (the low pressure of the cycle) it was selected to be equal to the critical one, thus p_1=73.7 bar and the test temperature is also set at 0, thus equal to the critical temperature of 31.0 ^oC.
Using the equations (3.1)-(3.5) the pressure at all states can be determined. The isentropic efficiency of the pump can be determined as follows:

$$\eta_p = \frac{h_{2,is} - h_1}{h_2 - h_1} \tag{3.6}$$

In this way, the enthalpy of state 2 can be determined and with the already determined pressure, all thermodynamic properties at state 2 are estimated.

$$\eta_p = \frac{h_{2,is} - h_1}{h_2 - h_1} \tag{3.7}$$

Within the optimization solver, T4 is an independent variable, therefore guess temperatures are set in the solver and therefore on each execution of the code pressure and temperature of state 4 are easily determined, along with enthalpy and entropy via Coolprop.
In a similar way to the pump, the enthalpy at the discharge of the turbine (state 5) can be determined by the definition of the turbine's isentropic efficiency:

$$\eta_T = \frac{h_4 - h_5}{h_{4,is} - h_5} \tag{3.8}$$

Consequently, the temperature and the entropy can be also determined by Coolprop. Given the predefined pinch point at the recuperator, the temperature at state 6 will be equal to:

$$T_6 = T_2 + \Delta T_{pinch} \tag{3.9}$$

Once the temperature at state 6 is determined and given that the pressure is already estimated, enthalpy and entropy can also be determined via Coolprop.
Finally, state 3 can be determined by applying an energy balance in the recuperator.

$$\dot{Q}_{rec} = \dot{m}_{CO_2}(h_5 - h_6) = \dot{m}_{CO_2}(h_3 - h_2) \tag{3.10}$$

Given the known pressure and enthalpy by (3.10) at state 3, the rest thermodynamic properties can be also determined.

3.2.1 Performance indicators

For the specification of the heater's duty, the equation derived from the energy balance is the following [28]:

$$\dot{Q}_{heater} = \dot{m}_g\left(h_{g,in} - h_{g,out}\right) = \dot{m}_{CO_2}(h_4 - h_3) \tag{3.11}$$

On the other hand, the thermal power at the turbine is given by:

$$W_{th,turb} = \dot{m}_{CO_2}(h_4 - h_5) \tag{3.12}$$

Consequently, the electrical production of the turbine is equal to:

$$W_{el,turb} = W_{th,turb}\, \eta_{mech}\eta_{gen} \tag{3.13}$$

With the mechanical efficiency to be equal to 98% and the generator efficiency to be equal to 95%.
The pump consumption is equal to:

$$W_{pump} = \frac{\dot{m}_{CO_2}(h_2 - h_1)}{\eta_m} \tag{3.14}$$

With the motor efficiency to be equal to 95%.
Eventually, the net power output is equal to:

$$W_{net} = W_{el,turb} - W_{pump} \tag{3.15}$$

The heat rejection at the gas cooler is equal to:

$$\dot{Q}_{cond} = \dot{m}_{CO_2}(h_6 - h_1) \tag{3.16}$$

Hence, the thermal efficiency of the cycle is equal to:

$$n_{th} = \frac{W_{net}}{\dot{Q}_{heater}} \tag{3.17}$$

On the other hand, the exergy efficiency is equal to:

$$n_{ex} = \frac{W_{net}}{Ex_H} \tag{3.18}$$

With,

$$Ex_H = \dot{m}_{CO2}\left[(h_4 - h_3) - T_{ref}(s_4 - s_3)\right] \tag{3.19}$$

Eventually, the results for the base case can be found below in Table 3.1.

Table 3.1. Thermodynamical properties of the s-CO_2 cycle

State	*1*	*2*	*3*	*4*	*5*	*6*
Density (kg/m³)	534.03	727.46	213.24	146.15	47.46	133.09
Pressure (bar)	73.8	305.2	304.2	303.2	75.8	74.8
Temperature (⁰C)	31.0	85.7	451.7	750	563.3	95.7
Enthalpy (kJ/kg)	317.91	361.29	904.13	1284.3	1060.9	518.7
Entropy (kJ/kgK)	1.386	1.410	2.489	2.929	2.959	2.010

Table 3.2. Performance results of the s-CO_2 cycle

Performance indicator	*Value*
$\dot{Q}_{heater}$ (kW)	950.5
$W_{th,turb}$ (kW)	558.2
W_{pump} (kW)	114.8
W_{net} (kW)	405.9
$\dot{Q}_{cond}$ (kW)	500.3
n_{th} (%)	42.71
n_{ex} (%)	65.18
Ex_H (kW)	453.5

3.3 Sensitivity analysis

In the following section, a sensitivity analysis is conducted to identify the key parameters that influence the performance of the s-CO_2 cycle.

3.3.1 Influence of turbine inlet temperature

The two figures below, show the influence of two parameters (Ttest,T_4) on the thermal efficiency, η_{th}. At first, it is important to mention that the further the temperature rises higher than the T_{crit}, the smaller the thermal efficiency is calculated. The reason for this result is that the temperature in state 1 has significant role in the net output of the pump. On the opposite, as the turbine inlet temperature increases, consequently the enthalpy in state 4 becomes higher and hence the turbine power output as well as the efficiency tends to increase. The acceptable level for the thermal efficiency is when the difference from the critical temperature is near 20°C. The same cross-evaluation of the above parameters is noticed with the exergy efficiency (Figures 3.4-3.5). The results are similar, as the heat has the same effect to the thermal and to the exergy efficiency. Again, the CO_2 stream at a supercritical state has to be at least 20° C above the T_{crit} in order to achieve a requisite number of exergy.

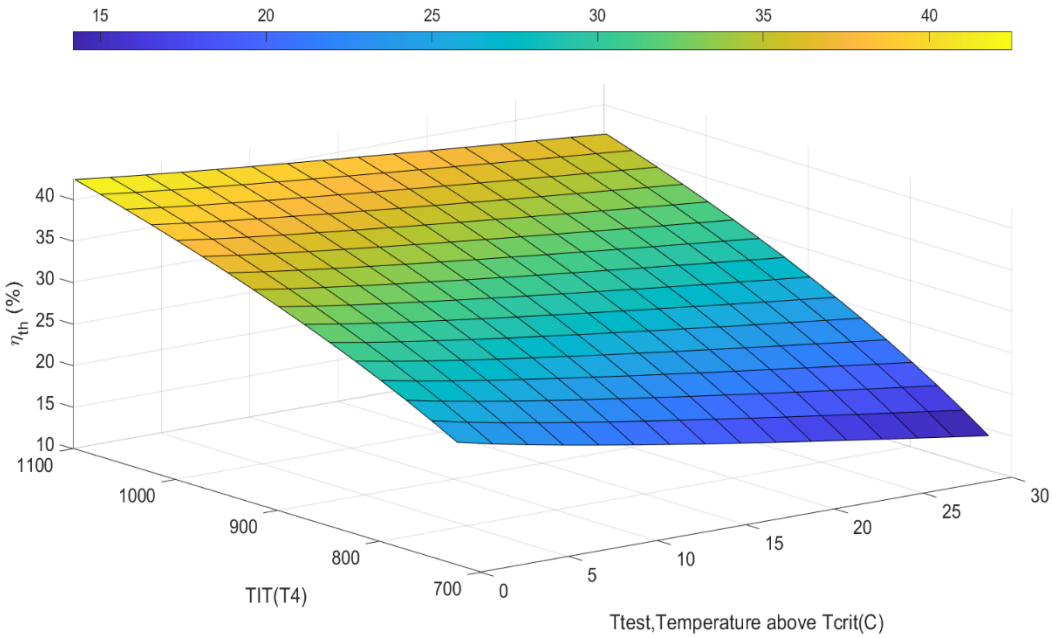

Fig. 3.2. 3D plot of thermal efficiency(z),Temperature above Tcrit(x) and TIT(y)

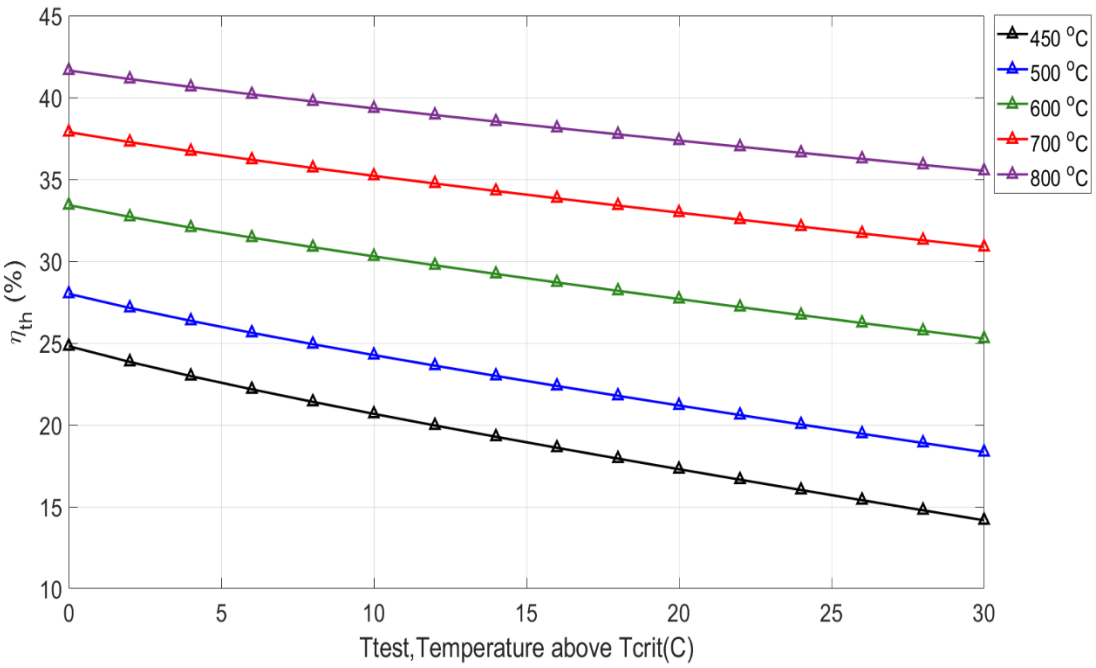

Fig. 3.3. 2D plot of thermal efficiency(x), Temperature above Tcrit(y), TIT(legend)

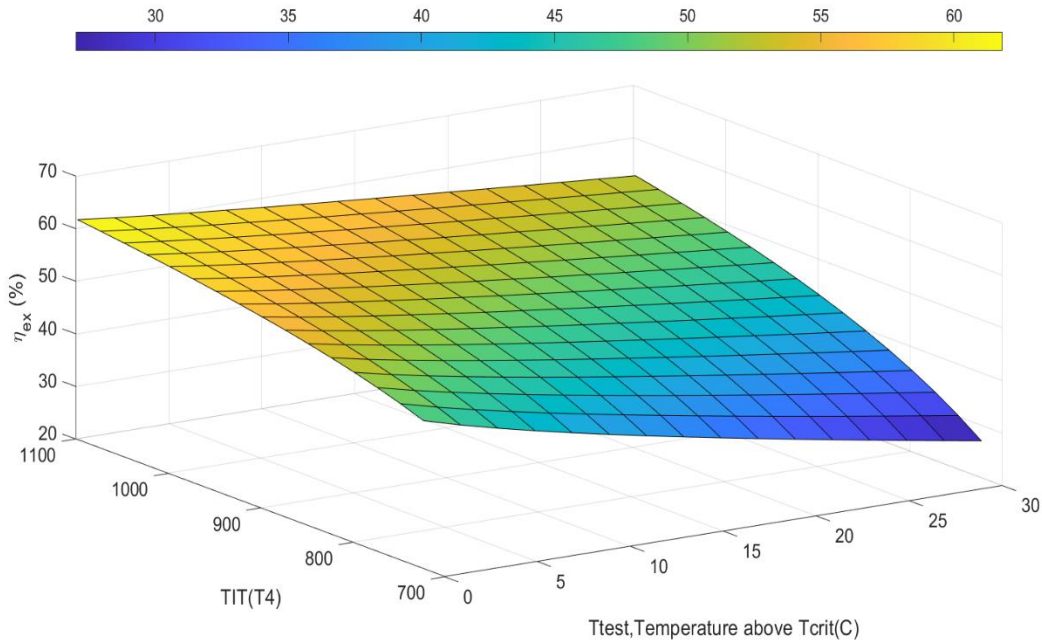

Fig. 3.4. 3D plot of exergy efficiency(z),Temperature above Tcrit(x),TIT(y)

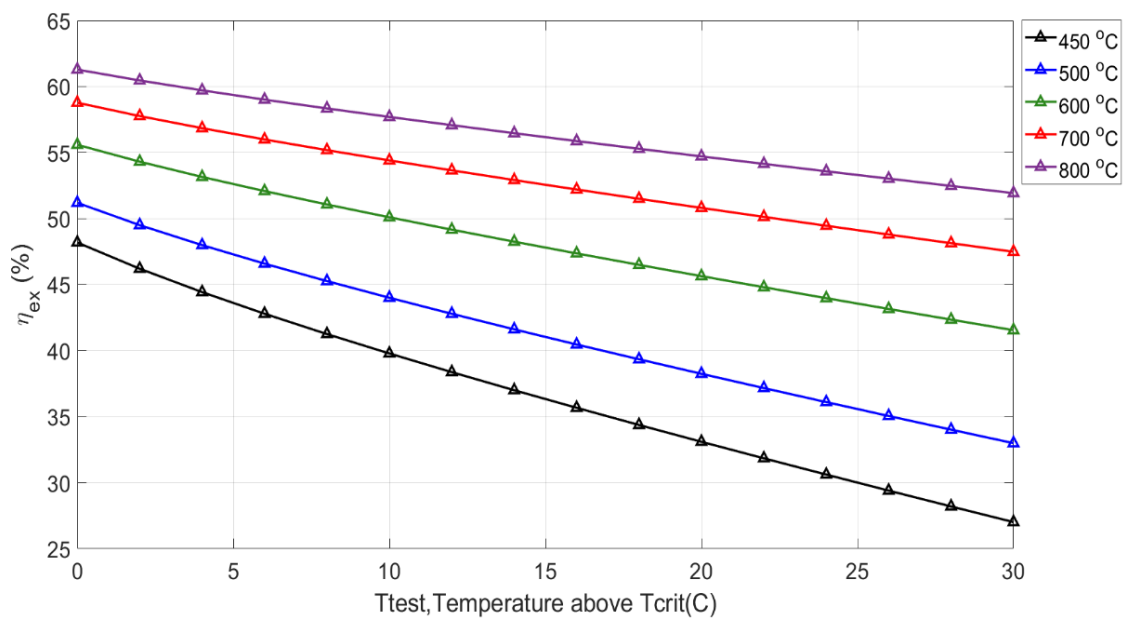

Fig. 3.5. 2D plot of exergy efficiency(z),Temperature above Tcrit(x),TIT(y)

3.3.2 Influence of pressure ratio

The most significant role towards the maximization of the thermal efficiency in a s-CO_2 cycle with a recuperator is the pressure ratio of the expander. Regardless of the turbine inlet temperature, when the pressure ratio is ranged from 4-6, the result is sharply enhancing the overall efficiency. If the TIT is additionally increased, the more heat which is produced, the more thermal efficiency is achieved. Fig. 3.6 shows that beyond a value of the PR of the expander, in combination with the turbine inlet temperature, the efficiency is negative and the layout is no more technically feasible. The reason is that the net output of the turbine is smaller than the pump, mainly because of the big difference between the two pressures (P_4 ,P_5), the decompression is enormous.

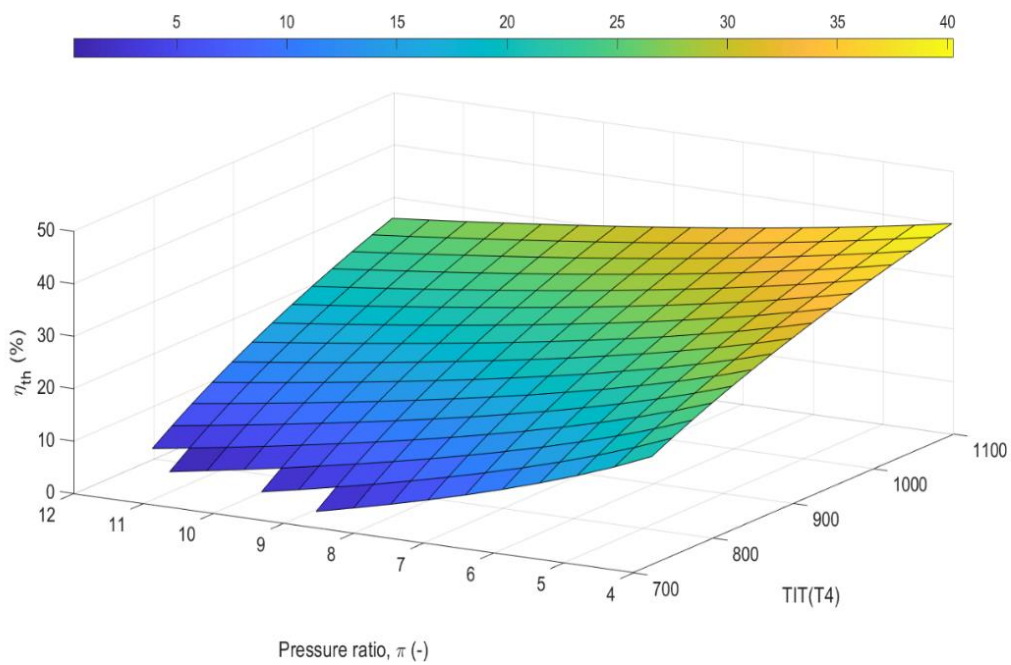

Fig. 3.6. 3D plot of thermal efficiency(z),pressiure ratio of expander(y),TIT(x)

Fig. 3.8 shows the connection between the exergy efficiency, the pressure ratio and the TIT. The diagram is similar with the thermal efficiency. The most significant role is the state before and after the heater. When the pressure ratio is small the net output of the expander is big so the fraction of exergy efficiency is getting bigger.

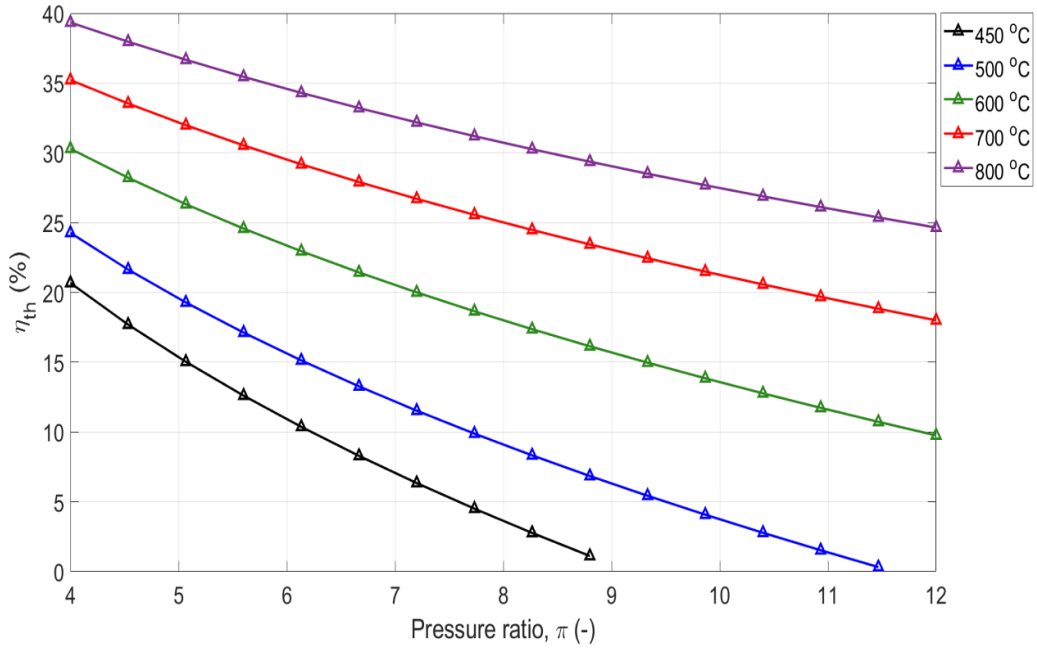

Fig. 3.7. 2D plot of thermal efficiency(x),pressure ratio of the expander(y),TIT(legend)

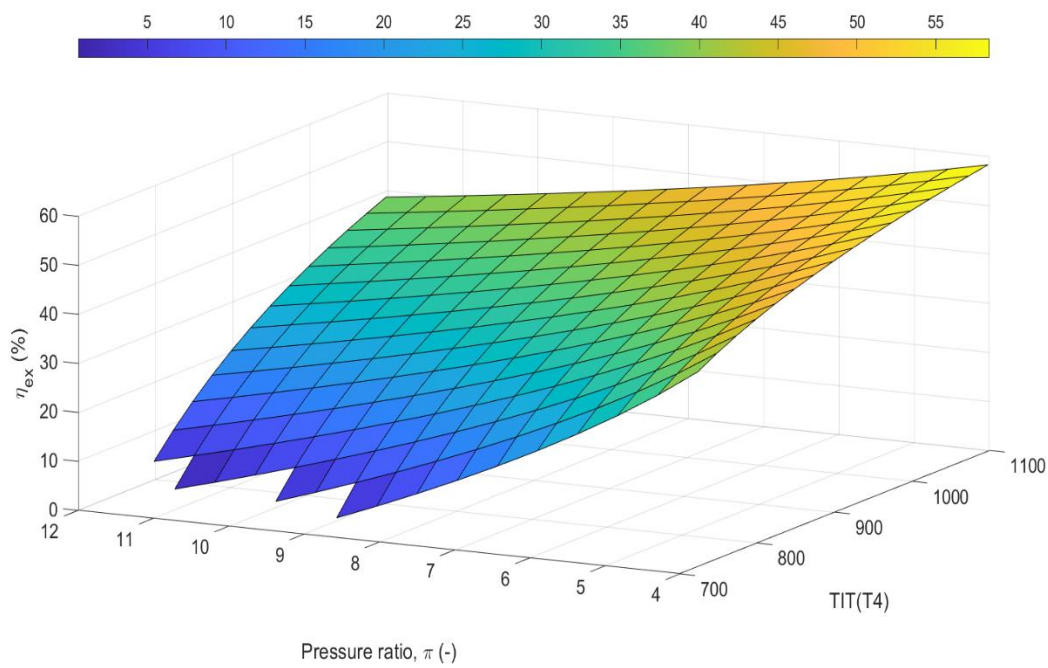

Fig. 3.8. 3D plot of exergy efficiency(z),pressure ratio of expander(y),TIT(x)

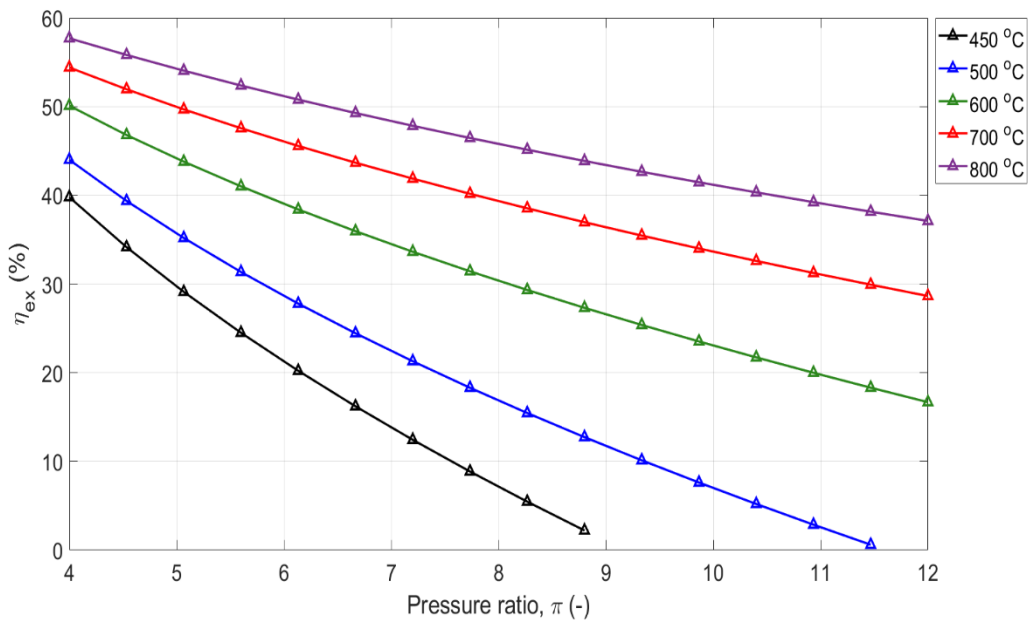

Fig. 3.9. 2D plot of exergy efficiency(z),pressure ratio of expander(y),TIT(x)

3.3.3 Influence of cycle's high pressure

Fig. 3.10 shows the effect of the upper pressure of the cycle (p_2) to the thermal efficiency. As expected, the increase of the upper pressure results in the increase of the $W_{th,turb}$ and consequently the W_{net}. As it is referred above, the boost of the turbine inlet temperature has as an outcome the production of heat and the net output rise. The 10 bar expansion makes a small difference to the thermal efficiency comparing with the 50 °C augmentation of the TIT.

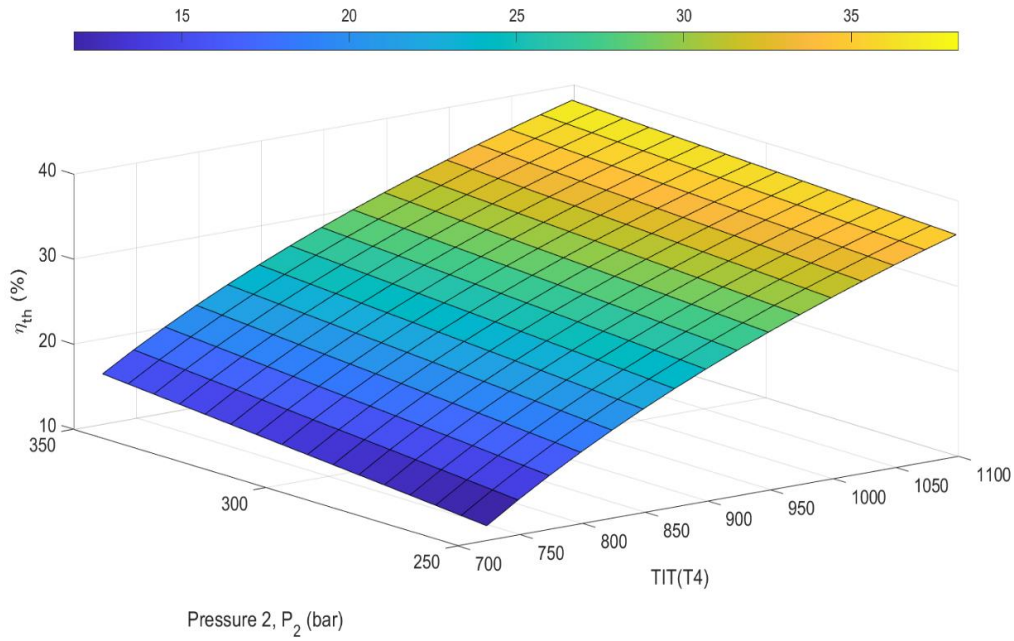

Fig. 3.10. 3D plot of thermal efficiency(z),upper pressure P_2 (y),TIT(x)

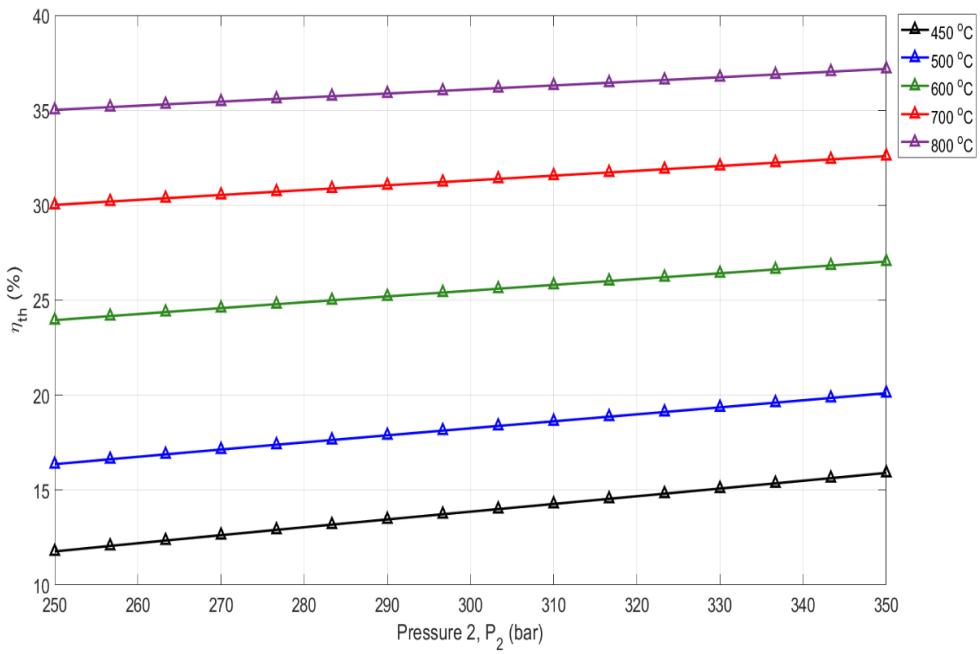

Fig. 3.11. 2D plot of thermal efficiency(x),upper pressure P_2 (y),TIT(legend)

Fig. 3.12 illustrates the same result with the thermal efficiencies. The exergy efficiency has a similar dependence in the two parameters(P_2,T_4) as the thermal efficiency, as the heat input is directly affected by P_2.

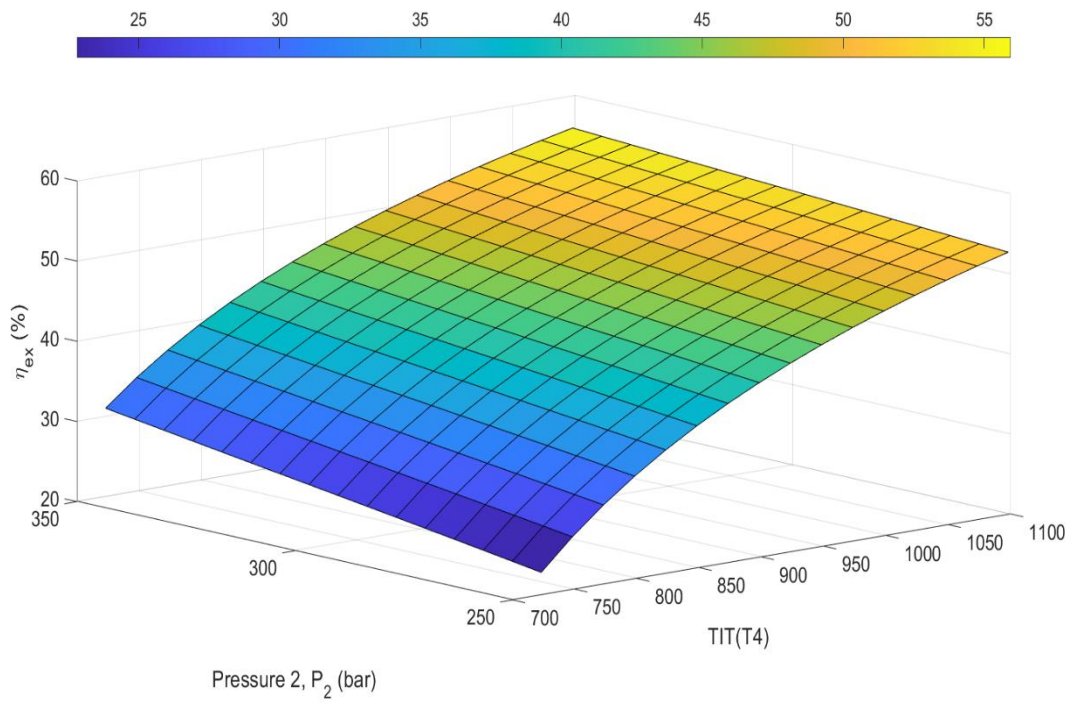

Fig. 3.12. 3D plot of exergy efficiency(z),upper pressure P_2 (y),TIT(x)

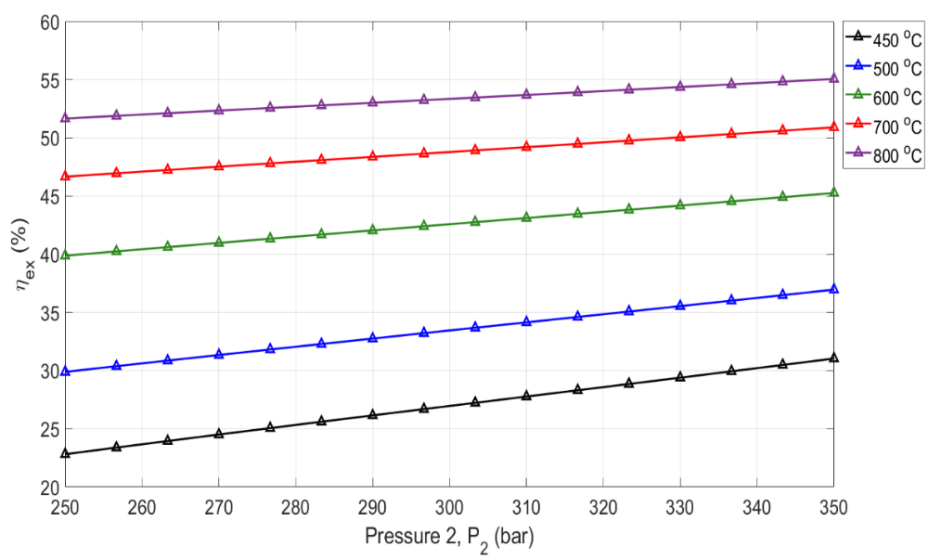

Fig. 3.13. 2D plot of exergy efficiency(z),upper pressure P_2 (y),TIT(x)

3.4 Influence of turbine inlet temperature without recuperation

In this scenario is investigated the influence of the TIT at the absence of a recuperator. Fig. 3.14 and 3.15 show the same results with Fig. 3.2 and 3.3 but the layout doesn't include a recuperator. The curves are similar and the effect of the parameters to the thermal efficiency is the same as it is analyzed before. The main difference is the maximum value of the efficiency is much lower than the maximum with recuperation, as the heat load at the heater is directly affected by the heat recovery.

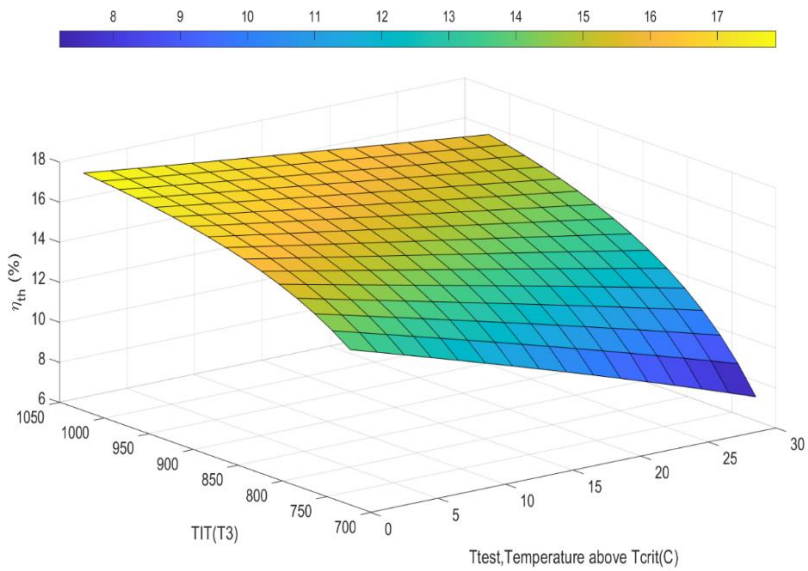

Fig. 3.14. [without HX] 3D plot of thermal efficiency(z),Temperature above Tcrit (x),TIT(y)

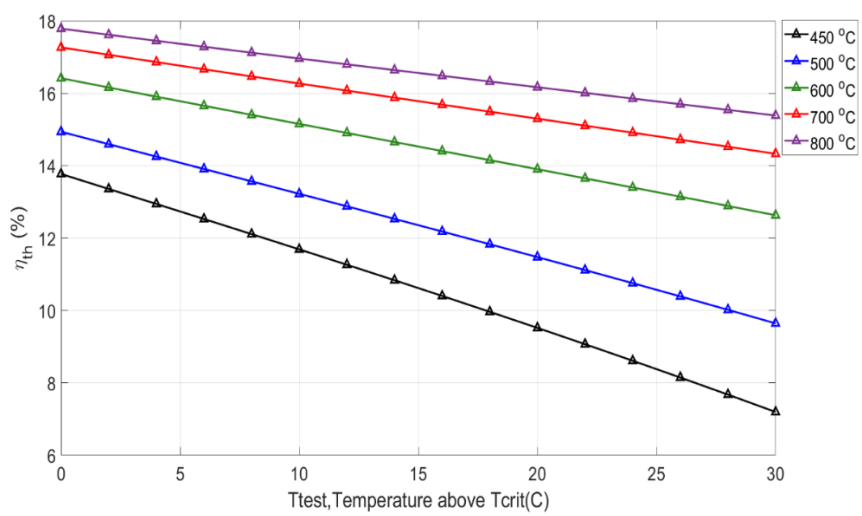

Fig. 3.15. [without HX] 2D plot of thermal efficiency(x),Temperature above Tcrit (y),TIT(legend)

The relation between turbine inlet temperature and temperature above the critical temperature is much like with or without heat exchanger. The behavior is similar in both cases as the dependence of the cycle's pressures and thus the available enthalpy change in the turbine is independent of the recuperation. Therefore, apart from the decreased results due to the increased heat load of the heater, the profiles are comparable in Fig. 3.16-3.17 with the ones in Fig. 3.4-3.5.

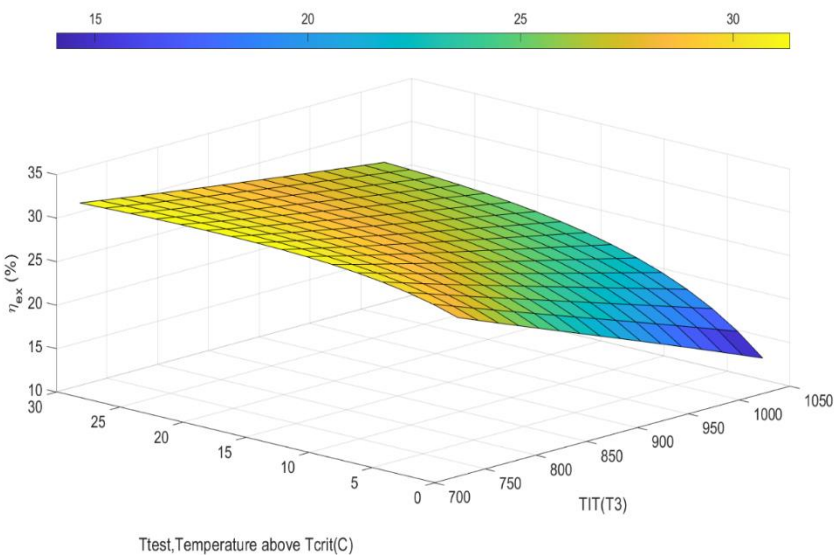

Fig. 3.16. [without HX] 3D plot of exergy efficiency(z),Temperature above Tcrit (y),TIT(x)

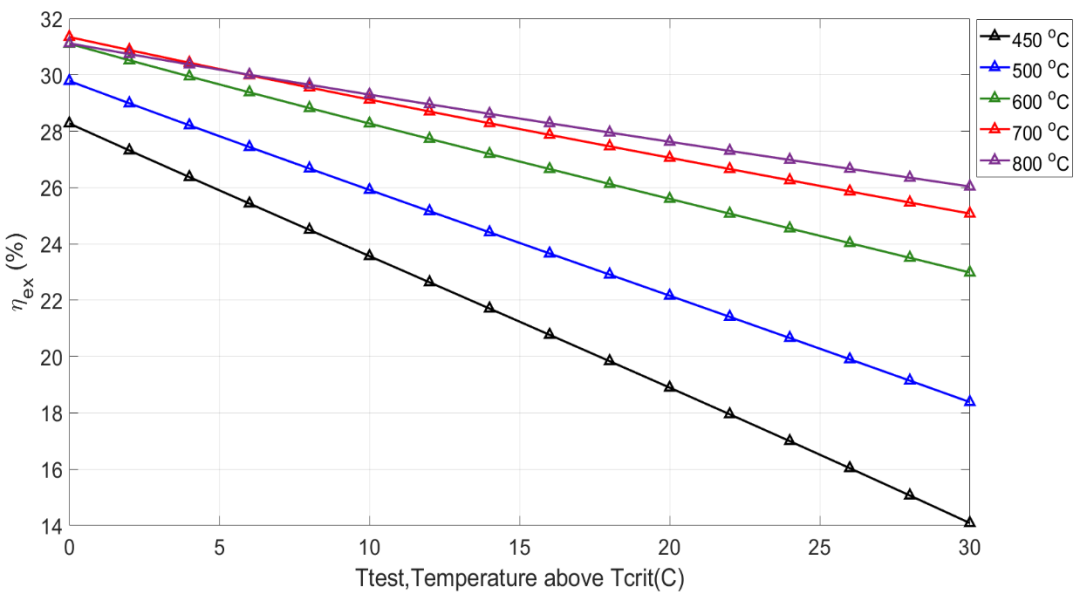

Fig. 3.17. [without HX] 2D plot of exergy efficiency(z),Temperature above Tcrit (y),TIT(x)

The 3D representation (Fig. 3.18) and 2D (Fig. 3.19) of pressure ratio, thermal efficiency and TIT without recuperation show a different image compared to Fig. 3.6-3.7. When the TIT is very low, the curve is similar with the curve of the recuperator layout; however, as the TIT increases, the curve's inclination decreases. This happens because on higher temperatures the heater's duty increases sharply and for lower pressure ratio tends to counterbalance the benefits by the increased power output.

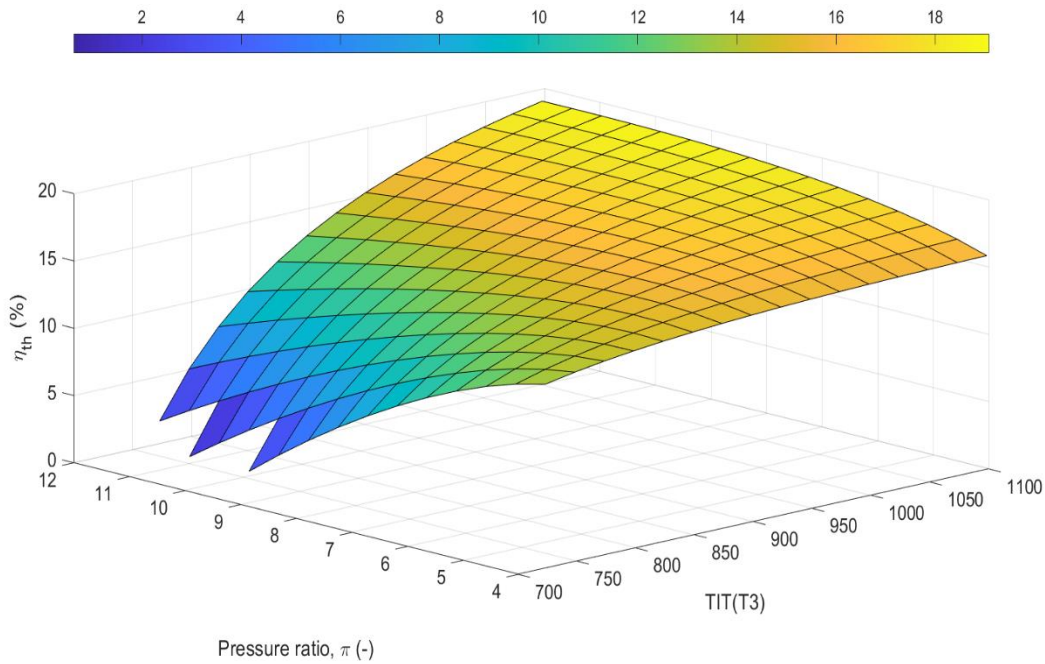

Fig. 3.18. [without HX] 3D plot of thermal efficiency(z),pressure ratio of the expander(y),TIT(x)

The same linear change of the curves is visible in Fig. 3.20-3.21. The exergy efficiency is higher than the previous analysis with temperature above Tcrit, but in comparison with Fig. 3.12 the optimal value has significant difference. The separate rise of the TIT or the small number of PR does not play significant role in the cycle; however, the simultaneous change of both provides the maximum exergy value (pressure ratio:8, TIT:800 ^{o}C).

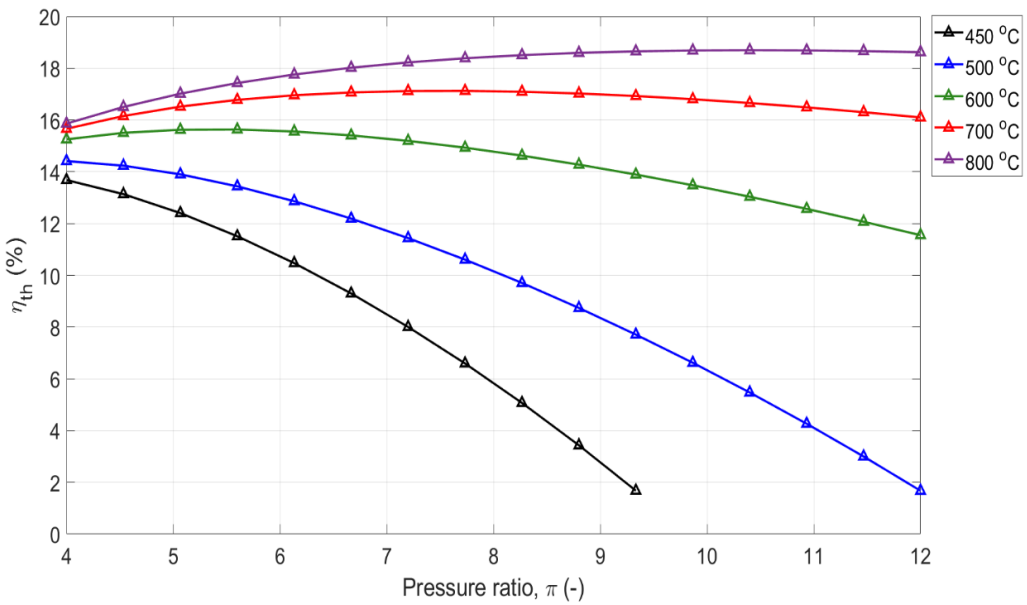

Fig. 3.19. [without HX] 2D plot of thermal efficiency(x),Pressure ratio of the expander (y),TIT(legend)

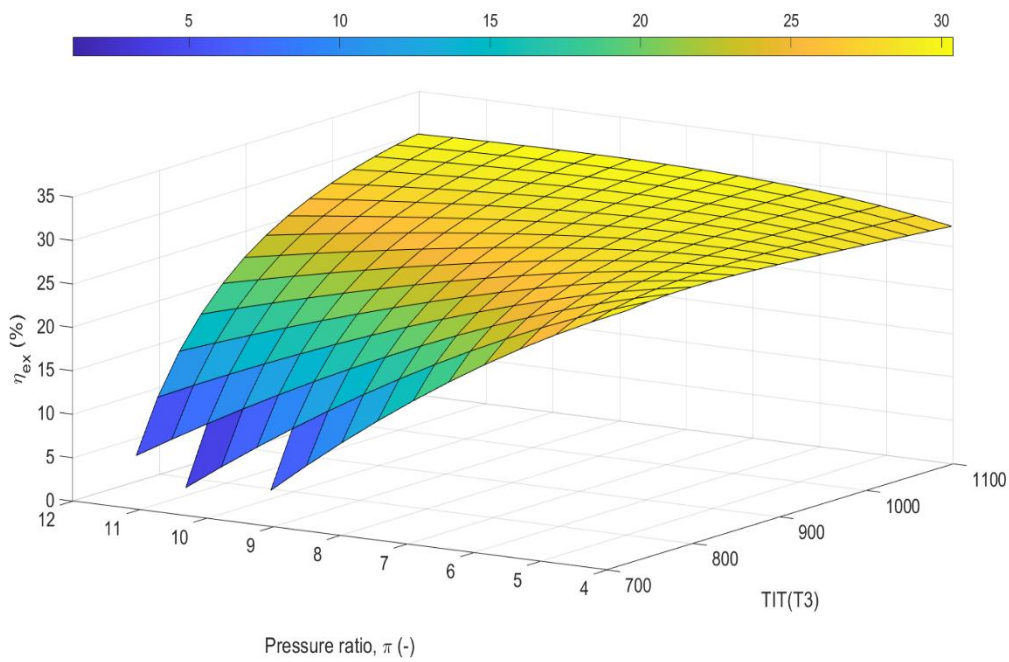

Fig. 3.20. [without HX] 3D plot of exergy efficiency(z),pressure ratio of the expander(y),TIT(x)

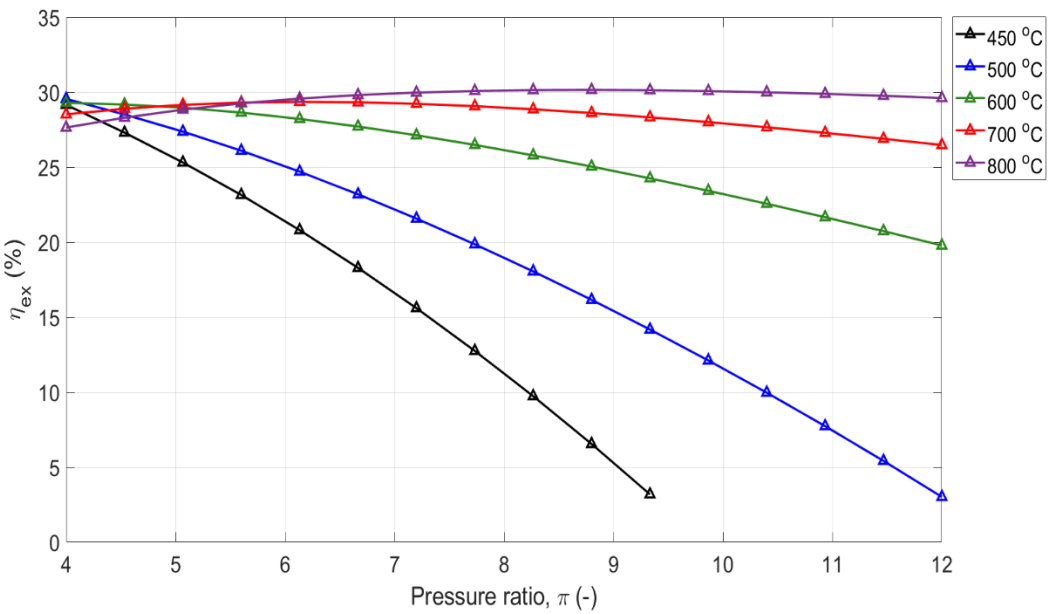

Fig. 3.21. [without HX] 2D plot of exergy efficiency(z),pressure ratio of the expander(y),TIT(x)

Fig. 3.22-3.23 show the dependence of thermal efficiency with the combination of the TIT and the upper pressure of the layout. This figure has the same effect as Fig. 3.10 with obviously smaller thermal efficiency. However, the significant observation is that after a big value of TIT the curve turns to be linear for every value of pressure as again the increase in the heater's duty neglects any increase in the turbine's power production.

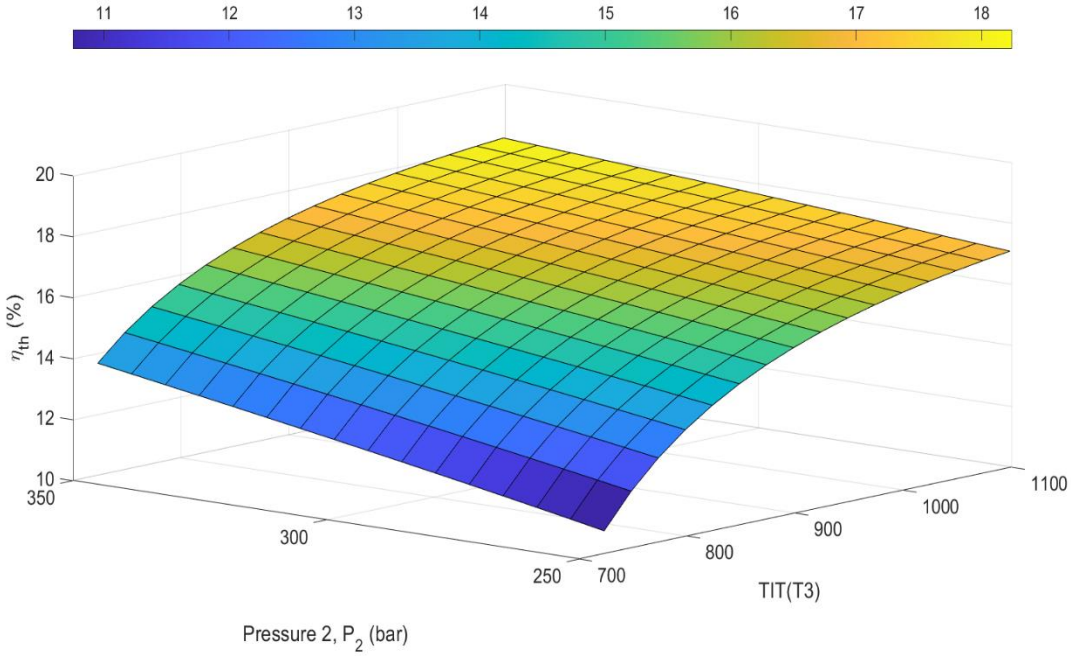

Fig. 3.22. [without HX] 3D plot of thermal efficiency(z), upper pressure P_2 (y),TIT(x)

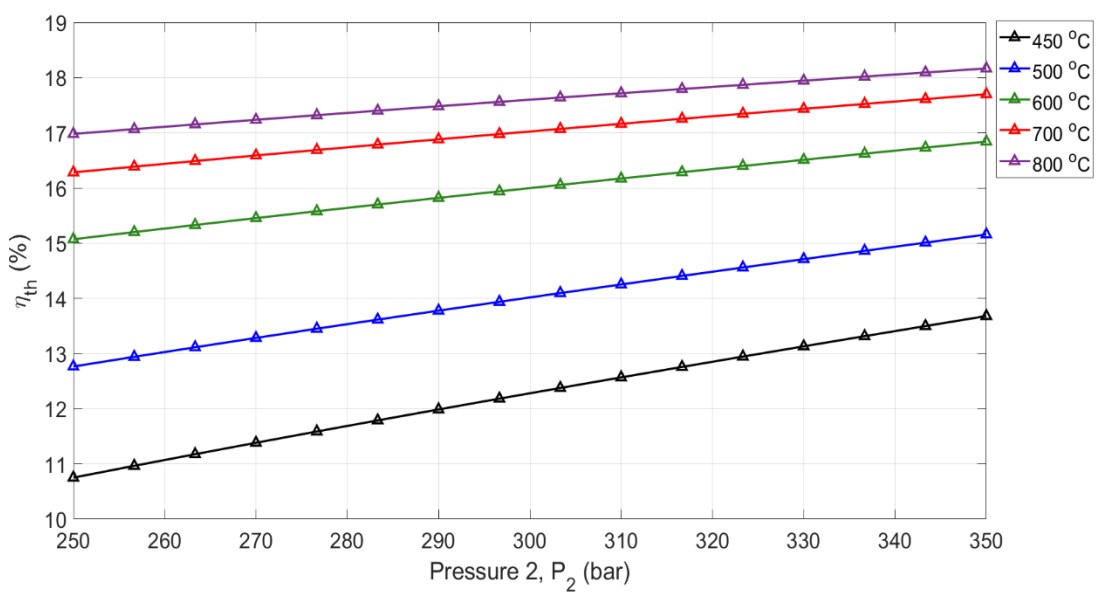

Fig. 3.23. [without HX] 2D plot of thermal efficiency(x),upper pressure P_2 (y),TIT(legend)

Fig. 3.24 shows the exergy efficiency result for different values of TIT and upper pressure. The shape is similar with the shape of the Fig. 3.12 but with smaller maximum values. It was noticed for the exergy efficiency without recuperator, after a certain value of turbine inlet temperature

(700°C), that the rise of this ignition temperature has no more benefits to provide, mainly due to the limitation of the high pressure which limits as a result the enthalpy increase at the suction of the turbine.

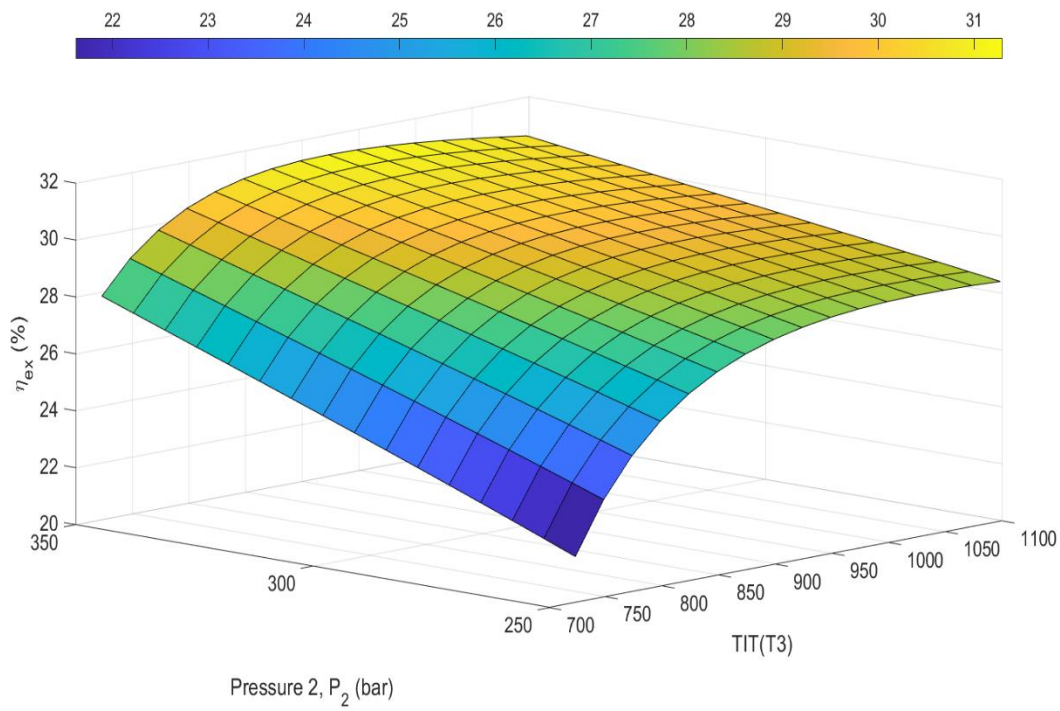

Fig. 3.24. [without HX] 3D plot of exergy efficiency(z), upper pressure P_2 (y),TIT(x)

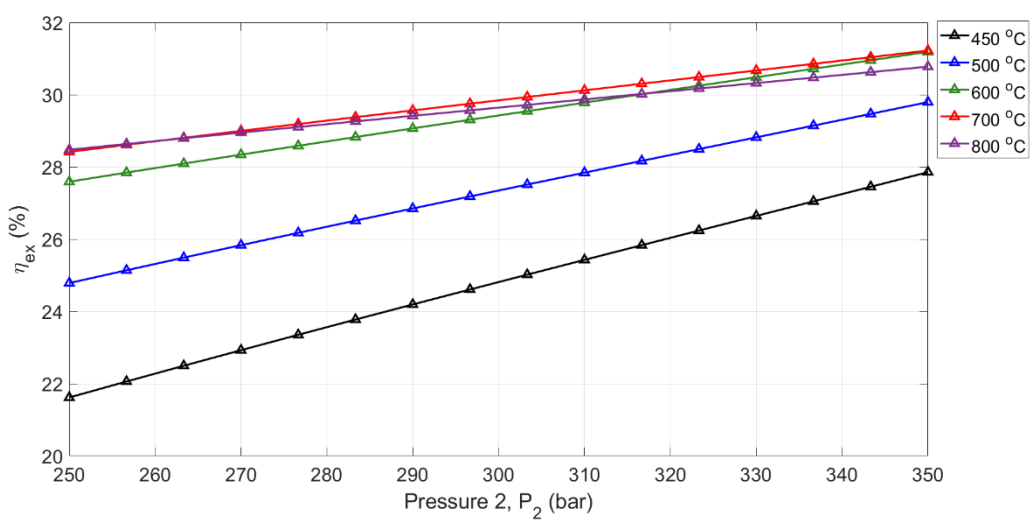

Fig. 3.25. [without HX] 2D plot of exergy efficiency(z), upper pressure P_2 (y),TIT(x)

4. Design, 3D depiction and specifications of each component

4.1 Heat exchangers: Recuperator

The recuperator is a shell and tube heat exchanger and more specifically a one-shell pass and two-tube passes shell and tube heat exchanger. Based on the results from MATLAB, which were occurred from the assumptions that were made in the previous section, the main dimensions for the suitable recuperator are listed in Table 4.1:

Table 4.1. Dimensions of recuperator

number of shell passes (-)	1
number of tube passes (-)	2
shell external diameter (mm)	626.8
shell internal diameter (mm)	601.5
bundle diameter (mm)	587.2
baffle diameter (mm)	586.3
baffle spacing (mm)	326.0
baffle cut percentage (%)	25
number of baffles (-)	8
square pitch arrangement with tube pitch (mm)	23
tube external diameter (mm)	18
number of tubes (-)	471
length of tubes (m)	7
Shell side fluid inlet diameter (mm)	90
Shell side fluid outlet diameter (mm)	76.2
overall heat transfer coefficient ($W/m^{2}{}^{0}C$)	351.3218

Fig.4.1 and Fig.4.2 explain some of the dimensions for a better understanding of the recuperator's geometry.

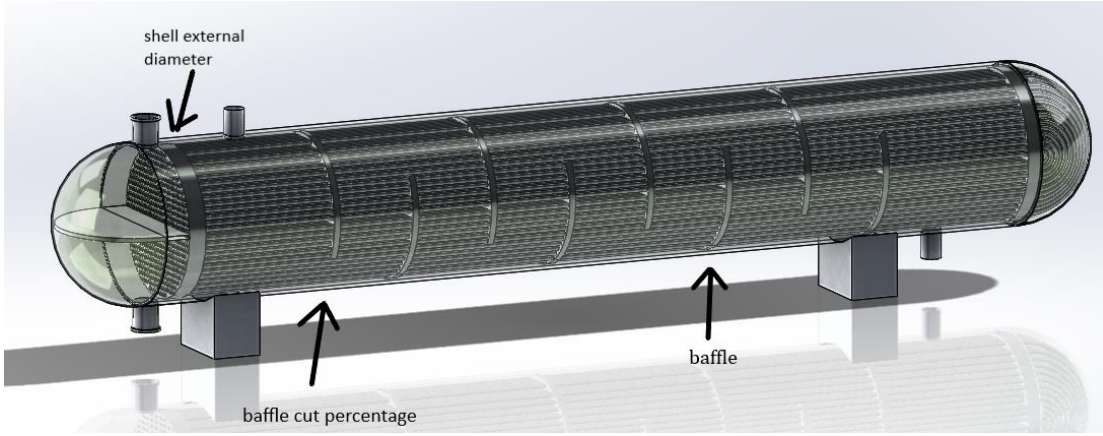

Fig. 4.1. realistic view of the internal of the shell of the recuperator at SOLIDWORKS

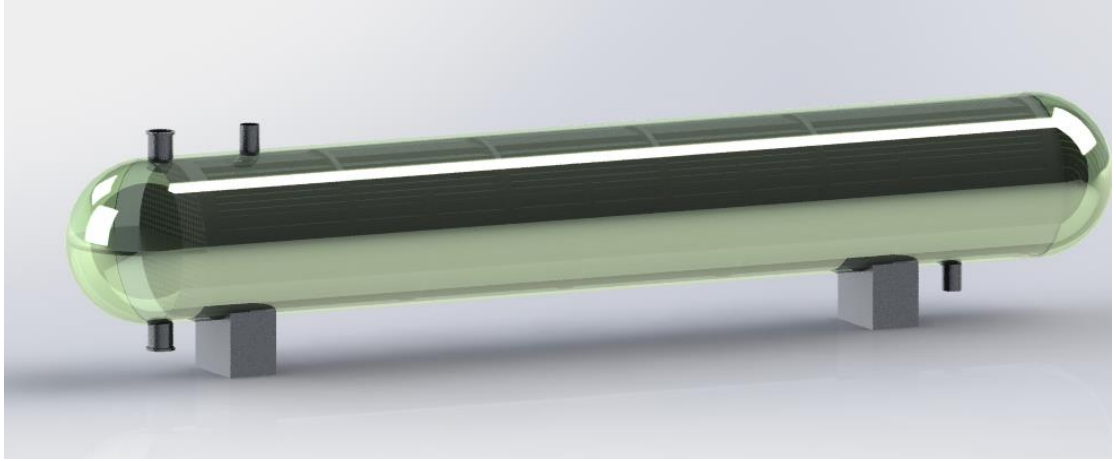

Fig. 4.2. realistic view of recuperator

4.1.1 Materials

- The saddles of the recuperator and the inlet and outlet holes are steel(AISI 304)
- The tubes are constructed by an aluminium alloy(1345 alloy)
- The shell of this recuperator is made of glass in order to make easier to see the details of the main body of heat exchanger(the common material is steel)

4.2 Heat exchanger: Heater

The heater is exactly the same type of heat exchanger as the recuperator.(one-shell pass and two-tube passes). The function of this HX is to give to CO_2 the appropriate heat input and increase its temperature in order to reach the nominal state for the introduction in the turbine. The main dimensions of this heater are the following:

Table 4.2. Dimensions of heater

number of shell passes (-)	1
number of tube passes (-)	2
shell external diameter (mm)	461.7
shell internal diameter (mm)	436.3
bundle diameter (mm)	422.6
baffle diameter (mm)	421.1
baffle spacing (mm)	240.1
baffle cut percentage (%)	25
number of baffles (-)	8
square pitch arrangement with tube pitch (mm)	22
tube external diameter (mm)	17
number of tubes (-)	259
length of tubes (m)	5
Shell side fluid inlet diameter (mm)	90
overall heat transfer coefficient($W/m^2\ ^0C$)	433.0355

The square pitch arrangement is the pattern of the tubes standing from a side cut view of the inner shell.

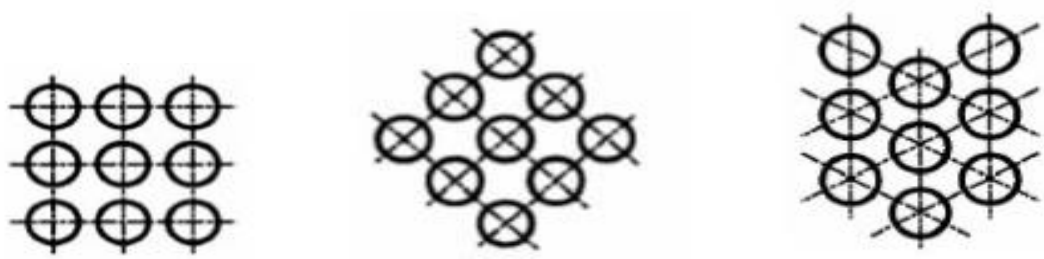

(a) (b) (c)

Fig. 4.3. Different pitch arrangements (a) square (b) square rotated (c) triangular

Triangle pitch is improving the heat transfer coefficient; however, with the square pitch arrangement is achieved the mechanical cleaning in an easier and more efficient way.

Furthermore, the square pitch arrangement is preferred when the pressure drop is low in contrast with the triangle pitch.

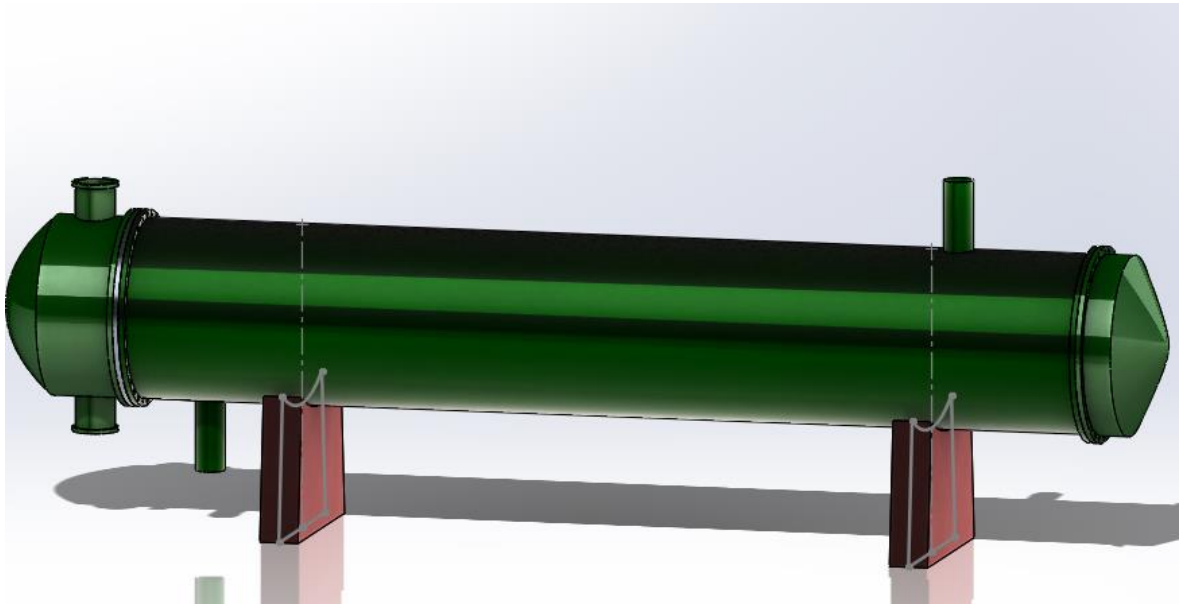

Fig. 4.4. Real view graphics of the heater at SOLIDWORKS

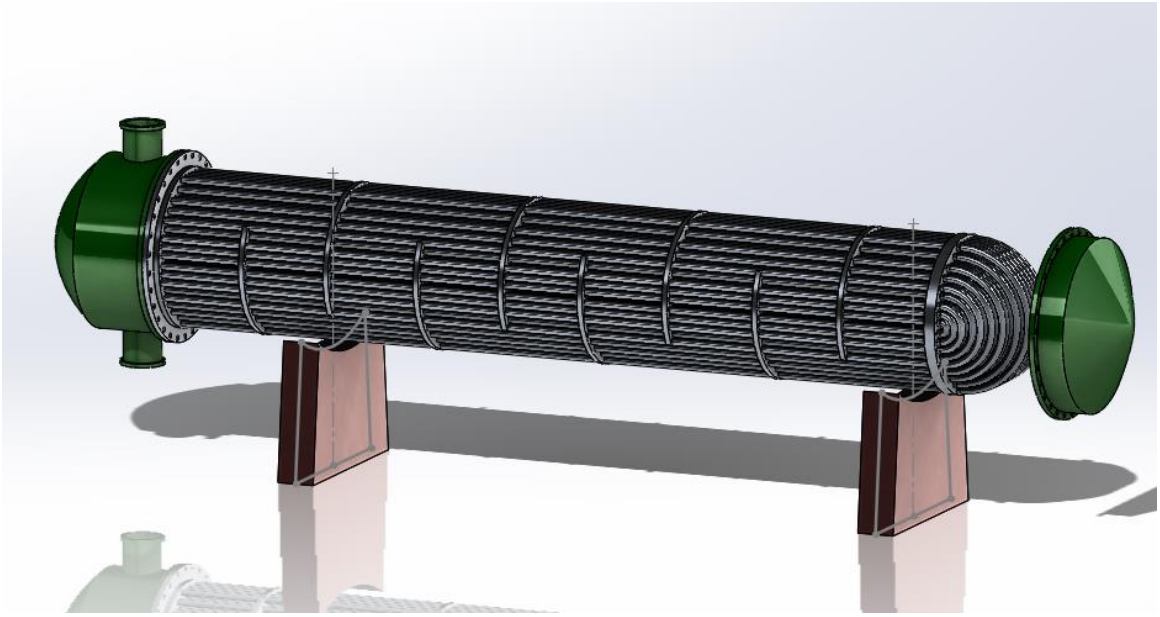

Fig. 4.5. Real view graphics of the internal of the heater

4.2.1 Materials

- The saddles(lightly pink) of the heater and the inlet and outlet holes are steel(AISI 304)
- The tubes are constructed by an aluminium alloy(6061-T4)
- The shell(green) of this heater is made of steel(AISI 304)

4.3 Heat exchanger:gas cooler/cooling tower

In order to convert the carbon dioxide from gas to liquid, it has been selected to make use of a custom-made cooling tower. The design of this component is a bit more complicated because of the finned tubes and the specific fluid allocation in the tubes, to minimize the components specific area.

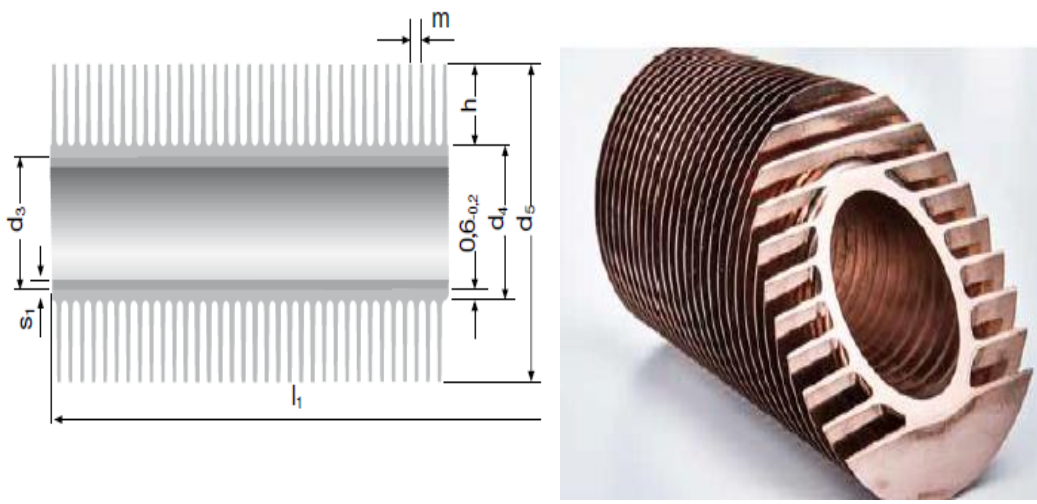

Fig. 4.6. Dimensions of the tubes and the fins

The carbon dioxide is inserted in the tubes of the cooling tower and the cold air (point 1, Fig. 4.7) that is inserted, with the help of the fans (point 2, Fig. 4.7), moves to the top of the cooling tower and converts the gas to liquid. It is significant to mention that the gas cooler is a whole custom structure, which was adjusted appropriately to the dimensions predicted by the sizing tool of the gas cooler.

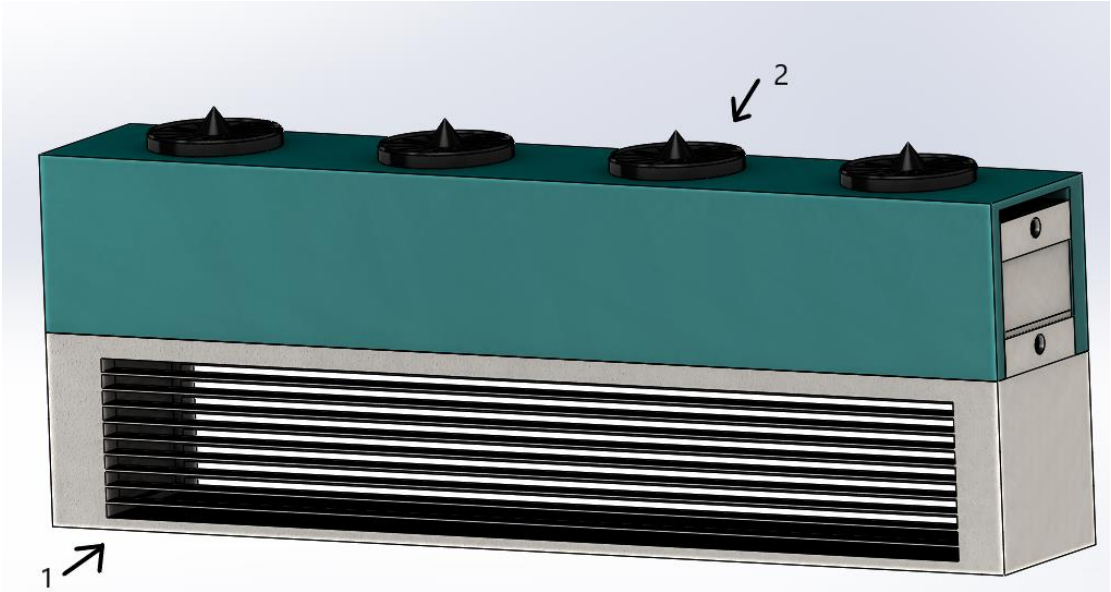

Fig. 4.7. Realistic view of the cooling tower

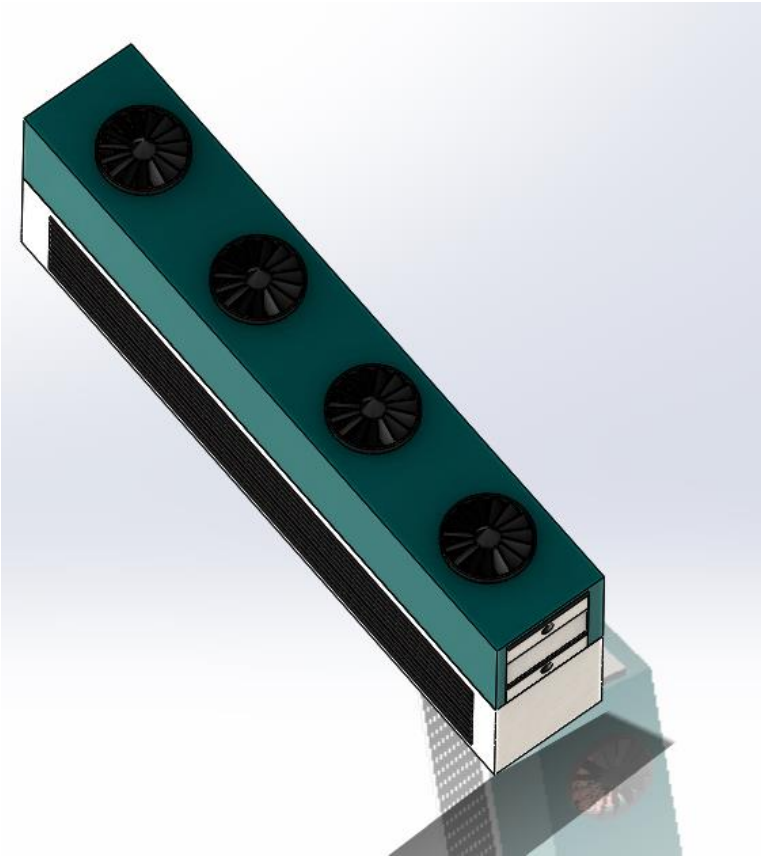

Fig. 4.8. Top view of the cooling tower

- length of the tube=3m.
- 2 arrays per pass
- 4 passes
- 13 tubes per pass
- Height=1150mm
- Height of fin=10m
- Fin pitch=3.6mm
- Tube diameter=35mm
- overall mean heat transfer coefficient = 18.8908 W/m²2K

The most demanding part of this component was the connection between the tubes. The use of 2 reducers was necessary, 2 elbows and one tube completed this complicated part, as shown in the detail of Fig. 4.9.

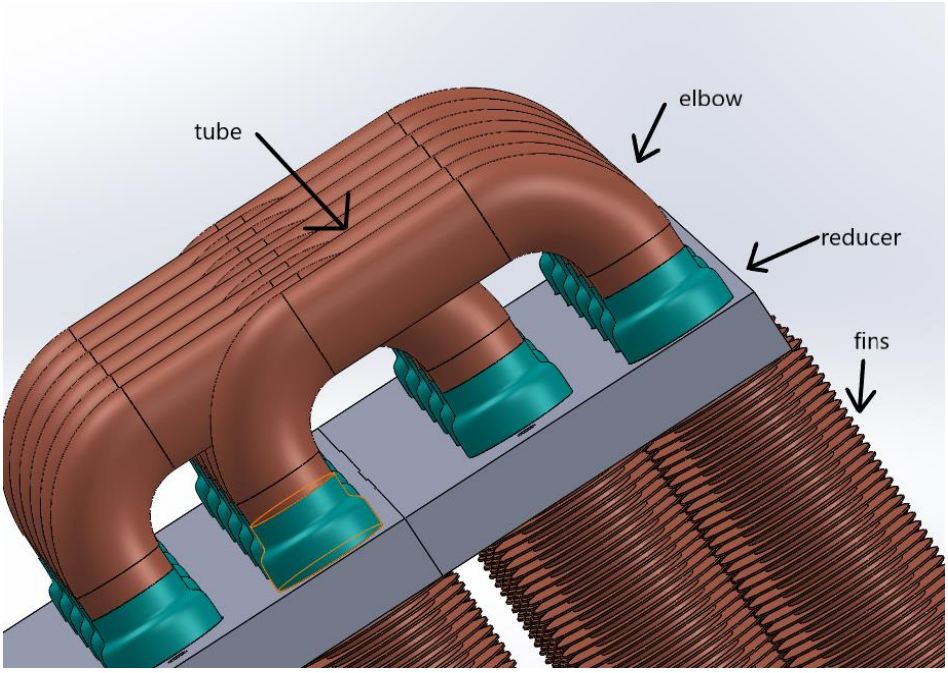

Fig. 4.9. The connection between the tubes

The length of the tube is 3m, every pass has two rows and thirteen tubes. The layout of the tubes in the pass is depicted below in Fig. 4.10.

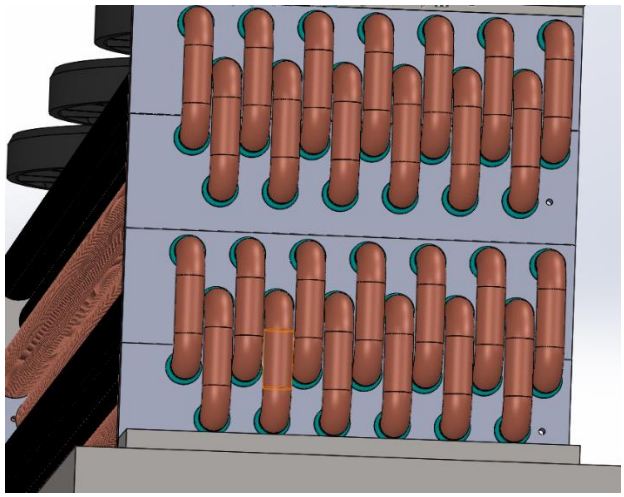

Fig. 4.10. The layout of the tubes in a pass (s_1=60 mm, s_1=52 mm)

4.3.1 Materials

- The air entry box and the whole shell of the cool tower is built by cast alloy.
- The tubes are constructed by copper
- The connection part (reducers, tubes and the elbows) is made of copper
- The fans are constructed by steel (stainless steel)

4.4 Buffer Tank

The buffer tank is implemented after the gas cooler as the function of this component is inextricable with the function of the cooling tower. The existence of a buffer tank allows the user to store the fluid every time maintenance is required as well as to absorb the thermal expansions within the closed circuit. When the layout is not in use and is under maintenance or construction, the storage of the fluid allows the drainage of a pipeline. Last but not least, the existence of the buffer tank in a Rankine cycle layout is significant because it absorbs the expansion stresses induced by the large temperature differences in some components.

Fig. 4.11. Buffer tank

4.5 turbine/expander

The analysis of the finding of the suitable dimensions and design for the turbine is reffered in a previous chapter.

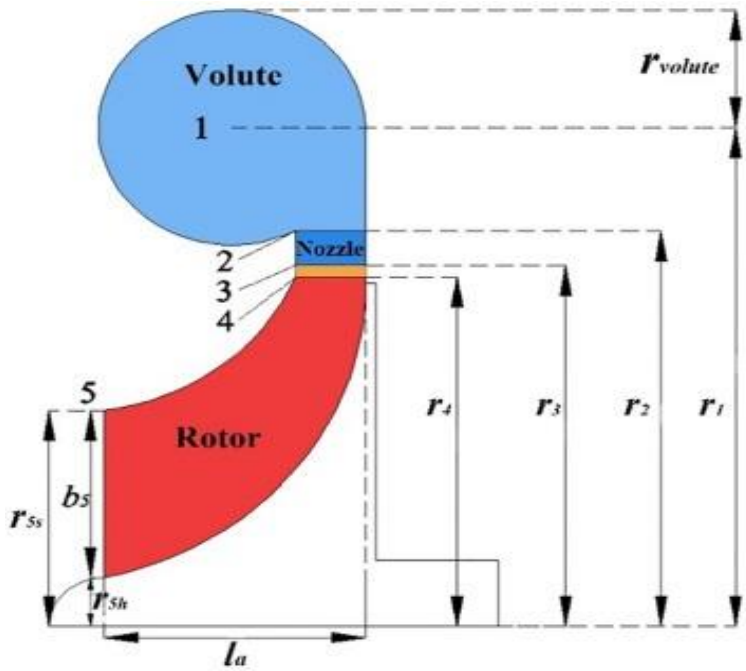

Fig. 4.12. Depiction of the dimension of the rotor,nozzle,and volute of a turbine

Because the article that is used to find the dimensions for the turbine is referred to a specific turbine's power output, it is necessary to implement an equation of similarity. According to [29], when the fluid-dynamic motors are being analyzed and the geometry relations are valid then the existence of a relation between the rotation speed the inlet rotor radius, the density and the power output is the most common equation that can be used to extrapolate the values into the size of the considered system. The assumptions are the same rotational speed and density, yielding:

$$\frac{N_1}{\rho_1 n_1^3 D_1^5} = \frac{N_2}{\rho_2 n_2^3 D_2^5} \tag{4.1}$$

$$D_2 = \frac{D_1}{1{,}16} \tag{4.2}$$

With D_2 to be the rotor inlet radius(r_4) and the r_4 as an input and using all the equations that are referred in the chapter above, the design results of the S-CO_2 turbine are listed in Table 4.3:

Table 4.3. Dimensions of the rotor and stator

Parameter	*Symbol*	*Value*
Degree of reaction	Ω	0.44
Diameter ratio	μ	0.35
Velocity ratio	x_a	0.66
Nozzle velocity coefficient	ϕ	0.92
Rotor velocity coefficient	ψ	0.8
Rotor inlet absolute flow angle (°)	α_4	17
Rotor inlet relative flow angle (°)	β_4	90.46
Rotor outlet absolute flow angle (°)	α_5	102.19
Rotor outlet relative flow angle (°)	β_5	38
Number of nozzle blades	Z_s	12
Nozzle installation angle (°)	α_s	29
Nozzle inlet radius (mm)	r_2	80.73
Nozzle outlet radius (mm)	r_3	60.66
Nozzle blade height (mm)	b_2	2.90
Number of rotor blades	Z_r	12
Rotor inlet radius (mm)	r_4	62.80
Hub radius at rotor outlet (mm)	r_{5h}	16.66
Shroud radius at rotor outlet (mm)	r_{5s}	27.30
Blade height at rotor inlet (mm)	b_4	2.871
Blade height at rotor outlet (mm)	b_5	10.635
Power output of turbine(kW)	W_t	557.1116

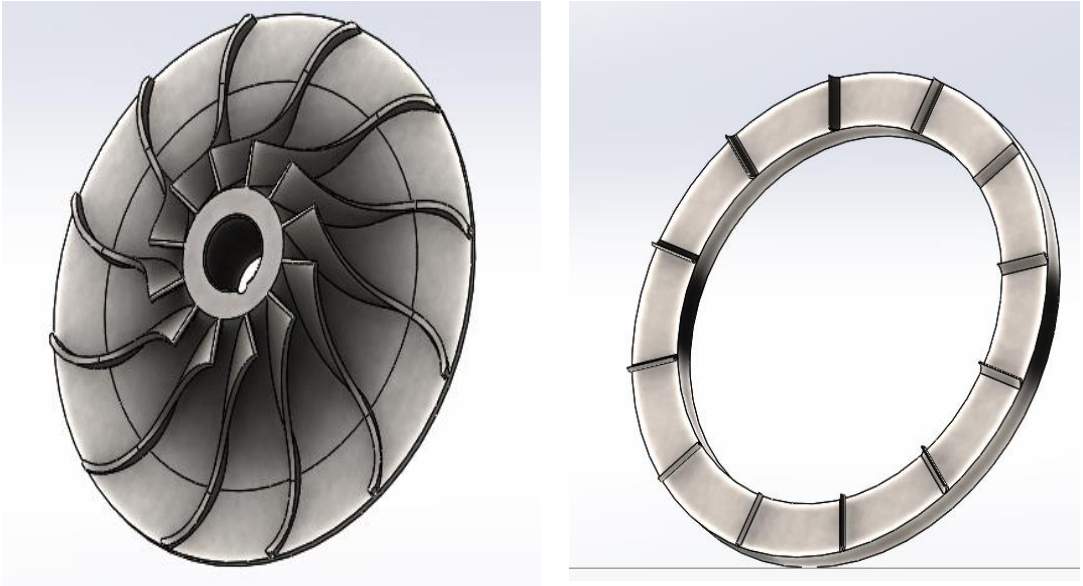

Fig. 4.13. Left is the rotor and right is the stator of this layout's turbine

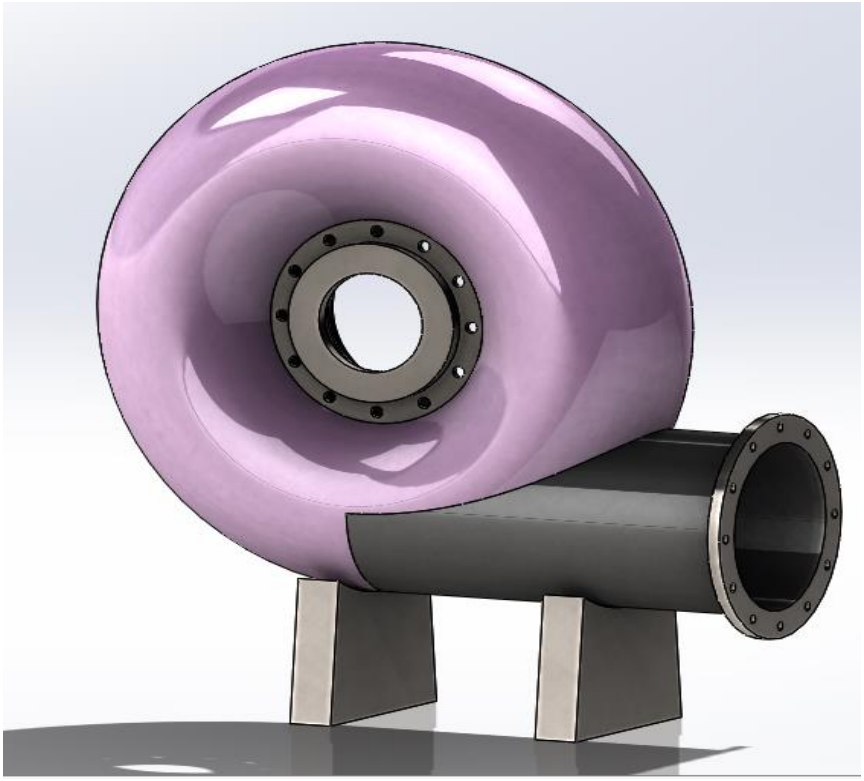

Fig. 4.14. Turbine shell

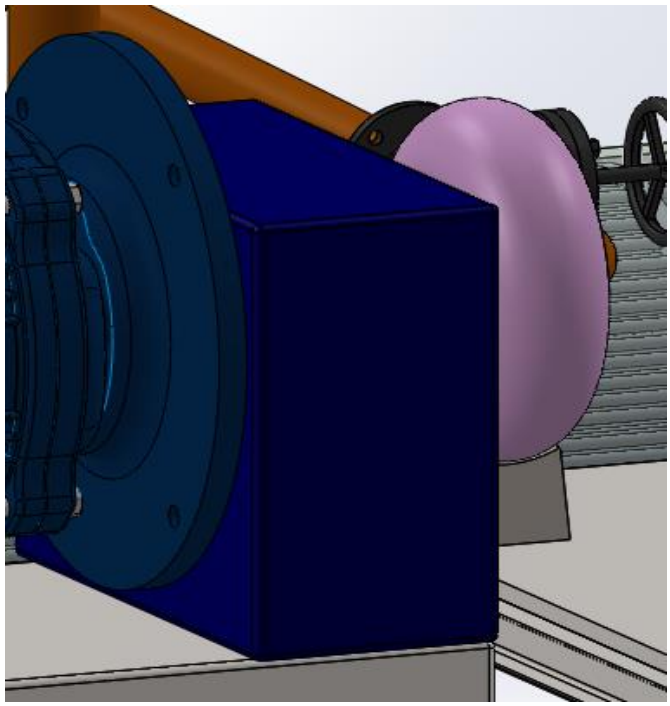

Fig. 4.15. Transmission system

It is important to refer that the use of the transmission is to synchronize the rotation of the motor to the rotation of the turbine.

4.5.1 Materials

- The rotor is built by alloy steel.
- The stator is constructed by stainless steel (AISI 316)
- The saddles are made of stainless steel (AISI 316)
- The volute is made of stainless steel (AISI 316)
- The transmission system is made of stainless steel

4.6 Pump

The pump that is chosen to the examined cycle is a triplex (three plunger rods) positive displacement, reciprocating, plunger pump, constructed of an unchromed forged brass manifold, 304SS valve assemblies, solid ceramic plungers and standard NBR (Buna-N) seals and o-rings. The triplex design results to higher efficiency and the concentric plungers provide a true wear surface and extended seal life. Furthermore, is equipped with stacked stainless steel valve design for long life and easy servicing.

Table 4.4. Specifications of the pump

Max flow	4.7 gpm/17.8 lpm
Max pressure	345 bar
RPM	1750
Material	brass

The flow rate is 2.5kg/s in the cycle and is obvious that this pump is not sufficient for these specifications. In order to use it, the scale of the pump is necessary to be magnified (4 time bigger than the original from cat pumps [30]) and for a stable operation, it was sensible to place two such scaled pumps.

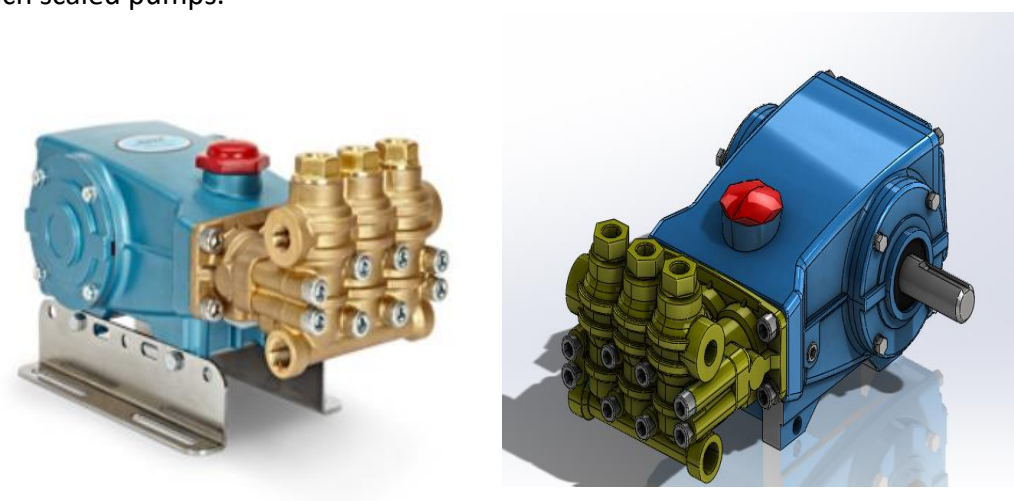

Fig. 4.16. left is the real depiction of the pump and right is the depiction at SOLIDWORKS

4.6.1 Motor

The motors used for the pumps are identical; however, the turbine generator has other specifications. The reason is simple: the work output of the pumps is extremely lower than the work output of the turbine.

The dimensions of the motors are based on the drawings from Valiadis Motors [31] and their drawings are located below in Fig. 4.17-4.19.

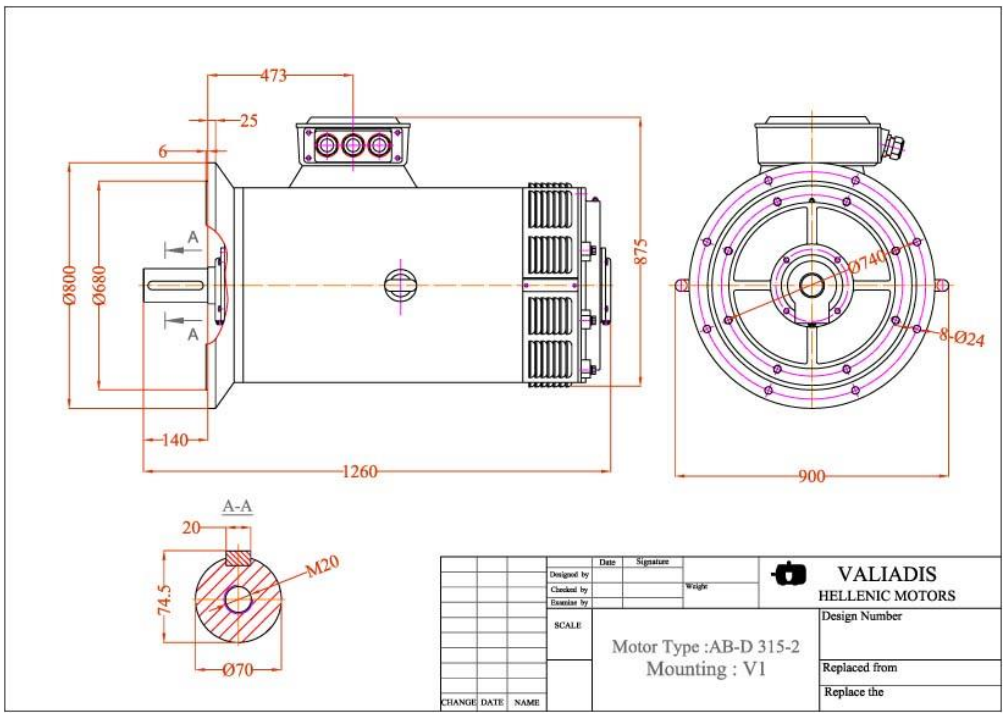

Fig. 4.17. Drawing for the motor of the pump by Valiadis motors [31]

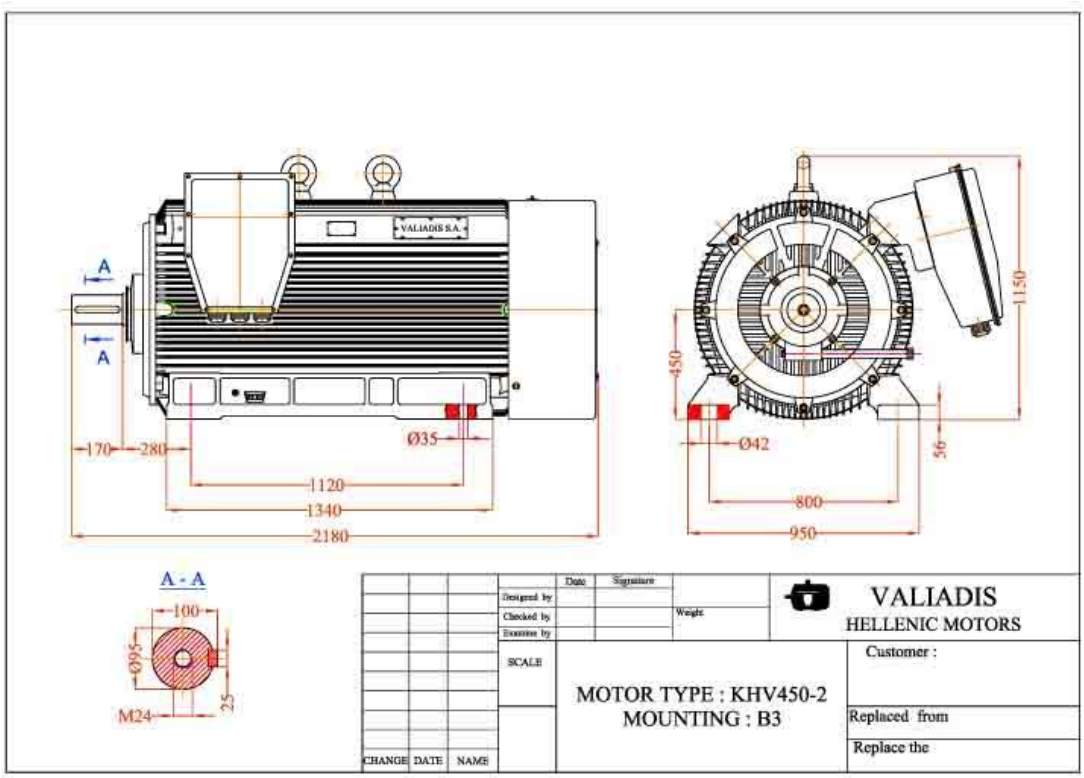

Fig. 4.18. Drawing for the turbine generator by Valiadis motors [31]

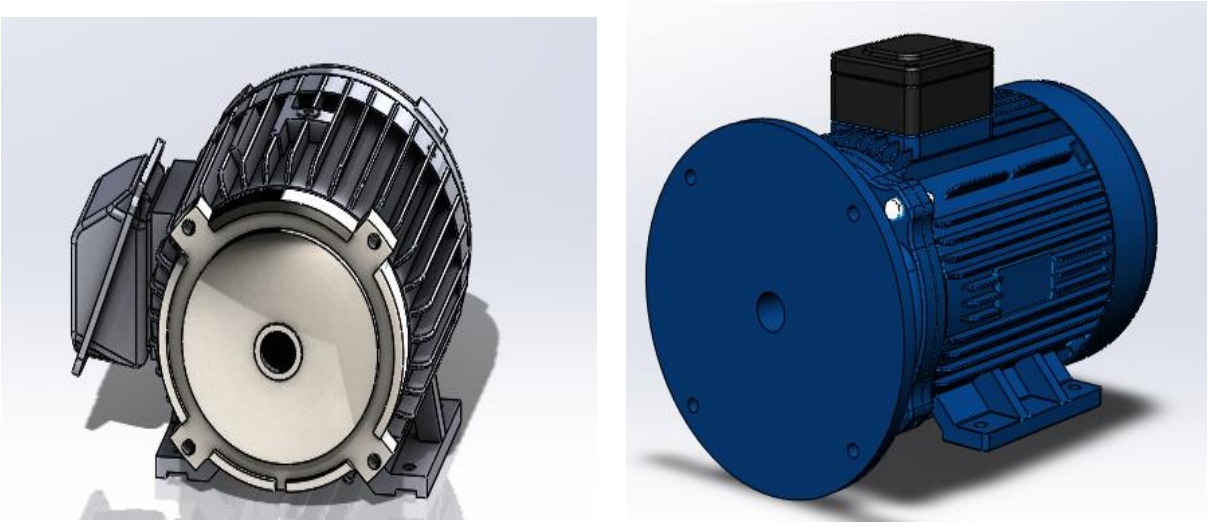

Fig. 4.19. Left is the motor of the pump and right is the motor of the turbine

The motor is necessary for the pump so as to rotate the shaft of the plunger and to pressurize the fluid. On the other hand, the generator of the turbine is the component that produces the electricity of the layout.

4.7 Supports

The supports located in the assembly are custom so as not to block the routing and to achieve the lowest possibility for a collapse.

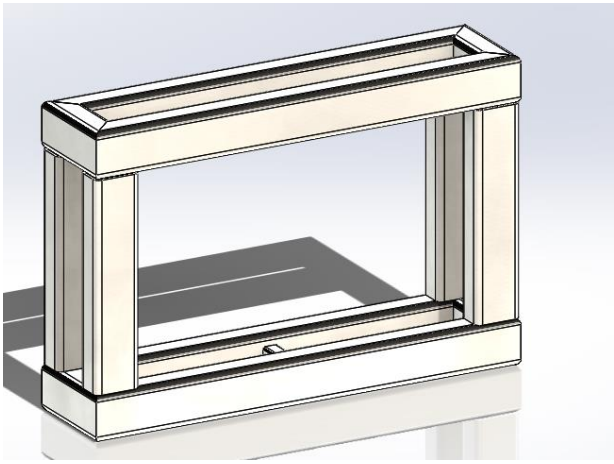

Fig. 4.20. Support for the recuperator

The support for the recuperator is built by carbon steel. The design of this support is based on the placement of the saddles and in order not to break down. The quantity of the material is not being optimized to be the less possible to achieve the fixing.

Table 4.5. Dimensions of the recuperator's support

Dimensions	*Value(mm)*
Height(y)	1960.3
Length(z)	675
Width(x)	2809.6

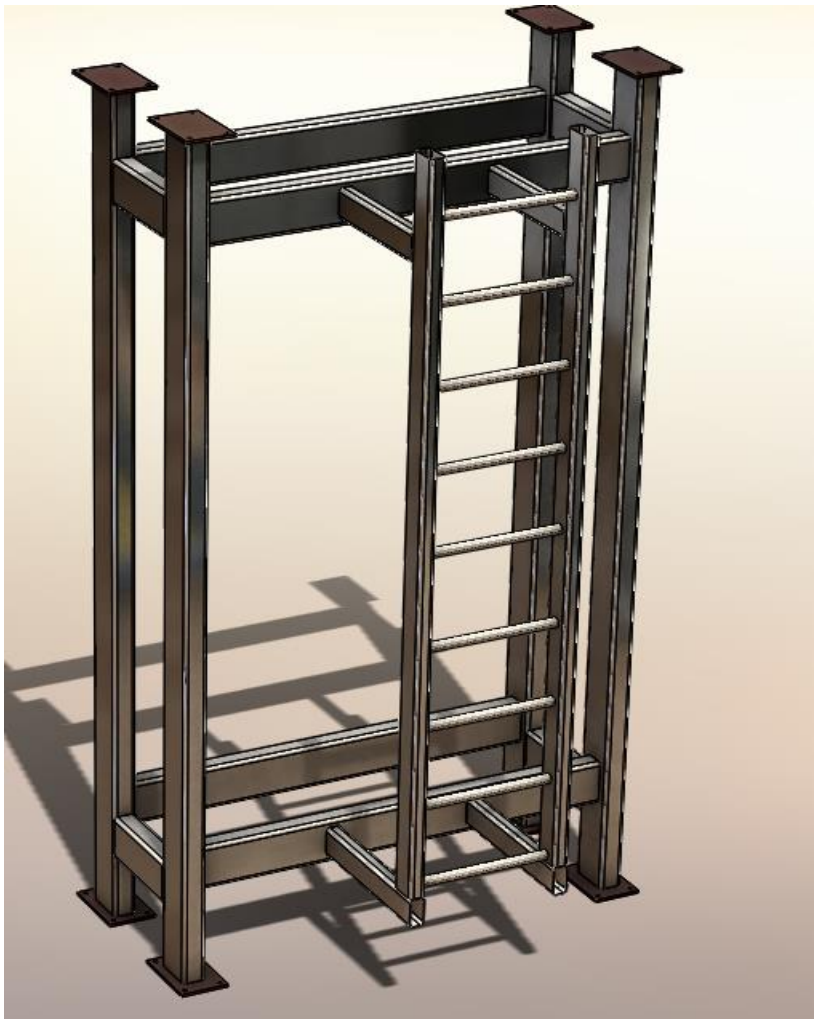

Fig. 4.21. Support for the heater

The support for the heater is constructed by carbon steel too and has four executive floor plates and four plates so as to place the heat exchanger. The ladder is an addition that helps for the maintenance and for an emergency (damage, improvement etc.).

Table 4.6. Dimensions of the heater's support

Dimensions	*Value(mm)*
Height(y)	2901.4
Length(z)	1569.85
Width(x)	652.4

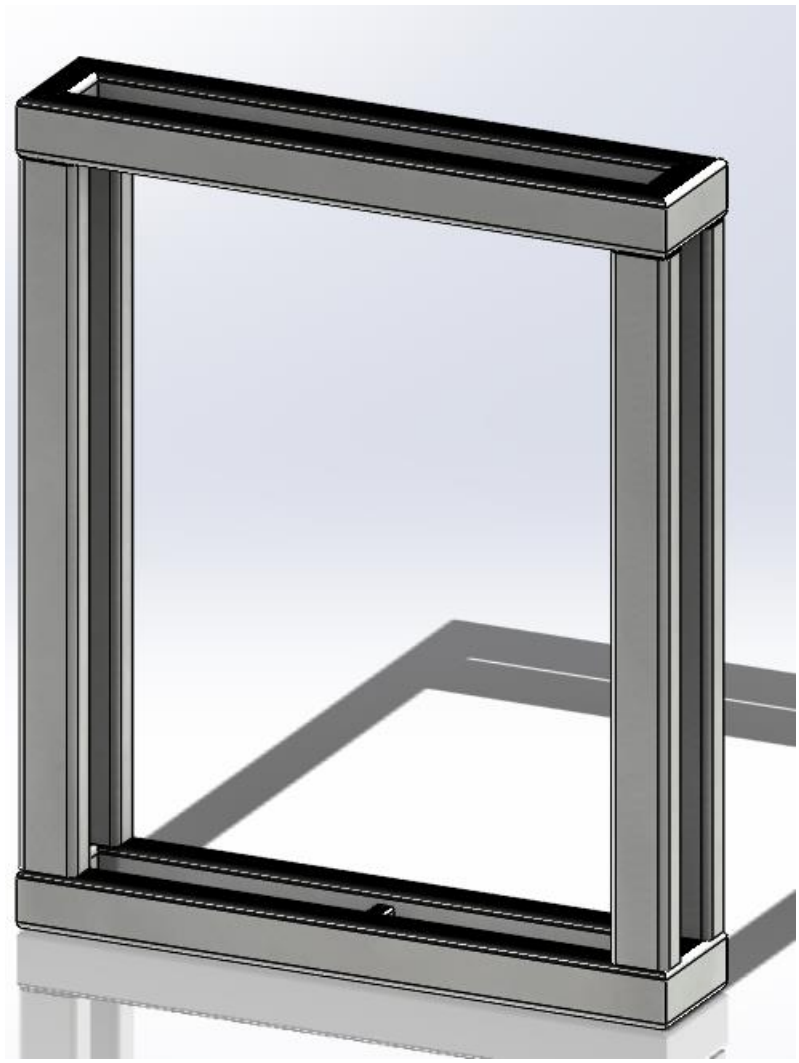

Fig. 4.22. Support for the cool tower(gas cooler)

The support of the gas cooler is built by carbon steel and it has to be the firmest construction of all the supports because of the weight of the gas cooler. As can be seen, it is the same with the support of the recuperator but the beams are stronger to carry on the weight.

Table 4.7. Dimensions of the gas cooler's support

Dimensions	*Value(mm)*
Height(y)	4070
Length(z)	3373
Width(x)	675

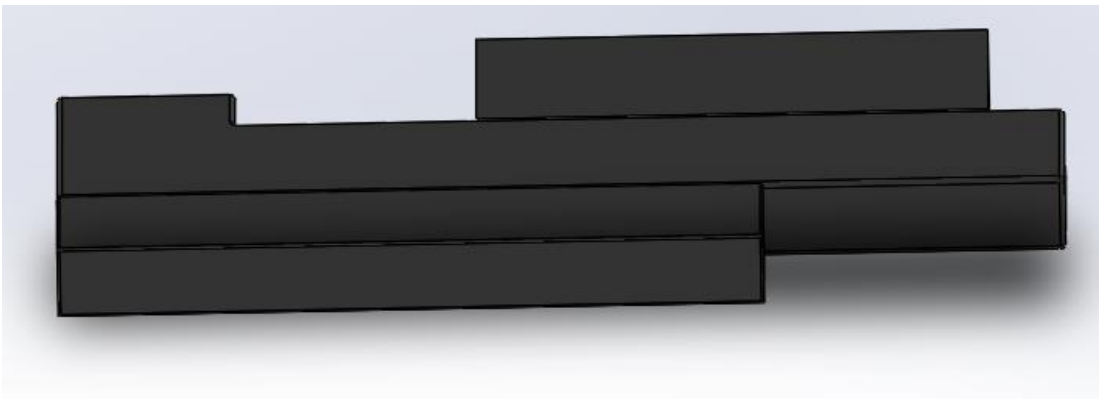

Fig. 4.23. Support for the pump

This is the floor support of the pumps and the motors of the pumps (made of carbon steel). In order to save space and not create a collision with the tubes and the rest of the construction, the design of this component is not a symmetric drawing as it would be suitable for the reason that it is used.

Table 4.8. Dimensions of the pump's support

Dimensions	*Value(mm)*
Height(y)	260
Length(z)	3800
Width(x)	1425

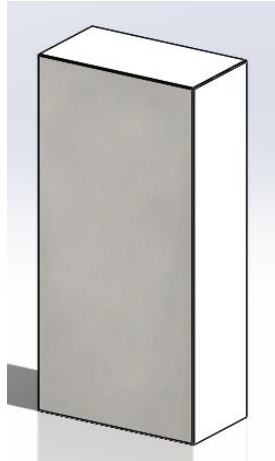

Fig. 4.24. Support for the turbine's generator and the rotate-down transformer

This is the support of the turbine's generator and the transmission system (carbon steel). The design is simpler than the other supports, and in a further analysis, it would be appropriate to examine the benefits and the disadvantages of this design and the previous.

Table 4.9. Dimensions of the motor's support

Dimensions	*Value(mm)*
Height(y)	2642.7
Length(z)	680
Width(x)	1280

Table 4.10. Dimensions of the turbine's support

Dimensions	*Value(mm)*
Height(y)	2642.7
Length(z)	1680
Width(x)	1060

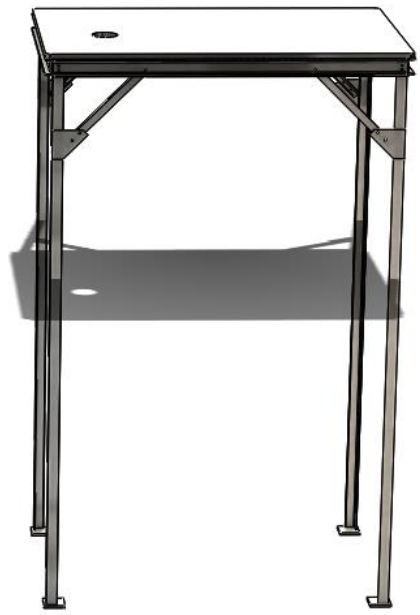

Fig. 4.25. Support for the buffer tank and the turbine

The last but not least support is the table of the buffer tank (carbon steel). The hole was created to help the routing to be simpler. The design of this support is completely different but extremely effective as well.

4.7.1 Routing

The piping is broken down to 5 categories of measurement:

Table 4.11 Routing dimensions

Diameter (in)	*Length (mm)*
2	36283
2 ½	9877
3	4147
3 ½	3691
4	2969

The flanges and elbows are compartmentalized to the similar categories based on the

Table 4.12 Flanges list

Diameter (in)	Quantity
2	6
2 ½	2
3	3
3 ½	6
4	1

Table 4.13 Elbows list

Diameter (in)	Quantity
2	25
2 ½	3
3	5
3 ½	0
4	3

The categories for the reducer are a bit different:

Table 4.14 Reducers list

Diameter (in)	Quantity
4 x 3	1
2 ½ x 2	1
3 x 2 ½	1
3 ½ x 2	5

Last but not least component of routing are the tee:

Table 4.15 Tees dimensions/quantities

Category	*Quantity*
2in all	5
3.5in to 3.5in and 2in	2

The last components that are inserted in the layout and are used to control the flow (valves),the pressure(pressure sensors) and the temperature (temperature sensors):

Table 4.16 Quantities of valves ,pressure sensors and temperature sensors

Valves	13
Pressure sensor	13
Temperature sensor	13

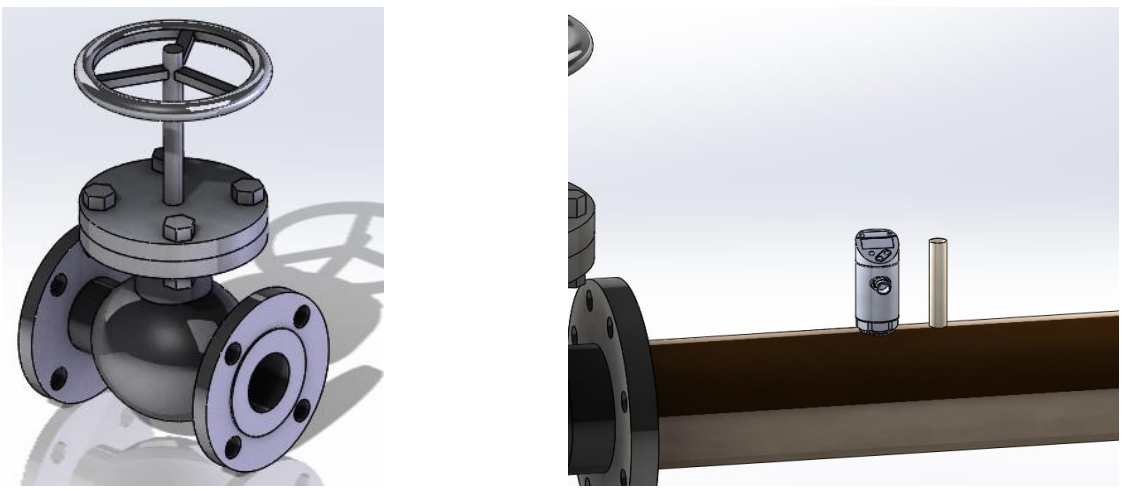

Fig. 4.26. Left is the valve and right is the pressure and temperature sensor

In Fig. 4.27 is presented the final layout of the investigated system, with all the components commissioned.

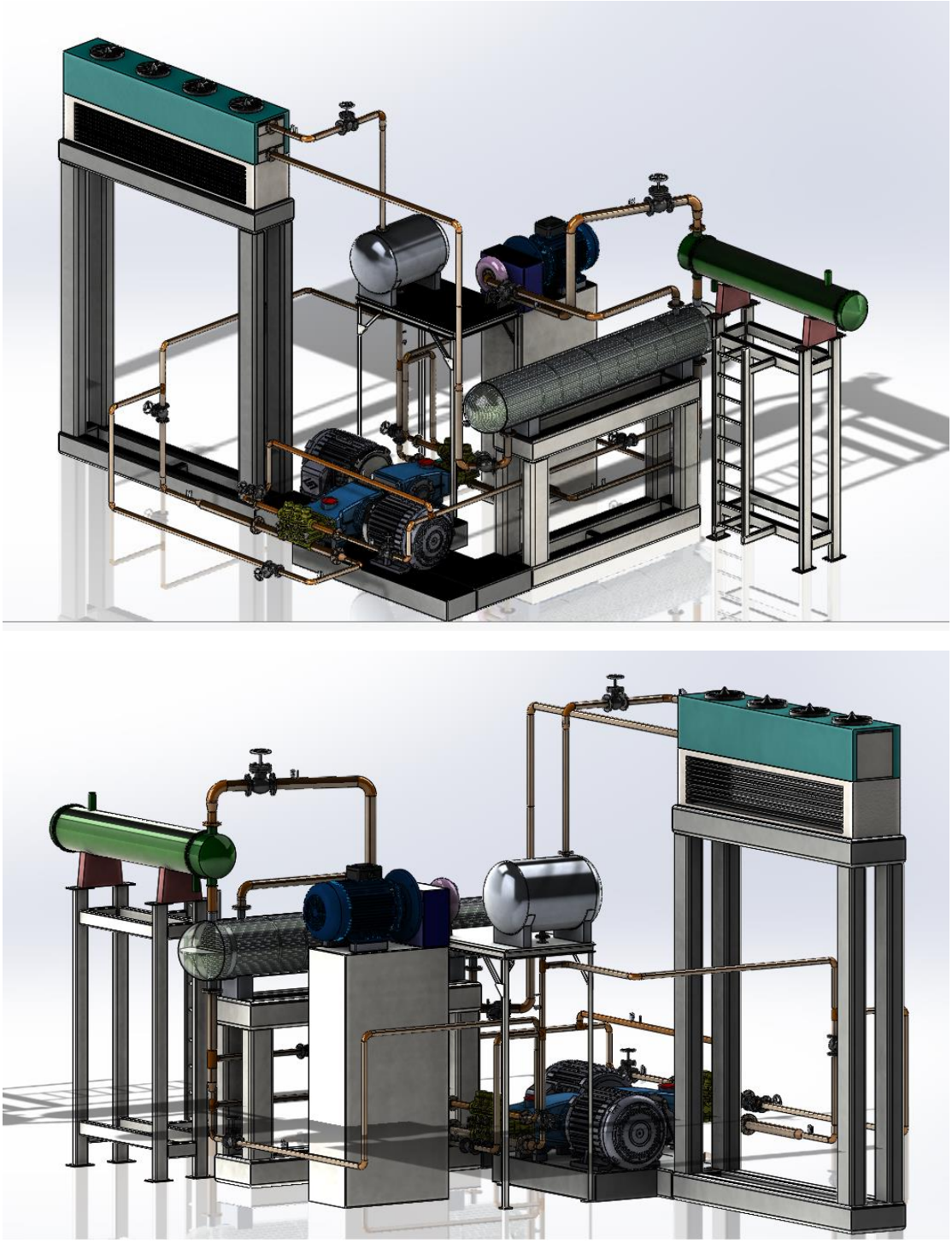

Fig. 4.27. The assembly of the layout

5. Techno-economic analysis

Every analysis about a new technology has to be combined with an economic model in order to make it not only efficient but also sustainable financially. Because of the similarity of supercritical cycle with the helium Brayton cycle, the researches for this cycle will be helpful to our analysis [14]. Apart from the estimation of the cost of the main components, it is required to estimate the support systems, the maintenance costs and the capital costs of the cycle. In order to examine the economic feasibility of a system, there are several correlations to evaluate different components.

5.1 Components cost

5.1.1 Heat exchangers

As main and most significant components of the cycle, the cost of a shell and tube heat exchanger has to be investigated thoroughly. According to a recent research about the HX cost of s-CO_2 cycle[32], it was proposed a correlation that shows the cost is the product of the thermodynamical scale and a parameter(C_1) which depends on the type of heat exchanger.

$$C_{hx} = C_1 \, UA \tag{5.1}$$

Table 5.1. Coefficient C_1 for different types of heat exchangers and values of UA

UA (kW/K)	*5*	*30*	*100*	*300*	*1000*
Primary Heat Exchanger ($/(W/K))	1.9	1.3	1.1	1	1
Recuperator ($/(W/K))	6.3	1.4	1.3	1.1	1
Air Coolers / Gas coolers ($/(W/K))	7.6	2.4	1.3	1.1	1

On the other hand, Weiland [33] supports that the value of C_1 is 0.294 for the heaters and 1.318 for the high temperature recuperators.

A more reliable research about the cycle that has being investigated, is the PhD dissertation of Astolfi [34] who discussed an Organic Rankine cycle installation and tried to calculate the cost of a HX as a function of the heat exchanger surface.

$$C_{hx} = 450{,}000 \left(\frac{A}{100}\right)^{0.7} \tag{5.2}$$

In order to facilitate the additional tolerances required in the manufacturing due to the high pressures of the sCO_2, an equation is introduced that adjusts the costs according to the pressure factor of heat exchanger.

$$\log(f_p) = -3.35099 + 1.915216\, logp_{hx} - 0.28169 \log^2 p_{hx} \qquad (5.3)$$

The most significant parameter in the estimation of HX volume is the thermal conductivity:

$$U = \frac{1}{a_i \frac{A_{i,t}}{A_{o,t}}} + \frac{1}{a_o \frac{A_{o,ht}}{A_{o,t}}} + \frac{R_{f,i}\, A_{o,t}}{A_{i,t}} + \frac{R_{f,o}\, A_{o,t}}{A_{o,ht}} + R_m \qquad (5.4)$$

$A_{i,t}$, $A_{o,t}$:inner and outlet surface of the tube ($A_{i,t}/A_{o,t} \approx 0.87$, $A_{o,t}/A_{o,ht} \approx 1$) [35]

$A_{o,ht}$: surface of the heat transfer area

R_f: resistance of fouling

R_m: resistance of material

These two resistances are inappreciable because of the small influence

- Special conductivity of CO_2: 2500 W/m^{2}K
- Special conductivity of water:10000 W/m^{2}K

Atrens expressed the cost of a heat exchanger with the following equation for a transcritical cycle [36]:

$$C_{hx} = \frac{567{,}5}{397}\left(B_{1,hx} + B_{2,hx} f_{M,hx} f_{p,hx}\right) C_{hx}^{0} f_S \qquad (5.5)$$

where

f_S is an additional factor considering material, additional piping, freight, labor and other overheads,
$B_{1,hx}$ =1.63 and $B_{2,hx}$ =1,66 are constants for the heat exchange type [37],
$f_{M,hx}$ is the material factor (for stainless steel) of the heat exchanger,
$f_{p,hx}$ is the pressure factor,

$$\log(f_{p,hx}) = C_{1,hx} + C_{2,hx}\log(p_{hx}) + C_{3,hx}\log^2 p_{hx} \quad (5.6)$$

where $C_{1,hx}$, $C_{2,hx}$ and $C_{3,hx}$ are constants for the heat exchange type, and p_{hx} is the design pressure of the heat exchanger.

Table 5.2. Coefficients and input values for equation (5.6)

$C_{1,hx}$	0.0016
$C_{2,hx}$	-0.0063
$C_{3,hx}$	0.0123
p_{hx}(bar)	305.2

and C_{hx}^0 is the basic cost for the heat exchanger made from carbon steel operating at ambient pressure,

$$\log(C_{hx}^0) = K_{1,hx} + K_{2,hx}\log(A_{hx}) + K_{3,hx}\log^2 A_{HX} \quad (5.7)$$

where $K_{1,hx}$, $K_{2,hx}$ and $K_{3,hx}$ are constants for the heat exchange type, and A_{hx} is the heat transfer area.

Table 5.3. Coefficients and input values for equation (5.7)

$K_{1,hx}$	4.3247
$K_{2,hx}$	-0.3030
$K_{3,hx}$	0.1634
$A_{hx,rec}$ (m^2)	239.7
$A_{hx,heat}$ (m^2)	73.8

In Fig. 5.1 (a)-(b) is depicted the difference of the above equations. Weiland and Carlson have the same results because the constant (C_1) is almost the same in their equations, but Astolfi's research is more reliable and near the Atrens' curve which is the same with the equation from CEPCI.

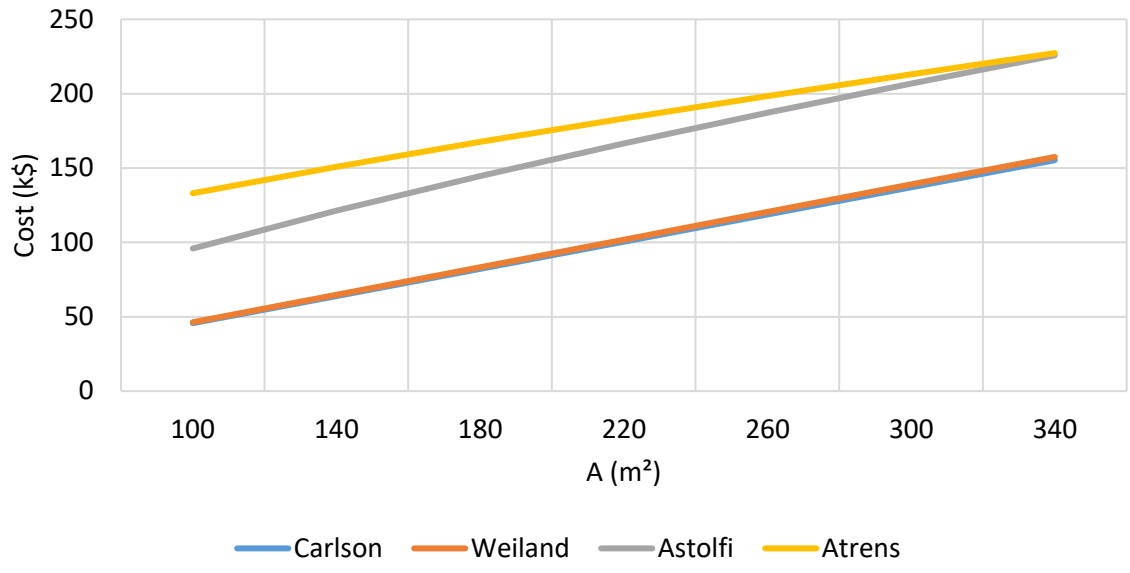

(a)

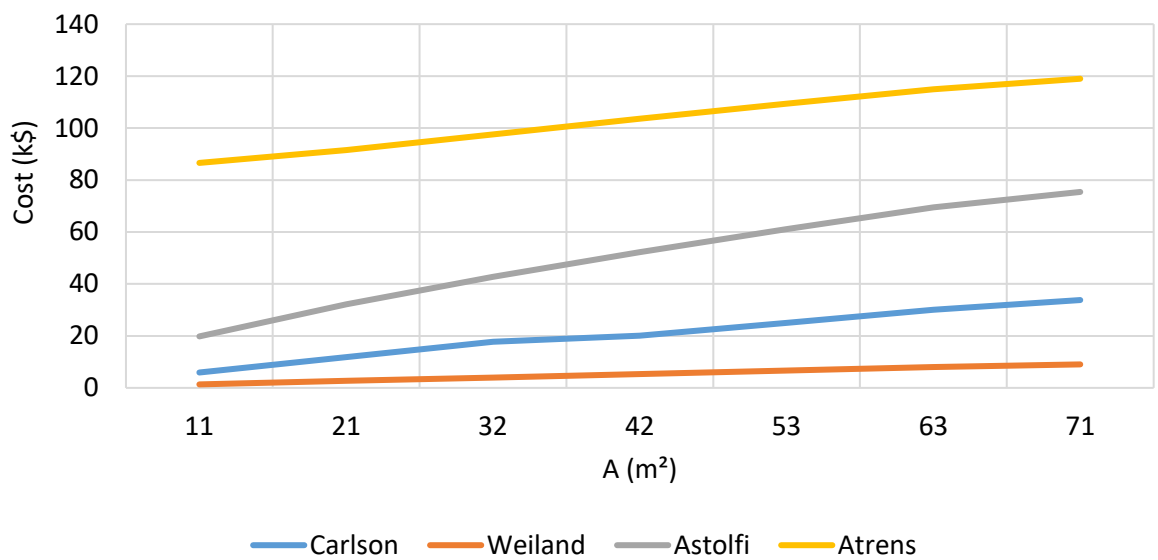

(b)

Fig. 5.1. The predictions of the proposed heat exchanger cost equations for the range of (a) recuperator and (b) heater surfaces

The cost of heater has similar results with the results for the recuperator but a significant difference is that the Astolfi's curve is not as close as it is in the recuperator's cost with the Atrens but closer to the other curves. For smaller heat transfer areas, the equation from Atrens

is not so reliable as it is for the recuperator; thus Astolfi's equation was chosen to calculate the cost of the heater.
The implementation of Astolfi's equation gives the total cost of recuperator and heater below:

- Cost of heater(€): 62,975
- Cost of recuperator(€): 150,265

5.1.2 Gas cooler

The gas cooler of this layout is an air-cooled heat exchanger. The equation of the basic cost estimation for the cooling tower is being developed by Smith [38] and the surface is referred to the bare-tube area:

$$C = 15600\left(\frac{A}{200}\right)^{0.89} \tag{5.8}$$

According to Le Kheiri[39] the constants for the pressure factor are listed in Table 5.4.

Table 5.4. Coefficients and input values for equation (5.6)

$C_{1,CT}$	0.03881
$C_{2,CT}$	-0.1127
$C_{3,CT}$	0.0818
$P_{CT}(bar)$	73.8

The comparison was conducted with the previous equations for the heat exchangers, because the references about the cost of a cooling tower were inadequate.

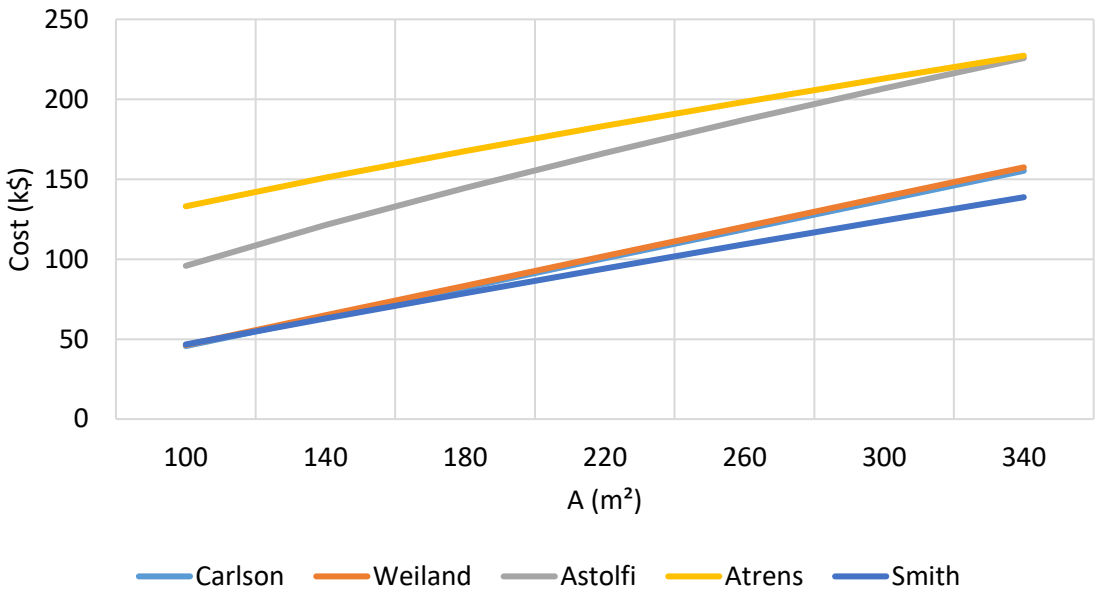

Fig. 5.2. The predictions of the proposed cooling tower cost equations

For the calculation of cooling tower's cost was selected the equation of Smith because the rest are not so reliable for this research. It is significant to note that the cost of buffer tank is included in the cost of the cooling tower:

- Cost of cool tower(€): 114,250

5.1.3 Expander/turbine

The evolution of expander and compressor is rapidly grown because of the major usefulness in every layout of almost every cycle. The components for the construction of a turbine or a compressor are complex and need to be carefully selected in order to achieve the effectiveness and quality that is required. These are the main reasons why these parts are the most expensive part of a layout. The finding of the costs for a compressor or an expander in a s-CO_2 cycle is relatively same with the cost of a gas turbine because the characteristics are the similar.(big inlet pressure, outlet temperature ranges from small to enormous numbers).The main difference is that, for a s-CO_2 rotary machine, the development is premature so the results are not so accurate from previous researches. Carlson[32] and Weiland[33] made a techno-economic research about a s-CO_2 cycle but the net output is significantly bigger than this layout. For this reason, the equation (5.9) is considered very useful in order to calculate the cost of this component in every research regardless the net output.

$$C = C_1\, W^{n_1} \tag{5.9}$$

C_1 and n_1 are 7790 and 0.6842, respectively by the theory of Carlson; on the other hand, Weiland claims that these constants are 186,200 and 0.5561, respectively, but the net output is calculated on MW. Weiland's research does not conclude states up to 550 °C and the turbine's or compressor's work is on MW, so the loss would be significant in other layouts. Finally, Astolfi, although his research is about organic Rankine cycle, could be of use for the estimation of the cost of a turbine.

$$C = C_1\, W_{st}^{n_1} + C_2 \left(\frac{SP}{SP_0}\right)^{n_2} \eta_{st}^{n_3} \tag{5.10}$$

$$SP = \frac{\sqrt{V_{out}}}{\Delta h_{is}^{0.25}} \tag{5.11}$$

With W to be in MW and SP_0=0.18.

According to Atrens,the cost of the turbine is given by:

$$C_{st} = \frac{567{,}5}{397} f_{MP} C_{st}^0 f_S \tag{5.12}$$

where f_{MP} is the material and the pressure factor (for stainless steel) of the turbine,
f_S is an additional factor about the material and the pressure
and C_{turb}^0 is the basic cost of the turbine, calculated as follows:

$$\log C_{st}^0 = k_{1,st} + k_{2,st} \log W_{st} + k_{3,turb} \log^2 W_{st} \tag{5.13}$$

where $K_{1,st}$, $K_{2,st}$ and $K_{3,st}$ are constants for the turbine, and W_{st} is the turbine's output power.

Table 5.5. Coefficients and input values for equation (5.13)

$k_{1,st}$	2.2897
$k_{2,st}$	1.3604
$k_{3,st}$	- 0.1027
$W_{st}(KW)$	558.2116

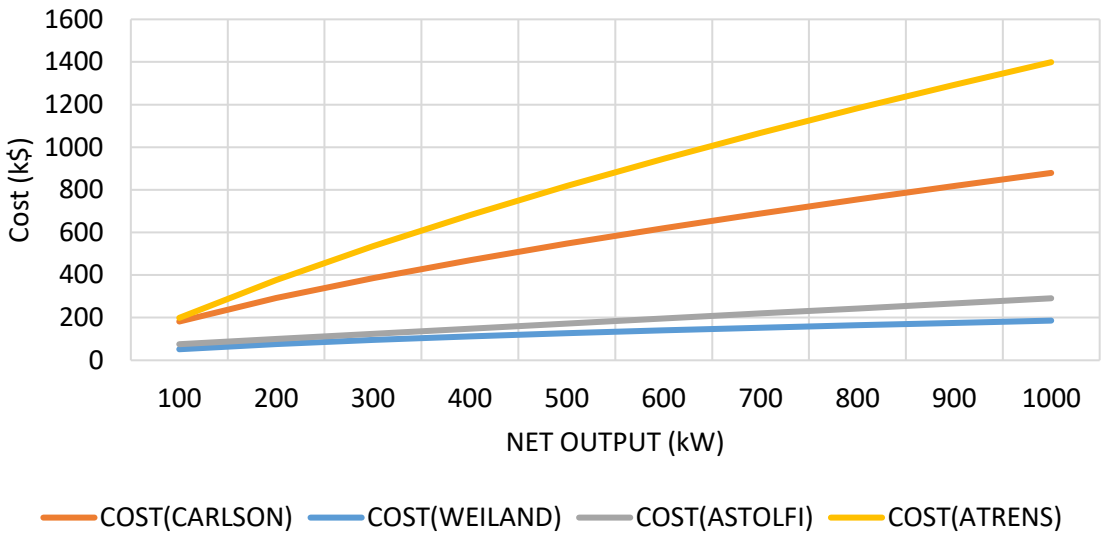

Fig. 5.3. The predictions of the proposed turbine cost equations

For the calculation of the turbine's cost Carlson's correlation was selected. It is noted that the cost of the transmission system is included in that of the turbine. The results are listed below:

- Cost of turbine(€): 500,869

5.1.4 Pump

The pumps used in the power cycle systems are of the centrifugal type and the costs of them can be calculated by[36]:

$$C_{PP} = \frac{567,5}{397}\left(B_{1,PP} + B_{2,PP} f_{M,PP} f_{P,PP}\right) C_{PP}^{0} \qquad (5.14)$$

where $B_{1,PP}$ =1.89 and $B_{2,PP}$ =1.35are constants for pump type (centrifugal)[37],
$f_{M,PP}$ is the material factor of the pump,
$f_{P,PP}$ is the pressure factor of the pump,
and C_{PP}^{0} is the basic cost of the pump made from carbon steel.

$$\log C_{pp}^{0} = k_{1,pp} + k_{2,pp} \log W_p + k_{3,pp} \log^2 W_p \qquad (5.15)$$

where $K_{1,pp}$, $K_{2,pp}$ and $K_{3,pp}$ are constants for pump type, and W_p is the consumption power in the pump. The constants for the pump are given by Jian Song,Kai Wang and Christos Markides in their research about the optimization of a combined supercritical cycle [37] and are listed in Table 5.6.

Table 5.6. Coefficients and input values for equation (5.15)

$k_{1,pp}$	3.3892
$k_{2,pp}$	0.0536
$k_{3,pp}$	0.1538
$W_p(KW)$	114.898

In order to find the pressure factor equation (5.16) is used which is

$$\log F_{pp}^{0} = C_{1,PP} + C_{2,PP} \log p_p + C_{3,pp} \log^2 p_p \qquad (5.16)$$

where $C_{1,PP}$, $C_{2,PP}$ and $C_{3,PP}$ are constants for pump type, and p_P is the design pressure of the pump.

Table 5.7. Coefficients and input values for equation (5.16)

$C_{1,PP}$	-0,3935
$C_{2,PP}$	0,3957
$C_{3,PP}$	-0,0023
$p_P(bar)$	280

Because of the lack of similar equations about the pump's cost, in this research, equation (5.14) is used for the calculation of this component's cost. Eventually, the cost of the pump was found to be:

- Cost of pump(€): 99,549

5.1.5 Motors/Generator

Last but not least is the estimation of the motor cost of the pump and the turbine's generator. Astolfi used in his PhD, the equation which is located below and is the main equation for the cost of the components:

$$\log C_{mot} = C_1 + C_2 \log W_{mot} + C_3 \log^2 W_{mot} \quad (5.17)$$

Table 5.8. Coefficients and input values for equation (5.17)

C_1	4,105466
C_2	0,057044
C_3	0,079664
W_{mot} (KW)	187,4898
W_{gen}(KW)	557,1116

It is significant that this equation is suitable for a range from 10KW to 10MW that yields to implement to both motors of the layout.
Weiland[33] claims that the estimation of the motor's cost, with the help of manufacturer's data, is calculated by the following equation:

$$C_{mot} = 108{,}900 W_{mot}^{0.5463} \quad (5.18)$$

The noteworthy annotation is that according to Weiland, this equation is referred to net output that reaches values of MWs.

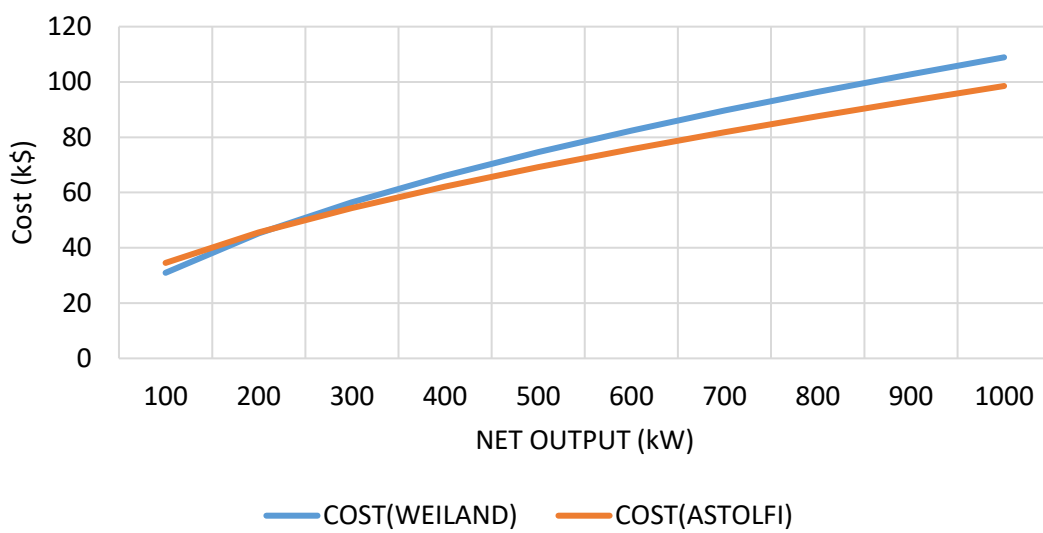

Fig. 5.4. The predictions of the proposed motor/generator cost equations

Because Weiland is referred to values that reach many MWs, Astolfi's equation is considered more valid for the range of the application and more reliable. Therefore, the results are listed below:

- Cost of pump's motor($): 37,681
- Cost of turbine's motor($): 61,972

5.1.6 Supports

All the profile costs were derived from [40]. Below are presented all the respective costs for the supports of the system.

Table 5.9. Cost estimation for recuperator's support

*Total profiles length (m)**	21
Cost estimation(€)	313.74

**Profiles considered of 50x30, Price of profile 14.94 €/m*

Table 5.10. Cost estimation for heater's support

*Total profiles length (m)**	29
Cost estimation(€)	433.26

**Profiles considered of 50x30, Price of profile 14.94 €/m*

Table 5.11. Cost estimation for gas cooler's support

*Total profiles length (m)**	43
Cost estimation(€)	642.94

**Profiles considered of 50x30, Price of profile 14.94 €/m*

Table 5.12. Cost estimation for pump's support

*Total profiles length (m)**	43
Cost estimation(€)	505.68

**Profiles considered of 31x26, Price of profile 11.76 €/m*

Table 5.13. Cost estimation for motor's support

*Total profiles length (m)**	43
Cost estimation(€)	270.48

**Profiles considered of 31x26, Price of profile 11.76 €/m*

Table 5.14. Cost estimation for turbine's support

*Total profiles length (m)**	29
Cost estimation(€)	341.04

**Profiles considered of 31x26, Price of profile 11.76 €/m*

5.1.7 Pipelines and miscellaneous

In this section are presented the costs as estimated for the pipelines, fittings and the rest instruments used in the s-CO_2 systems.

Table 5.15. Data for the used pipe costs

Category	*Length*	*Cost(€/m)*	*Total Cost(€)*
2(in)	36283(mm)	49.26	1787.2
2.5(in)	9876,98(mm)	61.89	611.5
3(in)	4147,4(mm)	74.97	311.5
3.5(in)	3691(mm)	88.48	326.5
4(in)	2969,22(mm)	102.16	303.4

Table 5.16. Data for the used flanges

Category	*Quantity*	*Cost(€/pc)*	*Total Cost(€)*
2(in)	6	83.48	500.9
2.5(in)	2	94.36	188.7
3(in)	3	97.67	293.0
3.5(in)	6	118.27	709.6
4(in)	1	136.53	136.5

Table 5.17. Data for the used elbows

Category	Quantity	Cost(€/pc)	Total Cost(€)
2(in)	25	17.41	435.5
2.5(in)	3	25.80	77.4
3(in)	5	38.63	193.2
3.5(in)	0	53.13	0
4(in)	3	70.12	210.4

Table 5.18. Data for the used reducers

Category	Quantity	Cost(€/pc)	Total Cost(€)
4in to 3in	1	51.9	51.9
2.5in to 2in	1	18.2	18.2
3in to 2.5in	1	26.1	26.1
3.5in to 2in	5	66.1	330.5

Table 5.19. Data for the used tees

Category	Quantity	Cost(€/pc)	Total Cost(€)
2in all	5	20.2	101.0
3.5in to 3.5in and 2in	2	101.8	203.6

Table 5.20. Data for the used valves

Category	Quantity	Cost(€/pc)	Total Cost(€)
2(in)	8	221.6	1772.8
2.5(in)	2	231.7	463.4
3(in)	2	239.7	479.4
3.5(in)	0	248.9	0
4(in)	1	257.8	257.8

Table 5.21. Data for the used sensors

Category	Quantity	Cost(€/pc)	Total Cost(€)
Pressure sensors	13	190	2470
Temperature sensors	13	99.2	1289.6
Energy meters	2	297.6	595.2

5.1.8 Total cost

The sum of the above costs of all the components and the routing parts gives the 80% of the total costs. There are two parameters that it is necessary to calculate in order to be specific and more reliable. The cost of employment is a significant branch of the costs and consists of 20% of the total cost. Last but not least is the maintenance cost which is calculated as the 1% of the total cost of the components.

Table 5.22. Total costs of system

Component	Price (€)
Recuperator	150,266
Heater	62,975
Turbine	500,869
Gas cooler	114,250
Pump	95,949
Motor(pump)	37,681
Motor(turbine)	61,973
Supports	2,507
Routing	14,145
Maintenance cost	13,008
Employment cost	260,153
Total cost	1,300,768

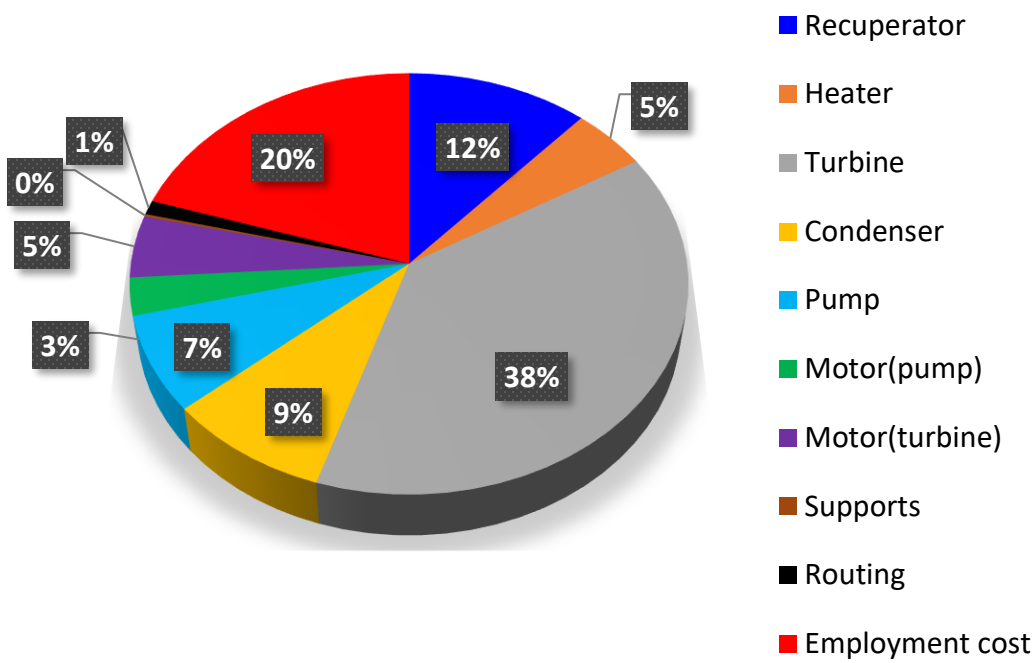

Fig. 5.5. Breakdown of capital cost for the system

5.2 Economic indicators

The most common indicators, that show if the combination of the effectiveness and the cost is sustainable, are the NPV (Net present value), the IRR (Internal rate of return), the PbP (Pay-back period) and the LCOE (Levelized cost of electricity). There are many other indicators that are very usable in order to examine every proposed system, thoroughly, but the above four parameters are the more frequently applied to measure the basic economic aspects of a proposed solution.

The Net Present Value is the amount of cash flows (negative and positive) discounted to the present for a specific period of investment. The formula for Net Present Value is:

$$NPV = -C_{cap} + \sum_{t=1}^{N} c_t \, (1+i)^{-t} \qquad (5.19)$$

Where

c_t is the cash flow of the t period,

t is the number of the year (1:first,2:second…)

i is the discount rate

N is the whole period of the investment
C_{cap} is the cash outflow in time 0

On the other hand, the Internal Rate of Return(IRR) is the discount rate when the NPV becomes zero.

$$-C_{cap} + \sum_{t=1}^{N} c_t \, (1 + IRR)^{-t} = 0 \tag{5.20}$$

To ensure the sustainability of the research is necessary to have a discount rate bigger than the IRR. The bigger this rate becomes; the more economical success is achieved.
One of the most important economic indicators is the Pay-back period (PbP) which is the period until the cash inflows overcomes the induced outflows. The payback period is equal to the ratio of the investment cost divided by the net annual income of the system, according to the equation:

$$PbP = \frac{C_{cap}}{C_{rev} - C_{main}} \tag{5.21}$$

Levelized cost of electricity allows also for a more direct conclusion on the potential of the proposed solution, providing a direct comparison with the conventional solution. On most occasions, has a similar profile to the NPV and can be calculated by the following formula:

$$LCOE = \frac{C_{cap} + \sum_{t=1}^{20} \frac{C_{main,t}}{(1+r)^t}}{\sum_{t=1}^{20} \frac{W_{net}}{(1+r)^t}} \tag{5.22}$$

The most significant parameters for the above indicators are the income and outcome. As an outcome is the operation and maintenance cost, while as income are considered the earnings from the sales of the electrical energy. The average value of the cost of the electrical energy is defined by Marginal System Cost (MSC) and is a price that changes every day, depending on the Greek market of energy. The swapping of this value for every month is located below in Fig. 5.6.

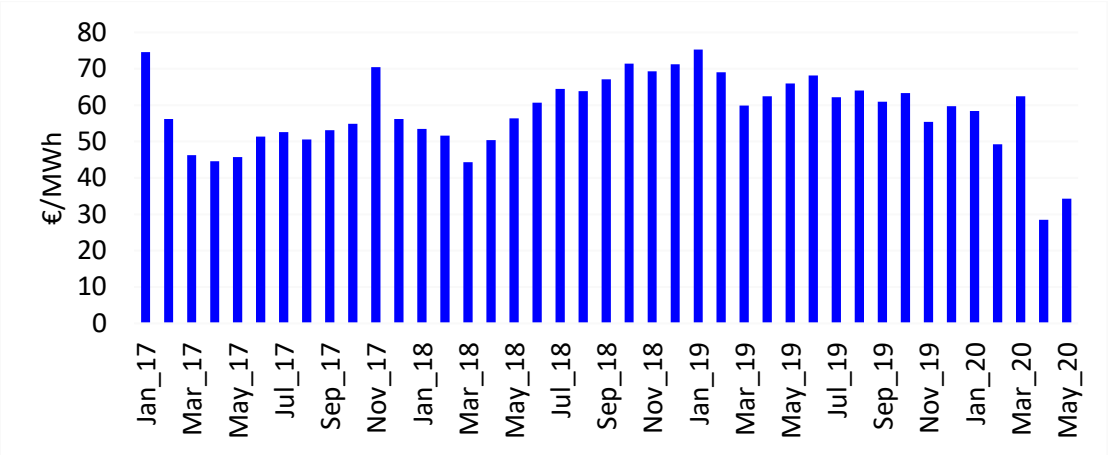

Fig. 5.6. Marginal System Cost for Greek market

The big decrease of the value of the electric energy's cost is down to the lockdown due to COVD-19 which bursts all over the country and the world. This makes it demanding to analyze the dependence of the average value of the electric energy's sale to the incomes in order to capture a larger range of a year's period.

Fig. 5.7 shows that the construction of the specific layout is not viable and not economically passable in most scenarios for a 15 year period of investment. Obviously, when the operating hours of the cycle become longer, then the revenues increase. The only profit is in the occasion of the maximum price of the electricity with the requirement to be in operation all day throughout the year (with an NPV of 93,530 €).The value of NPV for 6,570 hours per year is more realistic and it can be profitable in the case of an introduced carbon tax or the acquisition of a partial investment on the capital costs.

If the years of operation increase (N=20 instead of 15 considered in Fig. 5.7) then the results are different. For 8,760 hours, the layout is economically viable for two different values of sold electricity, with an NPV of 59,346€ for 0.065€/kWh and 406,345 € for 0.075€/kWh, respectively. A very important observation is that the more realistic value of 6,570 hours is almost viable because the loss is only 61,634€ and considering the benefits from the wasted heat that is used the loss is annihilated. Moreover, the possibility of an funding scheme, as discussed above, could make the proposed system even more competitive.

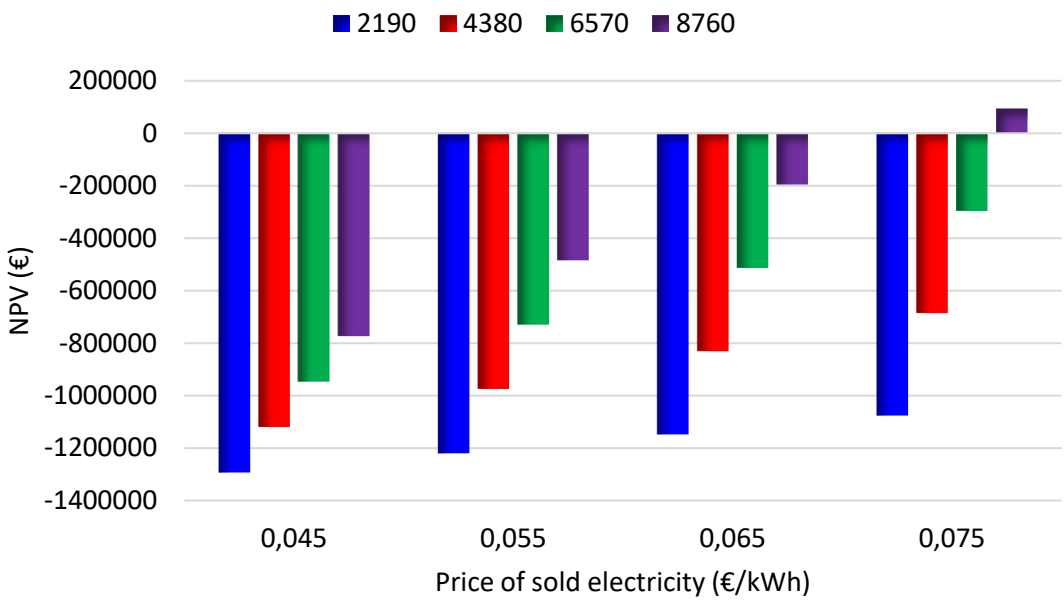

Fig. 5.7. Results for the NPV for N=15 and r=5% and for different marginal system costs and hours of annual operation

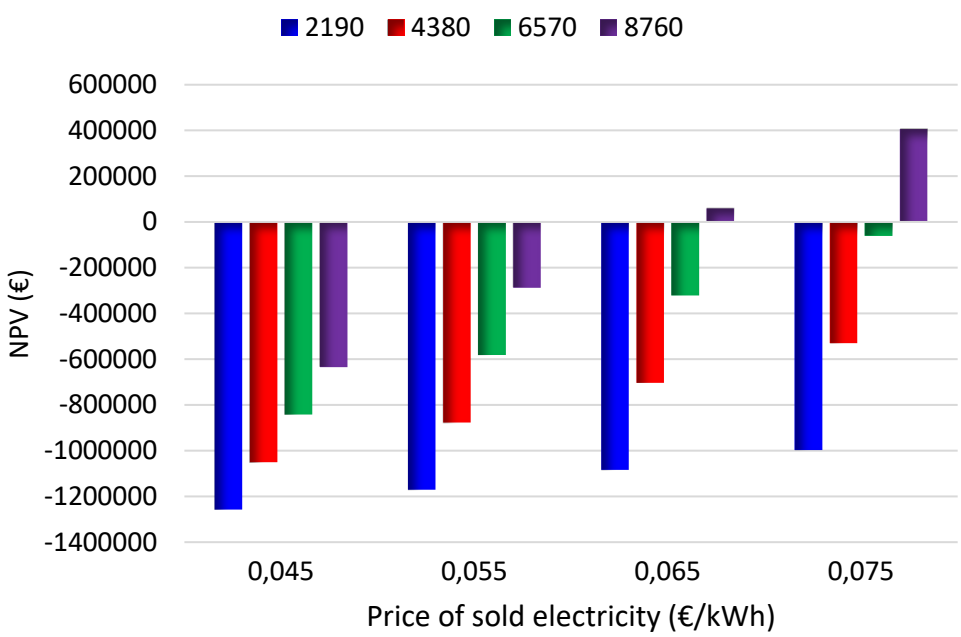

Fig. 5.8. Results for the NPV for N=20 and r=5% and for different marginal system costs and hours of annual operation

If the payback period is smaller than 20 years, then the proposed system is considered that can be materialized. For almost every price of sold electricity, if the operation is all day then the PbP is near 20 years for the lowest price and for the highest price of sold electricity is near 10 years (9,7 years). It is remarkable that if the operation time is 6,570 hours per year and the price of sold electricity is 0.055€/kWh then the payback period is 20,67 years while for the other prices, 0.065€/kWh and 0.075€/kWh, PbP is equal to 15,9 and 13 years, respectively. This figure provides the opportunity to understand more easily if the creation of this layout is profitable with respect to the operation time and the change of the price of the sold electricity

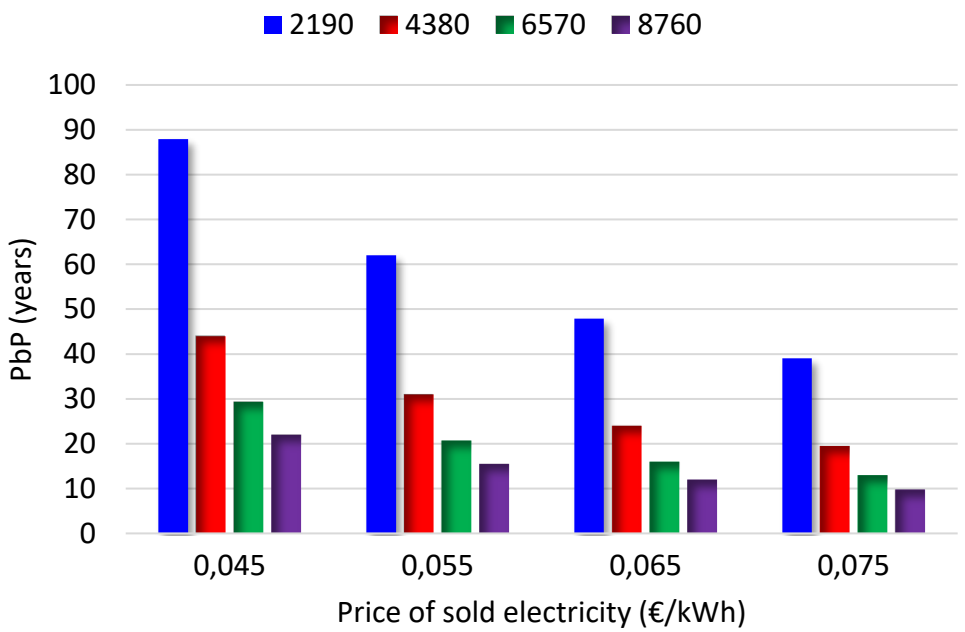

Fig. 5.9. Results for the payback period for different marginal system costs and hours of annual operation

Finally, the LCOE gives the price of the sold electricity in a standard period of investment in order to fully cover the total costs (both capital and operational/maintenance). If the LCOE is from 0.045€/kWh to 0.075€/kWh then the layout is viable. As it is obvious, the smaller the LCOE is, the better the profit will be. The smallest value is obtained for the maximum operation time and the maximum period of investment (0.047€/kWh) and the crucial value is for 6,570 hours per year and for 15 years (0.075€/kWh).

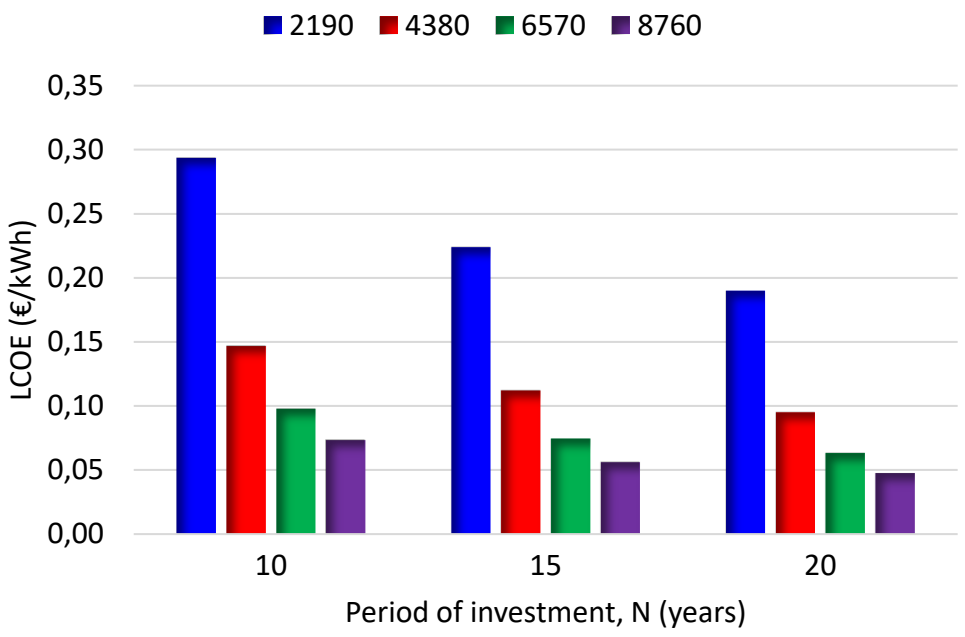

Fig. 5.10. Results for the LCOE for different periods of investment and hours of annual operation

6. Results and future research

Addressing the most significant factors to achieve the best thermal and exergy efficiency, which are the pressure ratio of the turbine the turbine inlet temperature and the temperature above the T_{crit}, the results can be summarized as following: the TIT reaches its peak value (750 ^{o}C) in order to achieve the highest efficiency. On the other hand, the pressure ratio has the smallest value possible (in this occasion is 4) and the pressure in state 2 must be as close as it can be to the critical pressure (73.8 bar) to maximize the thermal efficiency. Thus, the thermal efficiency is higher than 42% and the exergy efficiency exceeds 65%. The net output is 405.9 kW and the turbine gross output is 558 kW.

With respect to the thermodynamical values, this study emphasized to the depiction of the supercritical Rankine layout, in order to reveal the complicated design of the heat exchangers (recuperator, heater and gas cooler) as well as the turbomachinery and the pump. After the final placement of the supports and the minor components, the cost of the materials for the construction and the employment cost is estimated at 1,300,768 € with the most expensive to be the manufacturing of the turbine (38% of the total cost) and the heat exchangers with a 26% (of which 12% for the recuperator, 9% for the gas cooler and 5% for the heater). The employment cost constitutes, as well, a remarkable value of 20% of the total cost.

Lastly was conducted an economic analysis that provided significant results for the sustainability of the proposed system. For an interest rate 5% and for 15 years as the period of investment, the NPV is positive only in one occasion with a profit of 93,530 € (for a MSC equal to 0,075 €/kWh and for all day operation). If the period of investment increases then the NPV is profitable for both 0.065 €/kWh (NPV= 59,346 €) and 0.075 €/kWh (NPV=406,345 €). As it is referred above, the most realistic scenario is the operation time to be 6,570 hours per year and for the second occasion the loss is quite small, which with a small funding scheme could be turned competitive. The other two economic indicators (PbP, LCOE) provide slightly different images of when the layout will be viable and under which circumstances. The LCOE is an extremely significant factor because the changes that occurred globally (pandemic and economic crisis) the price of the electricity is very sensitive and can be completely different from one year to another.

In the first chapter, is discussed the meaning of cogeneration and trigeneration and how to realize them. The considered configuration of this research could have a dominant role for a combined heat power system, using the waste heat from the gas cooler to produce heating or exploiting the electricity to connect the Rankine cycle with a generator which is connected to a heat pump in order to produce cooling. Furthermore, the sensitivity of the main parameters in a future research may provide important results if the design of the turbine is different. In this study, is presented the optimization of the rotor but not of the stator. With a different design of the stator and the rotor the realization of smaller pressure ratios below 4 would be possible. Additionally, because of the environmentally friendly cycle, it is likely to achieve better economical results in a future research if the net output is not limited to only electricity but also to other energies and, moreover, a direct carbon tax would be introduced in Greek energy market, enhancing the competitiveness of CO_2-free systems. Moreover, since all the

components have been sized in detail a complete bill of materials has been developed, which could be used as future work to conduct a life cycle analysis and quantify the environmental footprint of the entire life cycle of the proposed system.

7. List of Tables

8. List of Figures

9. References

[1] "What is combined heat and power (CHP)?," 2016.

[2] C. Watford, "Combined heat and power (CHP) cogeneration," 2009.

[3] "Trigeneration," 2020.

[4] D. MacKay, *Sustainable Energy-without the hot air*: UIT cambridge, 2008.

[5] Butlins, "Combined heat and Power (CHP) simultaneously provides electricity and heat from a single source," 2020.

[6] "How does Micro CHP work?," 2015.

[7] "Triple points for some common substances," 2016.

[8] Emerson Climate Technologies, "Commercial CO_2 Refrigeration Systems Guide for Subcritical and Transcritical CO_2 Applications," 2014.

[9] A. Rozhentsev and C.-C. Wang, "Some design features of a CO2 air conditioner," *Applied Thermal Engineering,* vol. 21, pp. 871-880, 2001.

[10] B. T. Austin and K. Sumathy, "Transcritical carbon dioxide heat pump systems: A review," *Renewable and Sustainable Energy Reviews,* vol. 15, pp. 4013-4029, 2011.

[11] S. Karellas, T. C. Roumpedakis, N. Tzouganatos, and K. Braimakis, *Solar Cooling Technologies*: CRC Press, 2018.

[12] Y. Ahn, S. J. Bae, M. Kim, S. K. Cho, S. Baik, J. I. Lee*, et al.*, "Review of supercritical CO2 power cycle technology and current status of research and development," *Nuclear Engineering and Technology,* vol. 47, pp. 647-661, 2015/10/01/ 2015.

[13] S. A. Wright, R. F. Radel, M. E. Vernon, G. E. Rochau, and P. S. Pickard, "Operation and analysis of a supercritical CO2 Brayton cycle," *Sandia Report SAND2010-0171,* pp. 1-101, 2010.

[14] V. Dostal, M. J. Driscoll, and P. Hejzlar, "A supercritical carbon dioxide cycle for next generation nuclear reactors," Massachusetts Institute of Technology, Department of Nuclear Engineering …, 2004.

[15] A. T. Baheta, S. Hassan, A. R. B. Reduan, and A. D. Woldeyohannes, "Performance investigation of transcritical carbon dioxide refrigeration cycle," *Procedia Cirp,* vol. 26, pp. 482-485, 2015.

[16] C. Soares, "Chapter 3 - Gas Turbine Configurations and Heat Cycles," in *Gas Turbines (Second Edition)*, C. Soares, Ed., ed Oxford: Butterworth-Heinemann, 2015, pp. 93-171.

[17] S. C. Bhatia, "19 - Cogeneration," in *Advanced Renewable Energy Systems*, S. C. Bhatia, Ed., ed: Woodhead Publishing India, 2014, pp. 490-508.

[18] T. A. Adams II and J. H. Ghouse, "Polygeneration of fuels and chemicals," *Current Opinion in Chemical Engineering,* vol. 10, pp. 87-93, 2015.

[19] P. L. Georgios M. Kopanos, Michael C. Georgiadis, *Advances in Energy Systems Engineering*, 2017.

[20] R. Critoph, "Performance limitations of adsorption cycles for solar cooling," *Solar energy,* vol. 41, pp. 21-31, 1988.

[21] ©Mechanical Engineering Site. (2018). *Impulse Turbine and Reaction Turbine-Principle, Working and Difference*. Available: http://www.mechanicalengineeringsite.com/impulse-turbine-reaction-turbine-principle-working-difference/

[22] M. P. Boyce, "2 - Advanced industrial gas turbines for power generation," in *Combined Cycle Systems for Near-Zero Emission Power Generation*, A. D. Rao, Ed., ed: Woodhead Publishing, 2012, pp. 44-102.

[23] K. Zhou, J. Wang, J. Xia, Y. Guo, P. Zhao, and Y. Dai, "Design and performance analysis of a supercritical CO2 radial inflow turbine," *Applied Thermal Engineering,* vol. 167, p. 114757, 2020/02/25/ 2020.

[24] A. J. Glassman, "Computer program for design analysis of radial-inflow turbines," 1976.

[25] M. Marchionni, G. Bianchi, and S. A. Tassou, "Techno-economic assessment of Joule-Brayton cycle architectures for heat to power conversion from high-grade heat sources using CO2 in the supercritical state," *Energy,* vol. 148, pp. 1140-1152, 2018.

[26] D. Thanganadar, F. Asfand, and K. Patchigolla, "Thermal performance and economic analysis of supercritical Carbon Dioxide cycles in combined cycle power plant," *Applied Energy,* vol. 255, p. 113836, 2019.

[27] L. P. TIMKO, "Energy Efficient Engine high pressure turbine component test performance report," 01 JANUARY 1984 1984.

[28] X. Wang, Y. Yang, Y. Zheng, and Y. Dai, "Exergy and exergoeconomic analyses of a supercritical CO2 cycle for a cogeneration application," *Energy,* vol. 119, pp. 971-982, 2017.

[29] ΔΗΜΗΤΡΙΟΣ ΠΑΠΑΝΙΚΑΣ, *Αδιάστατοι χαρακτηριστικοί αριθμοί –Σχέσεις ομοιότητας – Ειδικός αριθμός στροφών -Εφαρμογές*, 2010.

[30] C. pumps, "7 Frame Plunger Pump."

[31] V. Motors, "Motors search-Dimension sheet," 2020.

[32] M. D. Carlson, B. M. Middleton, and C. K. Ho, "Techno-economic comparison of solar-driven SCO2 Brayton cycles using component cost models baselined with vendor data and estimates," in *Energy Sustainability*, 2017, p. V001T05A009.

[33] N. T. Weiland and C. W. White, "Techno-economic analysis of an integrated gasification direct-fired supercritical CO2 power cycle," *Fuel,* vol. 212, pp. 613-625, 2018.

[34] M. Astolfi, L. Xodo, M. C. Romano, and E. Macchi, "Technical and economical analysis of a solar–geothermal hybrid plant based on an Organic Rankine Cycle," *Geothermics,* vol. 40, pp. 58-68, 2011.

[35] M. Astolfi, "An innovative approach for the techno-economic optimization of organic rankine cycles," Italy, 2014.

[36] A. D. Atrens, H. Gurgenci, and V. Rudolph, "Economic optimization of a CO2-based EGS power plant," *Energy & Fuels,* vol. 25, pp. 3765-3775, 2011.

[37] J. Song, X. Li, K. Wang, and C. N. Markides, "Parametric optimisation of a combined supercritical CO2 (S-CO2) cycle and organic Rankine cycle (ORC) system for internal

combustion engine (ICE) waste-heat recovery," *Energy Conversion and Management,* vol. 218, p. 112999, 2020/08/15/ 2020.

[38] R. Smith, *Chemical process: design and integration*: John Wiley & Sons, 2005.

[39] V. Le, A. Kheiri, M. Feidt, and S. Pelloux-Prayer, "Thermodynamic and economic optimization of waste heat to power plant driven by a subcritical ORC using pure or zeotropic working fluid," *Energy,* vol. 78, pp. 622-638, 2014.

[40] McMaster-Carr. (2020). *Low-Carbon Steel Rectangular Tubes*. Available: https://www.mcmaster.com/metals/steel/low-carbon-steel-rectangular-tubes/